

Novel Host Materials for Blue Phosphorescent Organic Light-Emitting Diodes

Dissertation

zur Erlangung des akademischen Grades

Doktor der Naturwissenschaften (Dr. rer. nat.)

im Fach Chemie der Fakultät für Biologie, Chemie und Geowissenschaften

der Universität Bayreuth

vorgelegt von

Pamela Schrögel

geboren in Hof/Saale

Bayreuth, 2011

Die vorliegende Arbeit wurde in der Zeit von August 2007 bis Mai 2011 am Lehrstuhl für Makromolekulare Chemie I der Universität Bayreuth unter der Betreuung von Prof. Dr. Peter Strohriegl angefertigt.

Vollständiger Abdruck der von der Fakultät für Biologie, Chemie und Geowissenschaften der Universität Bayreuth genehmigten Dissertation zur Erlangung des akademischen Grades Doktor der Naturwissenschaften (Dr. rer. nat.).

Datum der Einreichung: 04. Mai 2011

Datum des wissenschaftlichen Kolloquiums: 27. Juli 2011

Prüfungsausschuss:

Erstgutachter: Prof. Dr. Peter Strohriegl

Zweitgutachter: Prof. Dr. Mukundan Thelakkat

Vorsitzender: Prof. Dr. Karlheinz Seifert

Prof. Dr. Anna Köhler

Table of Contents

1	Summary	1
2	Introduction	7
	2.1 Light Emission in Organic Semiconductors	8
	2.2 OLED operation principles	10
	2.3 OLED fabrication and relevant characteristics	14
	2.4 OLED architecture	16
	2.5 Materials for Organic Light Emitting Diodes	18
	2.5.1 Hole Transport Materials	18
	2.5.2 Electron Transport Materials	19
	2.5.3 Phosphorescent Emitting Materials	21
	2.5.4 Host materials for Phosphorescent Emitters	22
3	Aim of the Thesis	28
4	Overview of the Thesis	29
	4.1 High triplet energy host materials by introducing torsion	32
	4.2 High triplet energy host materials by <i>meta</i> -linkage	36
	4.3 High triplet energy host materials by non-conjugated linkage	39
5	References	46
6	A Series of CBP-derivatives as Host Materials for Blue Phosphorescent Organic Light-emitting Diodes	51
7	Meta-linked CBP-Derivatives as Host Materials for a Blue Iridium Carbene Complex	73
8	Phosphazene-based Host Materials for the Use in Blue Phosphorescent Organic Light-emitting Diodes	99
9	Appendix: Triplet Excimer Emission in a Series of 4,4'-Bis(<i>N</i> -carbazolyl)-2,2'-biphenyl Derivatives	121
10	List of Publications	147

1 Summary

Organic light-emitting diodes (OLEDs) have been commercially used in full-colour active matrix (AMOLED) displays for a couple of years. Only recently, a new application of OLEDs in the field of lighting has been opened up. For white emission monochrome systems of the three primary colours red, green and blue need to be combined. The major issue from the materials' point of view is still the lack of stable host-emitter systems for blue emission. This thesis deals with the development of new host materials for blue phosphorescent emitters.

The host material has to meet a complex profile of requirements. As most crucial feature the triplet energy of the host material has to exceed the triplet energy of the emitter. An increase of triplet energy of the host material is achieved by reducing the conjugated π -system in the host molecule. This thesis describes three synthetic approaches to high triplet energies by confining the π -conjugation: by introducing **torsion** in the molecular structure, by choosing a **meta-linkage** and by a **non-conjugated linkage**. The first and second approach was applied to carbazole-based host materials, whereas the third was demonstrated on phosphazene-based host materials.

In the first approach, the molecular structure of a well-known carbazole-based host material, 4,4'-bis(carbazol-9-yl)-2,2'-biphenyl (CBP), was optimised by introducing **torsion** via methyl or trifluoromethyl substituents in the 2- and 2'-positions of the central biphenyl moiety to yield twisted CBP-derivatives. By confining the conjugated system in combination with selective methyl substitution a series of host materials with superior thermal and photophysical properties was obtained. Compared with the triplet energy of 2.58 eV for CBP, high triplet energies of 2.95 eV could be realised for the twisted CBP-derivatives. In addition, appropriate substitution of the crystalline CBP results in amorphous materials with high glass transition temperatures of up to 120°C. In cyclic voltammetry the electrochemical properties were studied. Here, it was found that the systematic variation of the substitution patterns enables fine-tuning of the energetic positions of the HOMO and LUMO. This helps to avoid injection barriers at materials' interfaces in the OLED device. By blocking the activated sites in the host molecules a stability of the electrochemically oxidised species against dimerisation could be demonstrated.

2 | Summary

In the second approach, the conjugation in the same parent carbazole-based compound CBP was reduced by choosing a **meta-type of linkage** instead of the common *para*-linkage of the carbazole substituents to the central biphenyl unit. As a result of the *meta*-linkage, triplet energies of more than 2.90 eV were achieved. No further increase in triplet energy was observed by introducing additional torsion in the molecular structure as described in the first approach. Moreover, the thermal properties were optimised by selective methyl substitution to yield host materials with glass forming properties and high glass transition temperatures of up to 120°C. All host materials were tested in a comparative OLED device study in combination with a phosphorescent emitter with saturated blue emission. For the best host material of this series an external quantum efficiency of 9.7% and a high brightness of 10 800 cd/m² were achieved.

Both series of carbazole based host materials – the twisted and the *meta*-linked CBP-derivatives – were synthesised by Ullmann reaction of a dihalogenated biphenyl unit with two (substituted) carbazole units under classic conditions. Noteworthy is the intermediate 5,5'-diiodo-2,2'-dimethyl-biphenyl – a simple and versatile building block in the synthesis of materials with confined conjugation. The synthesis by direct iodination of 2,2'-dimethylbiphenyl, to the best of our knowledge, has not been described in literature before.

In the third approach, the class of low molecular weight phosphazenes, which is less described in the context of OLED-materials, was chosen as hosts for blue phosphorescent emitters. As a common characteristic all host materials consist of a six-membered ring of alternating phosphorus and nitrogen atoms. Each phosphorus atom bears two aromatic substituents attached via a **non-conjugated linkage**. Depending on the type of linkage to the central phosphazene core two sets of host materials can be distinguished: phenoxy substituted phosphazenes with phosphorus-oxygen bonds and phenyl substituted phosphazenes with phosphorus-carbon bonds. The phenoxy substituted derivatives were synthesized by nucleophilic substitution of the chlorine atoms in hexachlorocyclotriphosphazene with phenolates as nucleophils whereas the phenyl substituted derivatives were prepared by cyclocondensation of three equivalents of phosphinic amides. Due to their superior thermal properties compared to the phenoxy substituted series the phenyl substituted phosphazenes are better suited for

the use in OLED devices. They exhibit particularly high triplet energies of up to 3.4 eV. Thus, they can be combined with deep blue phosphorescent emitters. Another specialty of the phenyl substituted phosphazenes is a balanced charge carrier transport characteristic.

To conclude, each of the three presented approaches yields host materials with triplet energies high enough for a combination with blue phosphorescent emitters. Regarding the morphological stability the extensively studied carbazole based host materials exceed the novel phosphazene based host materials.

Zusammenfassung

Organische Leuchtdioden (OLEDs) finden seit einigen Jahren kommerzielle Verwendung in Aktiv-Matrix-Farbdisplays (AMOLEDs). Vor kurzem wurde ein weiteres Einsatzgebiet von OLEDs im Beleuchtungssektor erschlossen. Um weißes Licht zu erzeugen, müssen monochrome OLEDs der drei Primärfarben Rot, Grün und Blau miteinander kombiniert werden. Hierbei liegt die größte Herausforderung aus Material Sicht darin, dass keine stabilen Matrix-Emitter-Systeme für blaue Emission verfügbar sind. Diese Arbeit befasst sich mit der Entwicklung neuer Matrixmaterialien für blaue Phosphoreszenzemitter.

An die Matrix wird ein komplexes Anforderungsprofil gestellt. Als wichtigstes Kriterium muss das Matrixmaterial eine höhere Triplettenergie aufweisen als der Emitter. Eine Erhöhung der Triplettenergie des Matrixmaterials wird erreicht, indem das konjugierte π -System im Matrixmolekül verringert wird. Diese Arbeit zeigt drei synthetische Herangehensweisen auf, um durch eine Einschränkung der π -Konjugation die geforderten hohen Triplettenergien zu realisieren: durch Erzeugung von **Torsion** im Matrixmolekül, durch **meta-Verknüpfung** und durch **nicht-konjugative Verknüpfung**. Die ersten beiden Konzepte wurden auf carbazolbasierte Matrixmaterialien angewandt, wohingegen das dritte anhand von Matrixmaterialien auf Phosphazenenbasis gezeigt wurde.

Im ersten Ansatz wurde die Molekülstruktur einer der bekanntesten Matrixmaterialien auf Carbazolbasis, 4,4'-Bis(carbazol-9-yl)-2,2'-biphenyl (CBP), durch das Einbringen von **Torsion** optimiert. Dazu wird die zentrale Biphenyleinheit an den 2- und 2'-Positionen mit Methyl- oder Trifluormethylgruppen substituiert, um verdrillte CBP-Derivate zu

erhalten. Durch Verringerung der Konjugation und durch selektive Methylsubstitution entstand eine Reihe von Matrixmaterialien mit verbesserten thermischen und photophysikalischen Eigenschaften. Verglichen mit einer Triplettenergie von 2,58 eV für CBP konnten im Fall der verdrillten CBP-Derivate hohe Triplettenergien von 2,95 eV gemessen werden. Darüber hinaus führt eine geeignete Substitution der kristallinen Ausgangsverbindung CBP zu amorphen Materialien mit hohen Glasübergangstemperaturen von bis zu 120°C. Bei der Untersuchung der elektrochemischen Eigenschaften anhand von Cyclovoltammetriemessungen wurde beobachtet, dass die systematische Variation im Substitutionsmuster eine Feinabstimmung der Energielagen von HOMO und LUMO ermöglicht. Dadurch können Injektionsbarrieren an Materialgrenzflächen innerhalb eines OLED-Bauteils verhindert werden. Außerdem konnte gezeigt werden, dass durch die Blockierung aktivierter Positionen in den Matrixmolekülen eine Stabilität der elektrochemisch oxidierten Spezies gegen Dimerisierung erreicht wird.

Im zweiten Ansatz wurde die Konjugation derselben carbazolbasierten Ausgangsverbindung CBP dadurch eingeschränkt, dass für die Anbindung der Carbazolsubstituenten an die zentrale Biphenyleinheit eine **meta-Verknüpfung** anstelle der gewöhnlichen *para*-Verknüpfung gewählt wurde. Als Folge der *meta*-Verknüpfung liegen die Triplettenergien bei Werten von über 2,90 eV. Durch eine zusätzlich herbeigeführte Torsion in der Molekülstruktur – wie im ersten Ansatz beschrieben – wurde keine weitere Erhöhung der Triplettenergie beobachtet. Darüber hinaus konnten durch selektive Methylsubstitution die thermischen Eigenschaften weiter optimiert werden, so dass glasbildende Matrixmaterialien mit hohen Glasübergangstemperaturen von bis zu 120°C erhalten wurden. Alle *meta*-verknüpften Matrixmaterialien wurden in Kombination mit einem Phosphoreszenzemitter mit gesättigter, blauer Emission in einer OLED-Vergleichsstudie untersucht. Für die beste Matrix dieser Reihe wurden eine externe Quanteneffizienz von 9,7 % und eine hohe Leuchtdichte von 10 800 cd/m² erzielt.

Beide Reihen carbazolbasierter Matrixmaterialien – die verdrillten und die *meta*-verknüpften CBP-Derivate – wurden in einer Ullmann-Reaktion aus einer dihalogenierten Biphenyleinheit und zwei (substituierten) Carbazoleinheiten unter klassischen Bedingungen synthetisiert. Erwähnenswert hierbei ist die Zwischenstufe

5,5'-Diod-2,2'-dimethylbiphenyl – ein einfacher und vielseitiger Baustein in der Synthese von Materialien mit eingeschränkter Konjugation. Die Synthese durch direkte Iodierung von 2,2'-Dimethylbiphenyl wurde unseres Wissens nach bisher noch nicht beschrieben. Im dritten Ansatz wurde die für OLED-Materialien noch wenig bekannte Klasse niedermolekularer Phosphazenenverbindungen als Matrix für blaue Phosphoreszenz-emitter gewählt. Als gemeinsames Merkmal weisen alle Matrixmaterialien einen Sechsring aus alternierenden Phosphor- und Stickstoffatomen auf. Jedes Phosphoratom trägt zwei aromatische Substituenten, die durch **nicht-konjugative Verknüpfung** angebunden sind. Abhängig von der Art der Anbindung an den zentralen Phosphazenkern können zwei Serien von Matrixmaterialien unterschieden werden: phenoxy-substituierte Phosphazene mit Phosphor-Sauerstoff-Bindungen und phenyl-substituierte Phosphazene mit Phosphor-Kohlenstoff-Bindungen. Die Synthese der phenoxy-substituierten Derivate erfolgte über nukleophile Substitution der Chloratome in Hexachlorocyclotriphosphazenen mit entsprechenden Phenolaten als Nucleophile. Im Gegensatz dazu wurden die phenyl-substituierten Derivate durch Cyclokondensation von drei Äquivalenten Phosphinamid dargestellt. Durch die günstigeren thermischen Eigenschaften im Vergleich zu der phenoxy-substituierten Serie erwiesen sich die phenyl-substituierten Phosphazene als besser geeignet für den Einsatz in OLED-Bauteilen. Sie zeichnen sich durch besonders hohe Triplettenergien von bis zu 3,4 eV aus und können deshalb auch mit tiefblauen Phosphoreszenzemitern kombiniert werden. Als weitere Besonderheit zeigen phenyl-substituierte Phosphazene darüber hinaus einen ausgeglichenen Ladungsträgertransport.

Zusammenfassend führt jede der drei vorgestellten Synthesestrategien zu Matrixmaterialien mit den erforderlich hohen Triplettenergien, um mit blauen Phosphoreszenzemitern kombiniert werden zu können. Hinsichtlich der morphologischen Stabilität sind die umfangreich untersuchten Matrixmaterialien auf Carbazolbasis den neuen Materialien auf Phosphazenenbasis überlegen.

2 Introduction

In 2011, around 130 years after their commercialisation, incandescent light bulbs are still the most widely used light source in private households. Moreover, they are one of the most inefficient light sources with only 5 % of the consumed energy being converted into light – around 95 % are lost to heat.¹ Worldwide, governments are getting aware of the great potential to save energy and reduce the emission of greenhouse gases in the lighting sector. In 2009, the European Commission adapted a regulation (244/2009) for a gradual removal of inefficient incandescent light bulbs between September 2009 and September 2012.² Meanwhile, within the EU 100 W and 75 W bulbs are no longer commercially available. Alternative light sources like fluorescent lamps and compact fluorescent lamps have much higher efficiencies than incandescent light bulbs; however, they contain toxic mercury vapour. Inorganic light emitting diodes (LEDs) are currently among the most efficient light sources. As inorganic LEDs are point sources they can only be used as focused spotlight rather than as two-dimensional light source for surface illumination. Organic Light Emitting Diodes (OLEDs), which are, up to now, mainly used in flat full-colour displays, have been attracting attention for their use as illuminant in recent years. OLEDs offer a range of advantages: as their conceptual design differs from that of conventional light sources they emit diffuse light over a large area, they are thin and have a huge energy saving potential. Besides general lighting, signage, decorative and automotive interior lighting are being considered as fields of applications. Lighting companies like OSRAM and PHILIPS have already launched first commercial lighting panels as shown in Figure 1. In October 2010, OSRAM further announced to invest about 50 million Euros in a new OLED lighting pilot production and research facility in Regensburg, Germany.³ Due to the flexibility in design, the variety of innovative future applications is huge, for example, as lit-up blinds shown in a future study of General Electrics.⁴

The first white OLED device was presented in 1994 by Kido and co-workers.⁵ By doping red, green and blue fluorescent emitters into a poly(*N*-vinylcarbazole) matrix white emission covering a wide range of the visible spectrum was achieved. Yet, the power efficiency below 1 lm/W was still low.

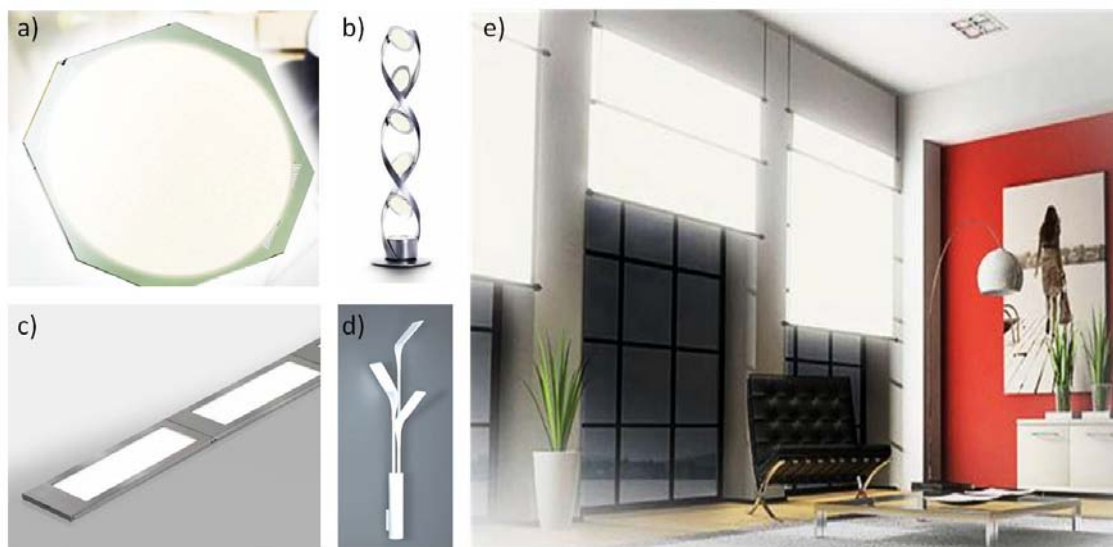


Figure 1. First commercial OLED panels and products: **a)** Orbeos (OSRAM),⁶ **b)** PirOLED (OSRAM)⁷ with five ORBEOS panels, **c)** Lumiblade (PHILIPS),⁸ **d)** O'Leaf wall light (PHILIPS),⁸ **e)** Vision of flexible blinds for interior illumination by GE.⁴

Since then much research has been focused on developing white OLEDs with high efficiencies to make them competitive and ready for the market. Only recently, a white OLED device was presented by the group of Karl Leo in 2009 with an impressive power efficiency of 90 lm/W comparable to a fluorescent tube.⁹ The development of energy saving substitutes for incandescent light bulbs is supported by many governments worldwide. In this course, the German Federal Ministry of Education and Research (BMBF) has been funding the project “OPAL 2008” and its follow up project “TOPAS 2012” as part of the “OLED 2015 initiative” for energy efficient lighting.

2.1 Light Emission in Organic Semiconductors

In an organic semiconductor a conjugated π -electron system with delocalised electrons is responsible for the inherent electronic and optoelectronic properties. The conjugated system is formed by the overlapping p_z -orbitals of sp^2 -hybridised C-atoms in the molecule. Compared to σ -bonds the π -bonds are considerably weaker. Thus, the π - π^* transition requires the lowest energy of electronic excitation. Due to the rather small energy gap (1.5 and 3 eV) between the highest occupied molecular orbital (HOMO) and

the lowest unoccupied molecular orbital (LUMO) in organic semiconductors the absorption of light in the visible region can lead to the excitation of one electron from the HOMO into the LUMO. With increasing extension of the conjugated π -electron system the energy gap declines. The possibility of tuning the materials properties by chemical modification is an essential advantage of organic semiconductors.¹⁰

Light absorption of an organic semiconductor causes an electron to be excited from its electronic ground state $S_{0,0}$ to its first excited electronic state $S_{1,n}$. Since the nuclei of the atoms are substantially heavier than the electrons, the electron transition has no effect on the equilibrium position of the potential surface. Therefore, only vertical transition of the electron take place into higher vibrationally excited $S_{1,n}$ states (Franck-Condon principle). The probability of each transition is determined by the Franck-Condon factor and results in fine-splitting of the absorption spectrum. By *internal conversion* (IC) which involves non-radiative deactivation processes the electron relaxes to the lowest electronic state $S_{1,0}$. Usually, radiative decay takes place from the lowest electronically excited state $S_{1,0}$ to the electronic ground state $S_{0,n}$ following again the Franck-Condon-principle (Kasha's rule). As a result, the *fluorescence* spectrum is always red-shifted compared to the absorption spectrum. The radiative decay in most organic molecules is limited to fluorescence as optical transitions take place under spin conservation.

The population of the triplet state requires spin flip by *intersystem crossing* (ISC) from the optically excited singlet state. By introducing heavy atoms spin-orbit coupling allows for mixing of the singlet and triplet states making ISC an efficient depopulation mechanism of the $S_{1,0}$ state. For example, in transition metal complexes, radiative decay takes place from the $T_{1,0}$ state under the emission of *phosphorescence*. The electronic transitions involved in absorption of light, fluorescence, phosphorescence, internal conversion and intersystem crossing are sketched in Figure 2.

Since intersystem crossing (ISC) involves the vibrational coupling between the S_1 and the T_1 states it becomes more effective, if the energy splitting between S_1 and T_1 , $\Delta E(S_1-T_1)$, is small.¹¹ This energy difference results from the interaction of the remaining electron in the HOMO with the electron in the LUMO. A smaller orbital overlap of HOMO and LUMO leads to a lower energy splitting $\Delta E(S_1-T_1)$. Thus, it can be significantly decreased if the optical transitions involve orbitals with different orientations in space like $n-\pi^*$

transitions or orbitals which are localised at different sites of the molecule. Such intermolecular charge transfer processes are common in organometal complexes resulting in a significant decrease of the energy splitting from ~ 1 eV for aromatic hydrocarbon compounds to 0.2 - 0.3 eV which leads to efficient intersystem crossing.¹²

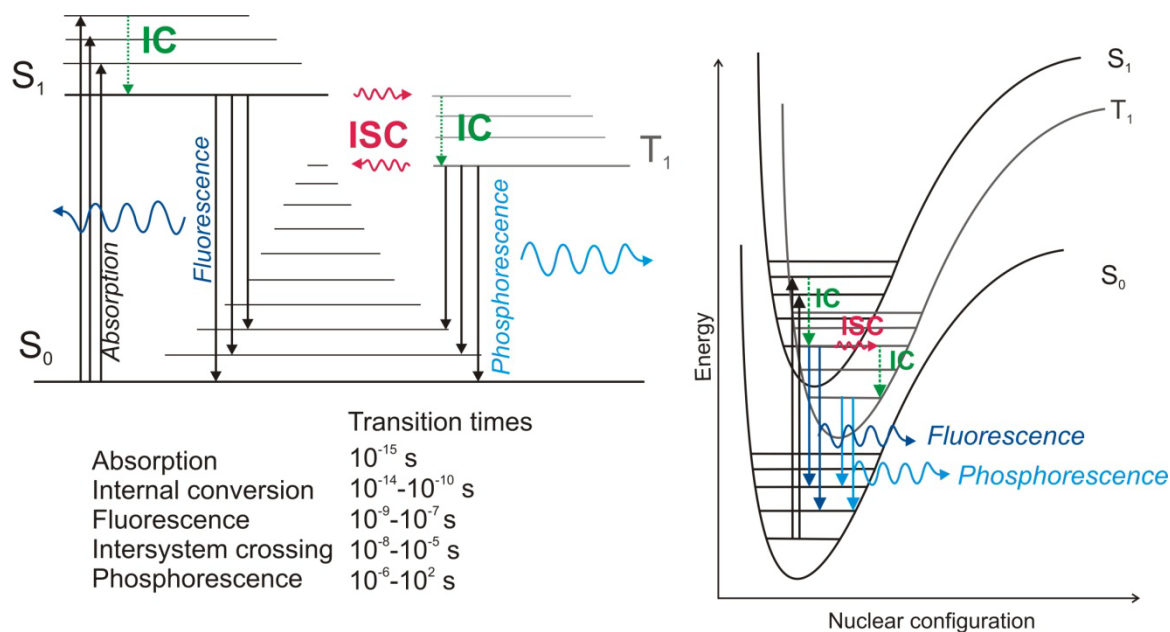


Figure 2. Left: Jablonski diagram sketching the electronic transitions involved during absorption of light (S_0 - S_1), fluorescence (S_1 - S_0) and phosphorescence (T_1 - S_0).¹³ **Right:** Potential diagram illustrating the vertical transitions following the Franck-Condon-principle, internal conversion (IC) and the intersystem crossing (ISC).

2.2 OLED operation principles

The basic principle of light emission in an OLED is electroluminescence. It was first discovered by Pope et al. in 1963 by applying high voltage to a single crystal of anthracene.¹⁴ Electroluminescence can be divided into three basic steps: (1) charge carrier injection, (2) charge carrier transport and (3) charge carrier recombination and emission of light. In Figure 3 these steps are sketched in a simple OLED device comprising an organic semiconducting layer sandwiched between two electrodes. One example of a simple device architecture is the first polymer OLED presented by R. Friend and co-workers in 1990.¹⁵ The device consists of 70 nm poly(phenylvinylene) (PPV) as active material, an indium-tin-oxide anode and aluminium cathode.

Charge carrier injection (1)

When a voltage is applied between the two electrodes charge carrier injection into the organic semiconductors occurs at the two interfaces with the electrodes. From a chemical point of view, injection of charge carriers leads to ionic molecular states. At the anode an electron is extracted from the HOMO level of the organic material to generate a radical cation (hole) while at the cathode a radical anion (electron) is formed by accepting an electron into the LUMO level.

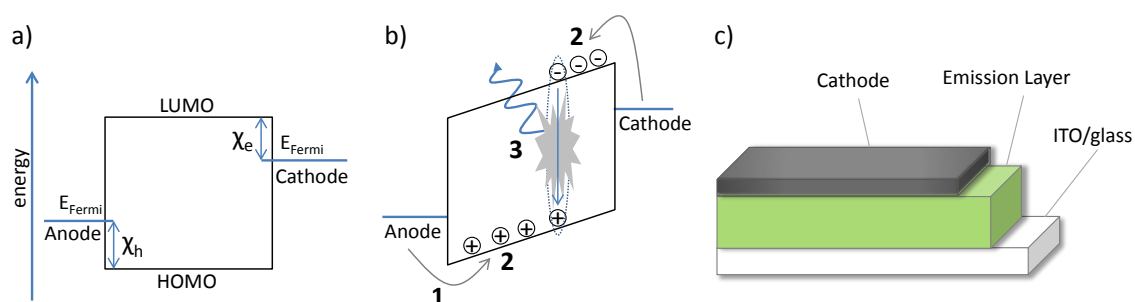


Figure 3. **a)** Energy diagram of a single-layer OLED: χ_h represents the hole injection barrier from the anode into the HOMO level and χ_e represents the electron injection barrier from the anode into the LUMO level of the organic layer. **b)** Energy level diagram of a single-layer OLED under applying an electric field. The three basic steps of light generation are included. **c)** Schematic of a single-layer OLED device with the emission layer sandwiched between a transparent anode and a metal cathode.

For efficient light extraction one of the electrodes needs to be transparent. In an ideal setup the contact between the electrodes and the organic semiconductors should have nearly no resistance, *i. e.* ohmic contacts should be formed. Therefore, the anode material has to reveal a high work function in order to enable hole injection into the HOMO level of the organic material. Here, transparent conductive oxides have proven to be suitable materials. Indium tin oxide sputtered on a glass substrate is the most common anode material. The work function (ϕ) of ITO is reported to be in the range of 4.7 - 5.0 eV depending on the pretreatment.¹⁶ Treatment with acids or bases can result in a shift of the ITO work function on the order of 1 eV.¹⁷ The barrier for hole injection from ITO into the HOMO can further be decreased by the deposition of a thin layer of hole injection materials with higher HOMO levels like copper phthalocyanine (CuPc, HOMO = 5.0 eV¹⁸) or the widely used poly(3,4-ethylene-dioxythiophene): poly(4-styrene-sulfonate) (PEDOT:PSS, HOMO = 5.2 eV¹⁹). For good electron injection into the LUMO

level of the organic semiconductor cathode materials with a low work function are required, as for example, magnesium ($\phi \approx 3.7$ eV) or calcium ($\phi \approx 3.0$ eV).²⁰ As a drawback, their low work functions render these materials highly reactive against oxygen and water. Because of the superior environmental stability very often high work function metals like aluminium ($\phi \approx 4.3$ eV)²⁰ are used as cathode materials. In combination with a thin interlayer of metallic lithium or LiF the electron injection barrier into the electron transporting material can be lowered.^{21,22} Instead of using separate hole or electron injection layers, the p-i-n technology provides ohmic contacts between the organic material and the electrodes by doping strong electron acceptors into the hole transporting material (p-doped HTM) and strong electron donors into electron transport material (n-doped ETM).^{23,24,25}

Charge carrier transport (2)

Driven by the external electric field injected holes and electrons will migrate through the organic semiconductor towards the opposite electrodes. The transport of charge carriers within an organic semiconductor is regarded to take place via hopping processes between molecule sites.^{26,27} Since ionic molecular states are involved it can be described by a sequence of redox reactions: a hole is transported by receiving an electron from the HOMO of a neighbouring neutral molecule. For the transport of electrons one electron is transferred from the LUMO level of a radical anion into the LUMO level of a neighbouring neutral molecule. The efficiency of charge carrier transport depends on the purity and morphology of the organic semiconductors. Impurities may act as trap states for holes or electrons,²⁸ whereas highly ordered systems, as in the case of defect free single crystals, result in higher charge carrier mobility than observed in amorphous organic materials.

Charge carrier recombination and emission of light (3)

Driven by Coulomb attraction, the recombination of electron and hole leads to localised excited states (excitons) with a binding energy between 0.4 - 1 eV.¹⁰ Due to spin statistics in standard quantum mechanics the spins of the hole and electron can be coupled to four new combined states: *one* singlet exciton and *three* triplet excitons. In most purely organic compounds only singlet excitons can decay under emission of

fluorescence, as radiative decay of triplet states is spin-forbidden. In these compounds, triplet excitons decay non-radiatively and do not contribute to light emission. However, by incorporation of a heavy atom strong spin-orbit coupling leads to efficient intersystem crossing (ISC) and emission of phosphorescence from the $T_{1,0}$ state into the ground state $S_{0,n}$ becomes an efficient relaxation path. Thus, in many transition metal complexes, as for example the green phosphorescent emitter tris(2-phenylpyridinato- N,C^2' -)iridium(III) ($Ir(ppy)_3$), all electrogenerated singlet (25 %) and triplet (75 %) excitations can be harvested for light emission. Forrest and Thompson et al. were the pioneers in triplet harvesting by incorporating the red phosphorescent emitter platinum octaethylporphyrin (PtOEP) into an OLED device.²⁹ Their finding was a breakthrough in the development of highly efficient OLED devices.

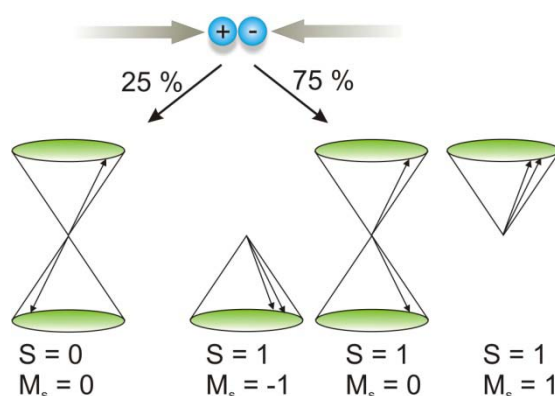


Figure 4: Recombination of charge carriers under the formation of 25 % singlet and 75 % triplet excitons. The two electron spins, represented by arrows, precess in z-direction. For the singlet exciton the relative orientations of the two electron spins are anti-parallel and 180° out of phase whereas they are in phase for the three triplet excitons. The quantum number of the spin angular momentum (S) and its z-component (M_s) are included.

Once formed an exciton can decay radiatively or diffuse according to its lifetime. Triplet excitons have a much longer lifetime (in the range of μs to s) than singlet excitons (in the range of ns) since the radiative decay from the first excited triplet state to the ground state is spin-forbidden. Thus, the triplet diffusion length is much longer (tens of nm) than for singlet excitons ($< 10 nm$). In order to prevent luminescence quenching the triplet emitter usually needs to be doped into a host material. Energy transfer in emitter-host-systems takes place via Förster energy transfer and Dexter energy transfer. Förster energy transfer is a long-range, non-radiative, dipole-dipole coupling of donor (D) and

acceptor (A) molecules. It requires spectral overlap between the emission of D and absorption of A and it only allows for energy transfer to the singlet excited state of A (singlet exciton). In the Dexter transfer the exciton diffuses from D to A sites via intermolecular electron exchange between D and A. Therefore, it requires orbital overlap between both molecules. Since this short-range process takes place under spin conservation both singlet-to-singlet and triplet-to-triplet energy transfer is allowed.³⁰

2.3 OLED fabrication and relevant characteristics

Depending on the nature of the organic materials basically two different fabrication methods of OLED devices are applied. Low molecular weight materials are usually deposited by thermal evaporation under high vacuum (10^{-6} mbar) which requires expensive technical equipment. On the other hand, polymeric materials are processed from solution: on a laboratory scale OLED preparation can be done by spincoating or doctor blading. Further developments towards printing techniques could be a way to low-cost mass production of large active areas. However, the production of multilayer devices with solution-based processes is facing the major problem of redissolving previously deposited layers.³¹ Therefore, the vapour-deposition technique is the prevailing process for OLED fabrication at the moment.

The most practical approach to generate OLEDs with white emission is to combine the emission of monochrome red, green and blue systems. Several different OLED architectures are possible: the different colour systems can be aligned horizontally as single pixels. An advantage is that each colour can be addressed separately for an easy colour adjustment while the fabrication of such a structure is not straightforward. In the vertical OLED structure the three colours are generated in a layered or in a stacked setup with single stacks for each colour. The stacked architecture requires internal electrodes whereas the layered structure is less complex, however, colour changes by differential aging of the different colours cannot be compensated.³¹

The light emitted by an OLED device can be described by several characteristics. The chromaticity of each colour is classified by its *x- and y-coordinates in the CIE-diagram* (Figure 5) which was developed by the Commission Internationale d'Eclairage (CIE) to

describe each colour with respect to the perception by the human eye. Besides the two colour approach, white light is most commonly generated by additive colour mixing of the three primary colours red, green and blue which span a triangle in the CIE-diagram. As each colour within this triangle can be obtained, the inclusion of the white point ($x = 0.33, y = 0.33$) into the triangle is crucial. Also shown is the emission colour of the temperature-dependant irradiation of a black body, the Planckian locus, which correlates the colour with a certain *colour temperature*. For lighting the temperature range between 3000 – 10 000 K is of interest where colour temperatures below 5000 K are regarded as “warm” white and temperatures above 5000 K as “cold” white.³² Another feature for the description of white light is the *colour rendering index (CRI)*. On a scale from 0 to 100 the CRI is a measure for the ability of a light source to resemble the colour appearance of test objects in comparison to a standard light source. For the application as indoor-lighting source a high CRI ≥ 80 is desired.

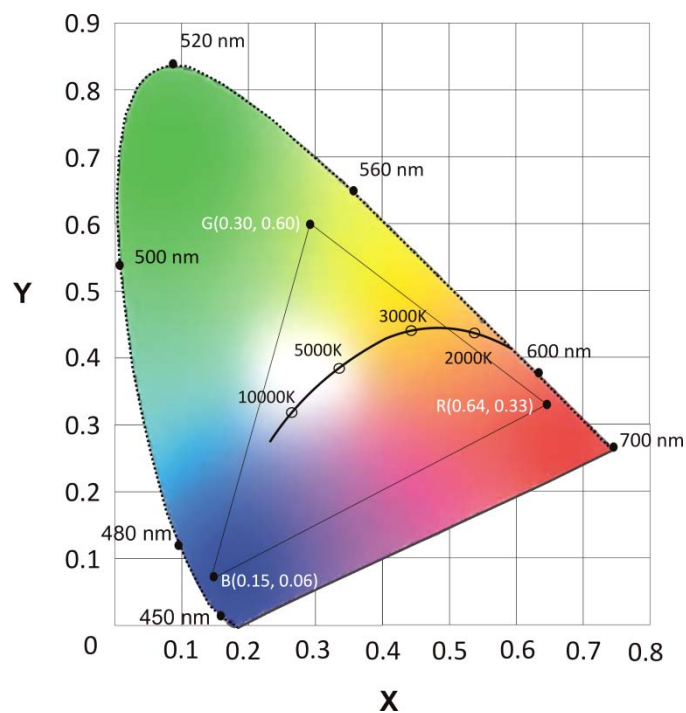


Figure 5. CIE-diagram with the chromaticities of the primary colours RGB (sRGB) defined as standards for colour displays, the Planckian locus (black curve) and the monochromatic colour curve (dotted line).

Another important figure-of-merit is the efficiency of an OLED device. OLED displays are usually classified by their current efficiency (η_c) given in candelas per ampere (cd/A). More common for OLEDs in lighting applications is the power efficacy (η_p) given in

lumens per watt (lm/W) which can be calculated from the current efficiency according to equation 1 under the assumption of Lambertian emission.

$$\eta_p = \eta_c \cdot (\pi/\text{voltage}) \quad (\text{eq. 1})$$

The external quantum efficiency (η_{ext}) is the ratio of the number of photons emitted by the device into the viewing direction to the number of electrons injected into the device. The external quantum efficiency is dependent on several single efficiencies which are taken into account in equation 2.³³

$$\eta_{\text{external}} = \eta_{\text{recombination}} \cdot \eta_{\text{spin}} \cdot \phi_{\text{PL}} \cdot \eta_{\text{outcoupling}} = \eta_{\text{internal}} \cdot \eta_{\text{outcoupling}} \quad (\text{eq. 2})$$

- $\eta_{\text{recombination}}$ – fraction of electrons that recombine with holes to form excitons
- η_{spin} – fraction of excitons formed which can result in radiative transitions;
0.25 for fluorescent emitters and 1 for phosphorescent emitters
- ϕ_{PL} – intrinsic quantum yield for radiative decay of the formed excitons
- $\eta_{\text{outcoupling}}$ – fraction of emitted photons that escape the device

2.4 OLED architecture

The first OLED device developed by Tang and VanSlyke in 1987 consisted of a simple two-layer structure with the aromatic amine TAPC as hole conductor and Alq₃ as electron transport material and emitter.³⁴ For highly efficient OLEDs a well-balanced injection and transport of both charge carriers is essential. To optimise these processes the OLED architecture has become more complex over the years by the addition of functional layers. Fig 6a shows a typical setup of a monochromic OLED device. For efficient charge carrier transfer the hole and electron transport materials should reveal high charge carrier mobilities. Nowadays, transport layers are usually doped to provide a high density of charge carriers and ensure high currents. The emission layer comprises the emitter doped host material. As the key step towards high efficiency the emission layer consists of a triplet emitter with a high phosphorescence quantum yield doped into a host material. Ideally, the host material performs charge carrier transport, charge carrier recombination and energy transfer to the emitter. Since the mobility of holes in most organic materials is higher compared to that of electrons³⁵ the insertion of an

additional hole blocking layer between the emission layer and the electron transporting layer helps to confine holes in the emission layer and improves the efficiency of recombination of charge carriers.

In the case of OLEDs with white emission in a layered configuration the design of the emission layer is most challenging. In 2009, the group of Karl Leo presented a highly sophisticated OLED design for white emission shown in Figure 6b. The emission of white light is accomplished by the use of three phosphorescent emitters: Ir(MDQ)₂(acac) for red, Ir(ppy)₃ for green and Flrpic for blue emission. The blue sublayer was located in the middle of the emission layer surrounded by red and green sublayers. At the interface of the two host materials TCTA and TPBI exciton formation takes place. Förster-type transfer is suppressed by 2 nm thin interlayers of pure host materials TCTA and TPBI. Additionally, the high triplet energy of TCTA also suppresses diffusion of blue excitons into the red emission layer. In contrast, unused triplet excitons from the blue region can be harvested by the green emitter by triplet diffusion. As the outcoupling efficiency depends on the difference of refractive indices n of the organic material ($n_{\text{org}} = 1.7-1.9$) and the glass substrate ($n_{\text{glass}} = 1.5$) losses by total internal reflections on the organic/glass interface can be prevented by matching the refractive indices. In this case this was accomplished by using high refractive index glass substrates ($n_{\text{glass}} = 1.78$). Light which is captured in glass modes can be extracted by using substrates of modified shapes like a patterned surface. With this optimised setup in combination with outcoupling techniques Leo's group achieved a power efficiency of 90 lm/W which matches the efficiency of a fluorescent tube. By using an additional half-sphere as outcoupling aid power efficiencies exceeding 120 lm/W could be demonstrated.⁹

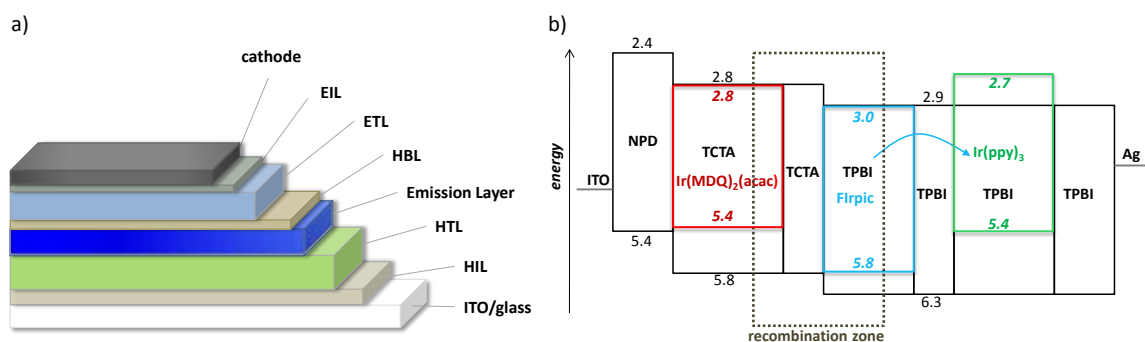


Figure 6. a) Schematic of a monochromatic multi-layer OLED device. **b)** Layered OLED architecture with sophisticated design of the emission layer for white emission.⁹

2.5 Materials for Organic Light Emitting Diodes

For a low drive voltage of the OLED device, the energy levels of all materials should be well-matched to avoid barriers for charge carrier injection and for charge carrier transport at the interfaces of two materials. Regarding a fabrication of the OLED device by thermal evaporation an important requirement for all small molecule materials used is their high thermal stability. Besides the thermal stability, a stable amorphous phase at operation temperature is beneficial for the morphological stability of the device.³⁶ In addition by forming uniform films amorphous materials help to avoid grain boundaries which may act as trap states during transport of charges.²⁸ While most small organic molecules tend to crystallize readily proper molecular design can lead to small molecules with a stable amorphous phase at room temperature. Such molecular glasses can be obtained by avoiding strong intermolecular forces like hydrogen bonding or π - π stacking between the molecules. A very common design concept for molecular glasses is the space-filling starburst topology.³⁷ Furthermore, the intermolecular distance can be increased by introducing bulky substituents to hinder packing of molecules and prevent crystallisation.

2.5.1 Hole Transport Materials

Hole transporting materials (HTMs) must reveal a low ionisation potential in order to facilitate hole injection and hole transport under the formation of radical cations. Typical hole transport materials have electron rich moieties and are therefore often based on triarylaminines. The molecular structures of several conventional hole transport materials are shown in Figure 7.

TPD has a HOMO level of ~ 5.3 eV³⁸ and a high hole drift mobility of $1 \cdot 10^{-3}$ cm²/Vs.³⁹ However, its low glass transition temperature (T_g) of 60°C⁴⁰ limits its use in OLED devices. The T_g of α -NPD is markedly increased to 100°C⁴¹ by replacing two phenyl substituent by naphthyl units. In addition, α -NPD has as well a high hole mobility of $8.8 \cdot 10^{-4}$ cm²/Vs⁴² and its HOMO level of ~ 5.4 eV^{38,43} is well suited for accepting holes from the hole injection layer or anode. A major drawback of both compounds is their low triplet energy of ~ 2.3 eV.⁴⁴ HTMs with triplet energies $\Delta E(T_1-S_0)$ higher compared to that of the emitter confine triplet excitons within the emission layer which increases the

efficiency of the device. For example, the molecular glass TCTA shows a high triplet energy of 2.8 eV⁹ and a very high T_g of 151°C.⁴⁵ The outer carbazole substituents lead to a deep HOMO level of 5.7 eV⁴⁵ and thus slightly reduced injection properties. Moreover, the hole mobility is one order of magnitude lower than for α -NPD and TPD. TAPC is a hole transport material with an excellent hole mobility of $1 \cdot 10^{-2}$ cm²/Vs⁴⁶ and a HOMO level of 5.4 eV.⁴³ Its high triplet energy of 2.9 eV⁴⁴ confines triplet excitons within the emitting layer. Yet, with a low T_g of 78°C³⁶ its morphological stability is rather poor.

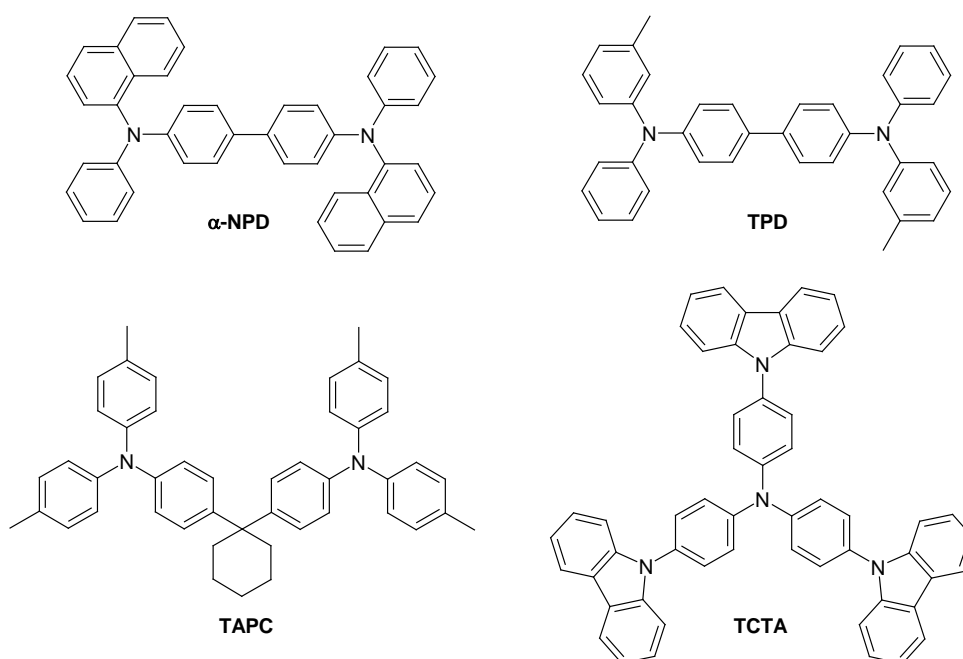


Figure 7. Molecular structures of: N,N'-di(naphtha-1-yl)-N,N'-diphenylbenzidine (α -NPD), N,N'-bis(3-methylphenyl)-N,N'-diphenylbenzidine (TPD), 1,1'-bis(4'-(N,N'-di(p-tolyl)aminophenyl)cyclohexane (TAPC), 4,4',4''-tris(carbazol-9-yl)triphenylamine (TCTA).

2.5.2 Electron Transport Materials

Electron transport materials (ETMs) facilitate the electron injection from the cathode, accept electrons and transport electrons to the emitting layer. Common electron transport materials are based on electron deficient heterocycles, like oxadiazoles, triazoles, pyridine, pyrimidine, imidazole or triazine. Among ETMs BCP and the metal chelate Alq₃ are the most commonly used materials. Figure 8 gives an overview of some ETMs frequently used in OLED devices.

Alq₃ has a suitable LUMO level of ~ 3 eV⁴⁷ to facilitate electron injection from the cathode. In Alq₃ the electron mobility in the range of $1 \cdot 10^{-5}$ cm²/Vs^{48,49} is rather low while the electron mobility of BCP is one order of magnitude higher.⁵⁰ BCP is also suited as hole blocking material due to its low HOMO level of 6.5 eV.⁵¹ However, films of Alq₃ are morphologically more stable due to its high T_g of 172°C.⁵² The star-shaped molecular glass TPQ also forms stable amorphous films (T_g = 147°C)⁵³ and has an electron mobility of $1 \cdot 10^{-4}$ cm²/Vs.⁵⁴ Among the class of triazines, BTB, for example, is known to have a high electron mobility of $7 \cdot 10^{-4}$ cm²/Vs.⁵⁵ Due to their low triplet energy most ETMs need to be combined with an additional hole and exciton blocking layer with higher triplet energy to confine excitons within the emission layer. When the benzimidazole-based TPBI with a triplet energy of 2.74 eV⁵⁶ and the pyridine-based TmPyPB with a triplet energy of 2.8 eV are used as electron transport materials triplets should not be quenched in green and light blue OLEDs. In addition, TmPyPB is a material with high electron mobility of $1 \cdot 10^{-3}$ cm²/Vs.⁵⁷

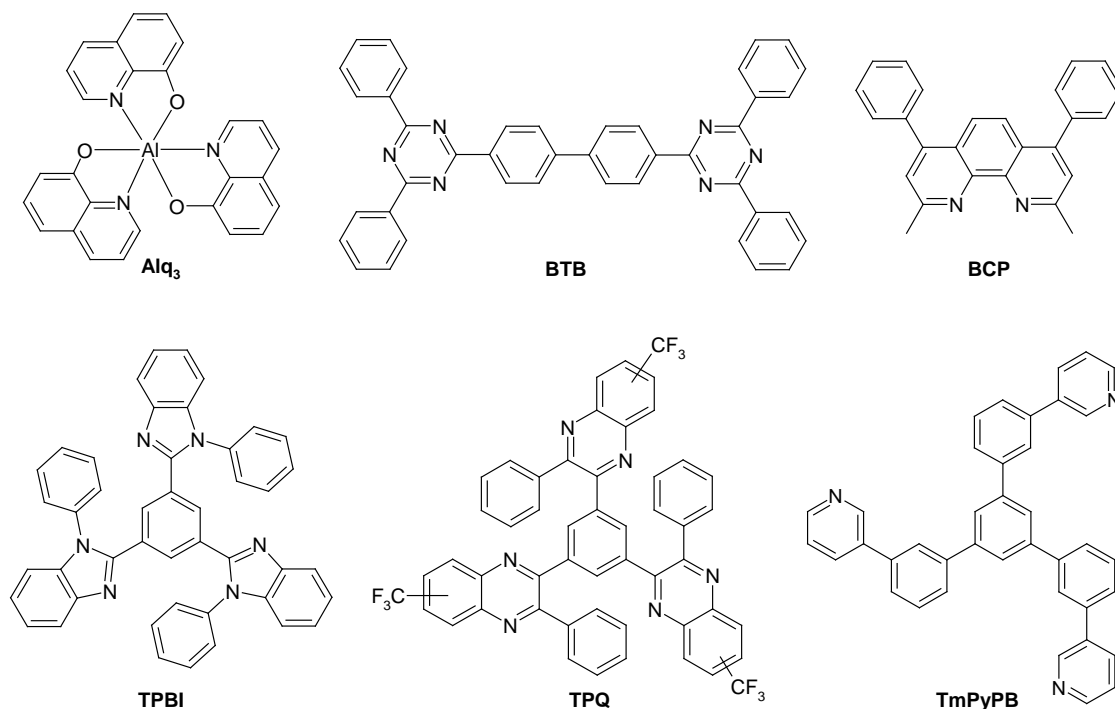


Figure 8. Molecular structures of: tris(8-hydroxyquinoline)aluminium (Alq₃), 4,4'-bis-(2-(4,6-diphenyl-1,3,5-triazinyl))-1,1'-biphenyl (BTB), 2,9-dimethyl-4,7-diphenyl-1,10-phenanthroline (BCP), 1,3,5-(tris-(N-phenylbenzimidazol-2-yl))-benzene (TPBI), 1,3,5-tris(3-phenylquinoxaline-2-yl)benzene (TPQ), 1,3,5-tri(m-pyridin-3-yl-phenyl)benzene (TmPyPB).

2.5.3 Phosphorescent Emitting Materials

The concept of triplet harvesting requires emitters with high phosphorescence quantum yields and short radiative lifetimes. The first phosphorescent emitter used in an OLED was the platinum-porphyrin-complex PtOEP with red emission ($\lambda_{\text{max}} = 650 \text{ nm}$).²⁹ As a result of its relatively long triplet lifetime of $\sim 90 \mu\text{s}$ ⁵⁸ a significant efficiency roll-off at higher current densities was observed. This phenomenon is associated with the process of triplet-triplet-annihilation (TTA) in which one excited state is lost for radiative decay.⁵⁹ In this process the interaction of two triplet excitons leads to the formation of one higher excited singlet exciton and one ground state molecule: $T_1 + T_1 \rightarrow S_n + S_0$. Only the singlet exciton - after intersystem crossing into the triplet state - can contribute to light emission.

Cyclometallated iridium(III) complexes have proven to be perfect candidates for phosphorescent emitters in OLEDs. They exhibit high quantum efficiencies and shorter lifetimes of the triplet excited states. Moreover, by suitable ligand design their emission energy can be shifted to span a large colour range from near infrared to near ultraviolet. The first example to be incorporated into an OLED device was the green ($\lambda_{\text{max}} = 520 \text{ nm}$) iridium complex *facial*-tris(2-phenylpyridinato-N,C^{2'})iridium(III) ($\text{Ir}(\text{ppy})_3$)⁶⁰ with a short radiative lifetime of $2 \mu\text{s}$.⁶¹ By expanding the π -conjugated system of the phenylpyridine ligand the triplet energy can be lowered resulting, for example, in red emission ($\lambda_{\text{max}} = 620 \text{ nm}$) of the complex bis(1-phenylisoquinolino-N,C^{2'})iridium(acetylacetonate) (piq)₂ $\text{Ir}(\text{acac})$.⁶² The introduction of electron withdrawing substituents like fluorine or cyano groups leads to a blue shift of the emission. The most common blue emitting iridium complex is bis(4,6-difluorophenyl)-pyridinato-N,C^{2'})iridium(III)picolinate (FIrpic) with greenish blue emission ($\lambda_{\text{max}} = 475 \text{ nm}$).⁶³ However, when using FIrpic as blue component in white OLEDs as in the case of the high efficiency white OLED of Leo's group, the generation of light is limited to a rather warm white with CIE colour coordinates of $x = 0.44$ and $y = 0.46$ and a CRI of 80.⁹ Here, the most crucial point towards more flexibility in rendering the whole range of white emission is the development of stable deeper blue emission systems. In Figure 9 three examples of phosphorescent iridium-complexes with different emission colours are shown.

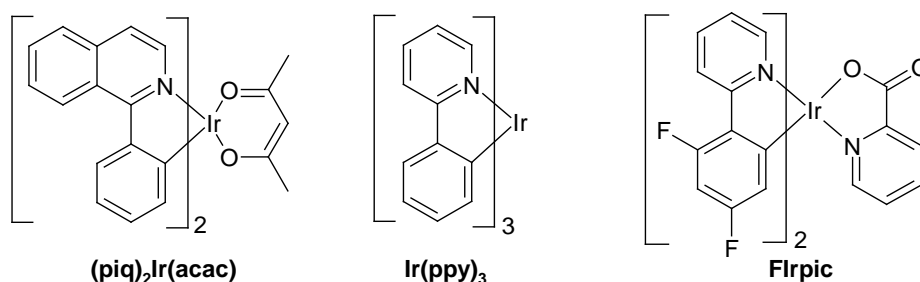


Figure 9. Molecular structures of the phosphorescent emitters bis(1-phenylisoquinolino- N,C^2')-iridium-(acetylacetonate) (**(piq)₂Ir(acac)**, red, $\Delta E(T_{1-}S_0) = 1.90$ eV, CIE x 0.68, y 0.32), tris(2-phenylpyridinato- N,C^2')iridium(III) (**Irppy₃**, green, $\Delta E(T_{1-}S_0) = 2.42$ eV, CIE x 0.27, y 0.63) and bis(4,6-difluorophenyl)-pyridinato- N,C^2')iridium(III)picolinate (**Flrpic**, blue, $\Delta E(T_{1-}S_0) = 2.65$ eV, CIE x 0.16 y 0.32).

2.5.4 Host materials for Phosphorescent Emitters

Usually, triplet emitters are diluted in an appropriate host material to prevent concentration quenching of the emission. Besides charge carrier transport the main task of the host material is energy transfer to the emitter. In Figure 10 two possible configurations of energy levels of host and emitter are shown.

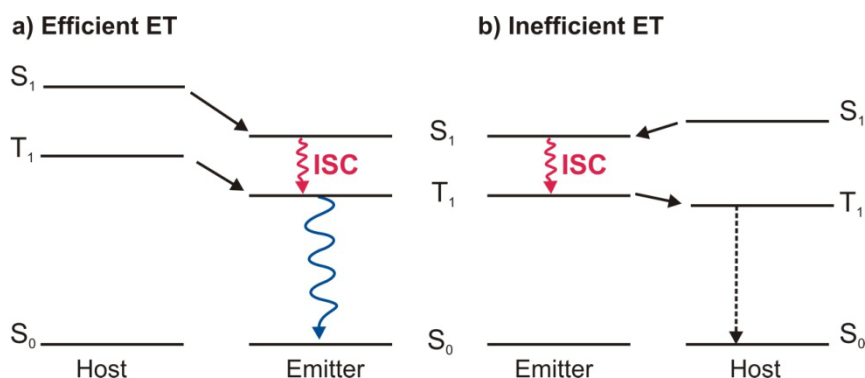


Figure 10. Energy diagram sketching **a)** efficient and **b)** inefficient energy transfer (ET) between host and emitter.

In the favoured scenario of efficient energy transfer shown in Figure 10 a) energy can be transferred from the singlet and triplet excited states of the host to the singlet and triplet excited states of the emitter. By efficient ISC all singlet excitons are converted to the triplet state to populate the $T_{1,0}$ state of the emitter which decays under emission of phosphorescence. In the case of inefficient energy transfer shown in Figure 10 b) the $T_{1,0}$ state of the emitter can be depopulated by energy transfer back into lower lying

triplet excited states of the host molecule. Since radiative decay from the $T_{1,0}$ of the host is spin-forbidden, the energy is lost for emission significantly lowering the quantum efficiency of the OLED device. Thus, the most crucial requirement for the host material is a triplet energy higher compared to the emitter. To confine triplet excitons on the turquoise emitter Flrpic ($\Delta E(T_1-S_0) = 2.65$ eV), for instance, the triplet energy of the host must be higher than 2.70 eV.⁶⁴ For deeper blue emitters host materials with even higher triplet energies $\Delta E(T_1-S_0) \geq 2.90$ eV are required. The development of host materials for deeper blue emitters has proven to be a challenging task. In general, the key to high triplet energies is to decrease the conjugation within a host molecule. Therefore, the variety of possible building blocks with high triplet energy is rather limited. Several design rules are valid for avoiding extended conjugation. In Figure 11 some trends in triplet energy related to the molecular basic structure are shown.

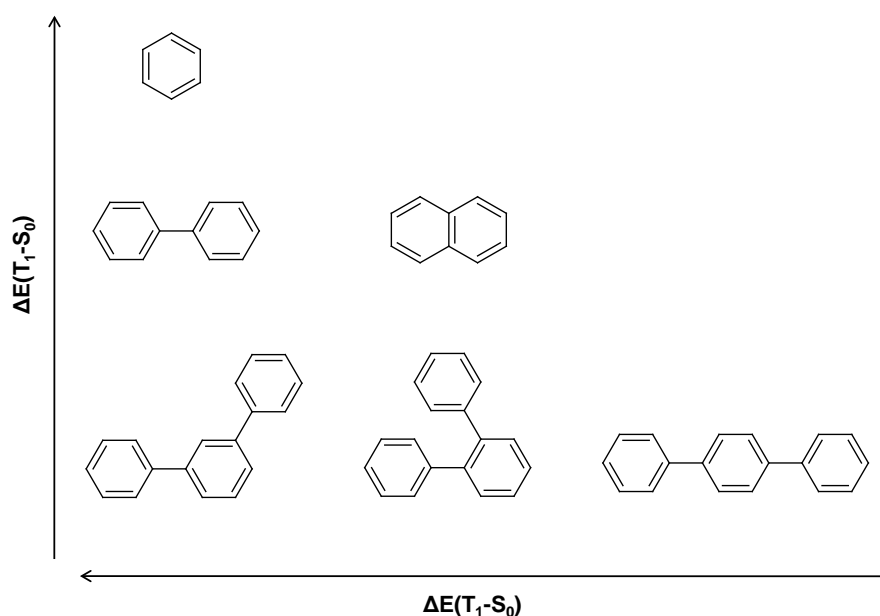


Figure 11. Dependence of the triplet energy $\Delta E(T_1-S_0)$ on the number of phenyl rings and on the type of linkage.

With increasing number of phenyl rings the conjugation increases and concomitantly the triplet energy decreases. Moreover, in fused ring systems lower triplet energy is expected as, for example, in the case of naphthalene ($\Delta E(T_1-S_0) = 2.64$ eV) compared with biphenyl ($\Delta E(T_1-S_0) = 2.82$ eV).⁶⁵ The possibilities for the connection of three phenyl

rings also influence the triplet energy. The *para*-linkage of the three phenyl rings allows for planarization and thus for the most extended conjugation resulting in a low triplet energy of $\Delta E(T_1-S_0) = 2.55$ eV for *para*-terphenyl. Compared with the *ortho*-linkage the *meta*-linkage leads to a lower degree of conjugation since the *meta*-positions are known to reveal the lowest electron densities in a phenyl ring. This translates into a larger triplet energy of $\Delta E(T_1-S_0) = 2.82$ eV for *meta*-terphenyl compared with 2.67 eV for *ortho*-terphenyl.⁶⁶

The probably largest class of host materials are based on carbazole which is a versatile building unit due to its high intrinsic triplet energy of 3.02 eV.⁶⁷ Some examples of carbazole based host materials are shown in Figure 12.

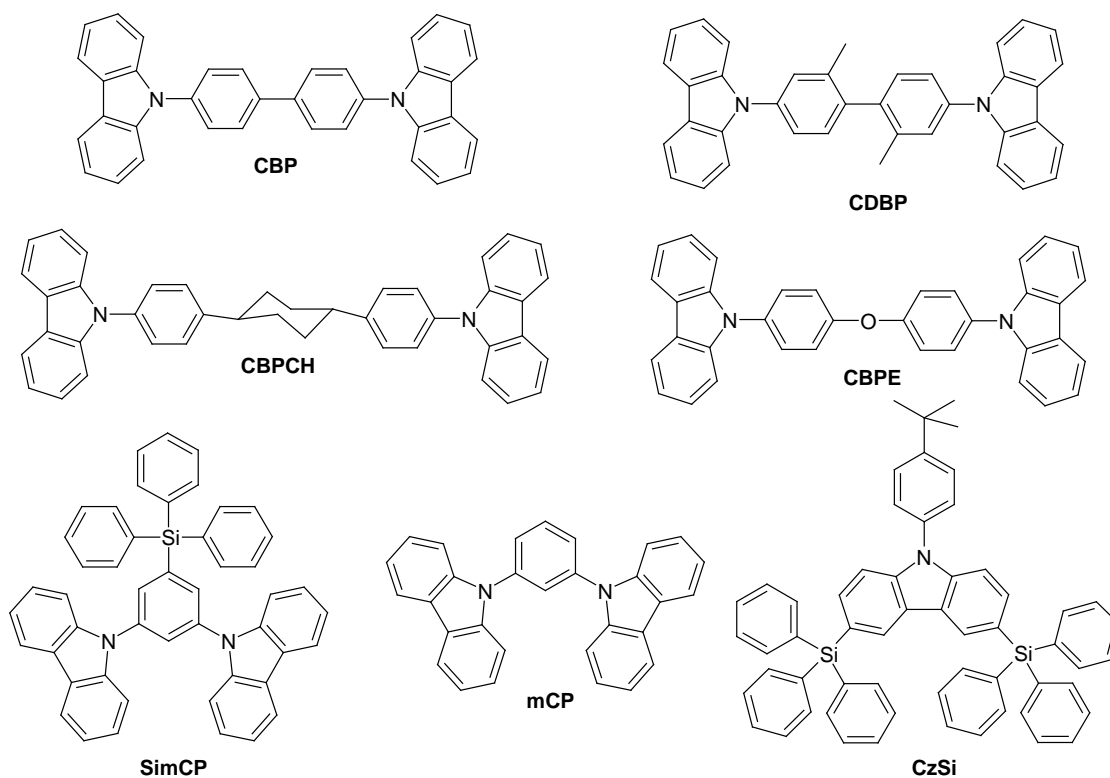


Figure 12. Molecular structures of carbazole based host materials. 4,4'-bis(carbazol-9-yl)biphenyl (**CBP**), 4,4'-bis(carbazol-9-yl)-2,2'-dimethyl-biphenyl (**CDBP**), bis(4-(carbazol-9-yl)cyclohexane (**CBPCH**), bis(4-(carbazol-9-yl)phenyl)ether (**CBPE**), 1,3-bis(carbazol-9-yl)-benzene (**mCP**), 3,5-di(*N*-carbazolyl)tetraphenylsilane (**SimCP**), 9-(4-*tert*-butylphenyl)-3,6-di(triphenylsilyl)-carbazole (**CzSi**).

The most commonly used host material is 4,4'-bis(9-carbazolyl)biphenyl (CBP) which is reported to have bipolar transport properties.⁶⁸ Basically, CBP is only suited as host for

red and green emitters because of its low triplet energy of 2.56 eV.⁶³ In green OLEDs based on Ir(ppy)₃ doped into CBP high power efficiencies up to 133 lm/W could be achieved.⁶⁹ Although, in combination with Flrpic ($\Delta E(T_1-S_0) = 2.65$ eV) endothermic energy transfer from CBP to Flrpic is partially possible, the efficiencies are unsatisfying.⁶³ Much effort has been made to design host materials with higher triplet energy in order to allow for exothermic energy transfer to blue emitters. One strategy to lower the conjugation within the molecule is the introduction of torsion shown in the host material 4,4'-bis(9-carbazolyl-2,2'-dimethylbiphenyl) (CDBP).^{70,71} The steric hindrance caused by methyl substituents in the 2- and 2'-positions of the biphenyl unit forces the two phenyl rings into a tilted conformation. As a result, the conjugation is limited. Due to the higher triplet energy of CDBP ($\Delta E(T_1-S_0) = 2.79$ eV), the external quantum efficiency in Flrpic-based OLEDs could be doubled from 5.1 % with CBP to 10.4 % with CDBP as host.⁷⁰ Another approach to lower the conjugation is to choose non-conjugated linkers between the two carbazole units such as a cyclohexyl group in CBPCH or an oxygen-bridge in CBPE.⁷² The high triplet energy of mCP ($E(T_1-S_0) = 2.90$ eV) is achieved by replacing the biphenyl unit by a single phenyl ring in combination with a *meta*-linkage of the carbazole units.^{73,74} In contrast to the high crystallisation tendency of mCP ($T_g = 55^\circ\text{C}$), the bulky triphenyl silyl groups render SimCP⁷⁵ and CzSi⁷⁶ morphologically stable host materials with high T_g s of 101°C and 131°C and high triplet energies of 3.01 eV and 3.02 eV, respectively. However, the separation of the conducting units by bulky substituents usually has detrimental effects on the charge carrier mobility.

Ideally, the host materials are able to perform both hole and electron transport to gain charge carrier balance within the emission layer. So-called bipolar host materials are usually tailored by combining electron rich with electron deficient moieties to provide suitable energy levels for the injection and transport of both charge carriers. Often used functionalities are carbazole units for the donor component and heterocycles or phosphine oxide groups as acceptor component. In such donor-acceptor type host molecules it is essential to suppress the electron delocalisation between donor and acceptor sites in the molecule in order to keep the optical band gap and the triplet energy at a high level. Some examples for bipolar host materials are shown in Figure 13.

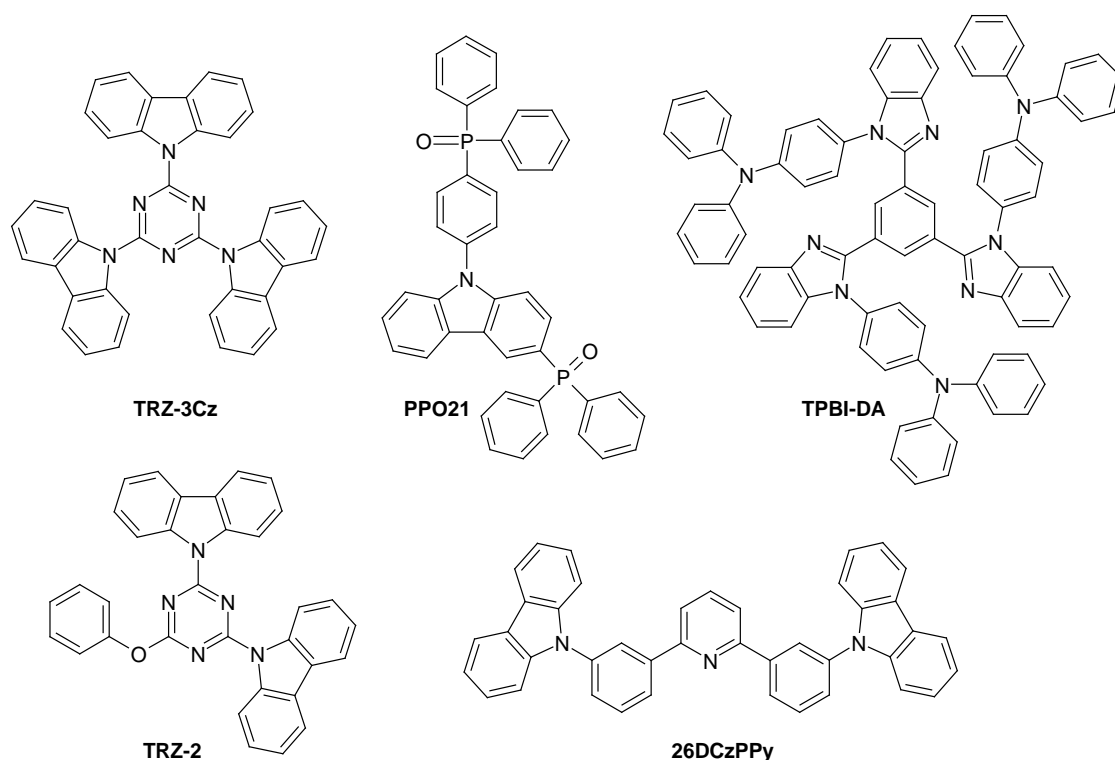


Figure 13. Molecular structures of the bipolar host materials 2,4,6-tricarbazol-9-yl-1,3,5-triazine (**TRZ-3Cz**), 3-(diphenylphosphoryl)-9-(4-(diphenylphosphoryl)phenyl)-9-carbazole (**PPO21**), 1,3,5-tris(N-(4-diphenylaminophenyl)benzimidazol-2-yl)benzene (**TPBI-DA**), 2,4-bis(carbazol-9-yl)-6-phenoxy-1,3,5-triazine (**TRZ-2**), 2,6-bis(3-(carbazol-9-yl)phenyl)pyridine (**26DCzPPy**).

The star-shaped TPBI-DA is a combination of the well-known electron transporting TPBI-core and diphenyl amine units.⁷⁷ Due to its triplet energy of 2.74 eV it is limited to the use as host for green phosphorescent emitters. In a simple OLED architecture based on the green emitter Ir(ppy)₂(acac) a high power efficiency of 70 lm/W was achieved compared to 21 lm/W for the control device using TPBI. The triplet energy of the donor substituted triazine host material TRZ-3Cz⁷⁸ of 2.81 eV can be further increased to 2.96 eV by replacing one carbazole unit by a phenoxy group in TRZ-2. In an OLED device with an emission layer comprising FIrpic:TRZ-2 an external quantum efficiency of 12 % was reported.⁷⁹ One of the highest efficiencies of FIrpic-based OLED devices up to now was achieved by using the bipolar host 26DCzPPy with pyridine and carbazole functionalities. At 100 cd/cm² an external quantum efficiency of 24 % and a power efficiency of 46 lm/W with only low efficiency roll-off at higher current densities were stated.⁸⁰ Among the phosphine oxide containing bipolar materials PPO21 proved to be

suites as host for even deeper blue phosphorescent emitters due to its high triplet energy of 3.01 eV. The OLED based on the deep blue emitter tris((3,5-difluoro-4-cyanophenyl)pyridine)iridium (FCNIr; CIE x 0.15, y 0.16; $E(T_1-S_0) = 2.80$ eV) gave more than 19 % external quantum efficiency.⁸¹

Besides carbazole-based and bipolar host materials the class of ultra high band gap host materials (UGH) was developed for the use in deep blue OLED devices.^{82,83} These UGH materials are often arylsilane-based and exhibit large optical energy gaps in the range of 3.8 eV and 4.4 eV and high triplet energies up to 3.5 eV. As a result, the excitation of the phosphorescent dopant takes place via direct charge trapping on the emitter. In Figure 14 some examples of UGH materials are shown.

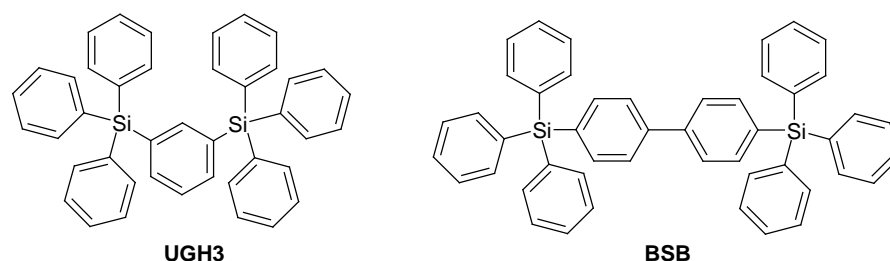
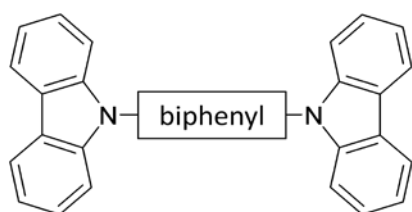


Figure 14. Molecular structures of ultra high band gap host materials (UGH). 1,3-bis(triphenylsilyl)benzene (**UGH3**), 4,4'-bis-triphenylsilyl-biphenyl (**BSB**).

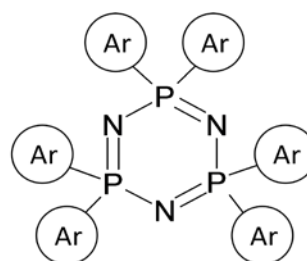
UGH3 has an undesirable low T_g of 46°C which can be increased to 100°C for the compound BSB⁸⁴ by insertion of a biphenyl unit. However, the triplet energy of BSB is concomitantly lowered to 2.8 eV compared to 3.5 eV for UGH3. An OLED device based on the blue phosphor bis(4,6-difluorophenylpyridinato)-4-(pyridin-2-yl)-1,2,3-triazolate iridium(III) (Flrpytz; CIE x 0.15, y 0.23, $E(T_1-S_0) = 2.70$ eV) gave a high external quantum efficiency of 19.3 %. However, in UGH materials the poor charge transporting properties due to the large energy band gap result in high drive voltages.

3 Aim of the Thesis

The development of highly efficient blue phosphorescent OLEDs is still one of the major obstacles which need to be overcome to realise OLED based lighting. Thus, stable blue host-emitter systems have to be found. The objective of this thesis is the synthesis and characterisation of novel host materials for blue phosphorescent emitters and their application in organic light-emitting diodes. In the design of the host material several aspects have to be taken into account: High thermal and morphological stability is essential to enable the fabrication by thermal evaporation and to ensure a long-term stability against crystallisation. Adequate energy levels help to reduce energetic barriers for charge carrier injection. Additionally, the host material should provide balanced transport of both types of charge carriers. A major focus, however, is set on the triplet energy of the host material which has to be higher compared to the emitter. Efficient energy transfer from the host to a blue phosphorescent emitter requires a triplet energy of the host of at least 2.8 eV. Therefore, the conjugation within the molecules has to be confined. Several approaches to high triplet energies are subject of this thesis. Novel host materials based on two classes of materials are considered in this thesis: the well-known class of carbazoles and the new class of low molecular weight cyclic phosphazenes. To gain a comprehensive understanding of structure-property relations with regard to thermal behaviour, optical and electronic properties the series of different host materials have to be thoroughly characterised. By incorporating the host materials in organic light-emitting devices their potential as host materials for saturated blue phosphorescent emitters is investigated.



Carbazole-based Host Materials



Phosphazene-based Host Materials

Figure 15. The two different classes of host materials with high triplet energies $\Delta E(T_1-S_0)$ described in the thesis. **Left:** Carbazole-based materials with different linker groups. **Right:** Cyclic phosphazenes with six aromatic substituents (Ar).

4 Overview of the Thesis

The thesis includes four publications. Three of them are presented in chapters 6 to 8 and one appears as appendix in chapter 9. Two publications have already been published, one is submitted to *Advanced Functional Materials* and one is intended for submission to *Chemistry of Materials*.

All chapters deal with the synthesis and characterisation of host materials for blue phosphorescent emitters and their application in organic light-emitting diodes (OLEDs). To be considered suitable as host for blue phosphorescent emitters the material has to fulfil several requirements. Thus, in the design of all new host materials the following aims were pursued: the most crucial requirement for the host materials is the triplet energy higher compared to that of the emitter. In the case of blue phosphorescent emitters the triplet energy of the host needs to be at least 2.8 eV. Moreover, the host materials should reveal morphological stability to ensure homogeneous mixing of the emitter in the matrix and to prevent grain boundaries which may act as trap states. In the course of this thesis novel host materials of two different classes, carbazole and phosphazene based materials, have been developed. The central point leading through the thesis is the extension of the triplet energy by confinement of conjugation. On the one hand, high triplet energy host materials based on carbazole were achieved either by introducing torsion in the molecular structure or by choosing a meta-linkage of the building blocks. On the other hand, in the phosphazene-based host materials a non-conjugated type of linkage of the substituents to the central phosphazene ring leads to high triplet energies.

All synthesised materials were thoroughly characterised by standard techniques. The triplet energies of the host materials were determined by low temperature emission spectroscopy. In addition, the electrochemical properties of the compounds were investigated by cyclic voltammetry (CV) or ultra-violet photoelectron spectroscopy (UPS). The thermal behaviour was characterised by thermogravimetric analysis (TGA) and differential scanning calorimetry (DSC). Additionally, computational calculations of

the electronic levels were carried out to facilitate the interpretation of experimental results. In devices the OLED performance of most of the materials could be tested.

Carbazole is an often used building block in the design of host materials due to its high triplet energy of 3 eV. During my thesis two series of carbazole-based host materials were synthesised. Both series comprise derivatives of the well-known host material 4,4'-bis(carbazol-9-yl)-2,2'-biphenyl (CBP). In the first approach described in chapter 6 the molecular structure of the parent CBP was modified with the aim to attain the desired properties. By applying a systematic variation of the substitution pattern a series of amorphous CBP-derivatives with high triplet energies was obtained. The synthesis of the CBP-derivatives was accomplished by Ullmann-coupling reactions of the (un)substituted carbazole units with the 4,4'-diiodobiphenyl units with either methyl or trifluoromethyl groups in the 2- and 2'-position. The steric hindrance due to the substitution of the central biphenyl introduces torsion, thus, leading to confined conjugation and high triplet energies of over 2.9 eV. By methyl substitution of the carbazole units electrochemical stability against oxidation could be demonstrated. Furthermore, the HOMO level of the compounds can be fine-tuned by methyl substitution on the carbazole moieties. A detailed study of the photo physical properties of the series of twisted CBP-derivatives is provided in chapter 9.

In the second approach the basic structure of CBP was optimised by choosing a different type of linkage. Contrary to the *para*-linked CBP, in the novel derivatives the carbazole units were linked to the central biphenyl unit at the 3- and 3'-positions. This *meta*-linkage in combination with a selective methyl substitution leads to a series of materials with high triplet energies and high glass transition temperatures. The synthesis was done in analogy to the previous series of CBP-derivatives. The design principle of introducing torsion from the first approach described in chapter 6 was also adopted, however, no further increase in triplet energy was observed. A publication dealing with the *meta*-linked CBP-derivatives can be found in chapter 7.

Besides the carbazole-based host materials, another class of host materials with confined conjugation was investigated. Phosphazene-based host materials for blue phosphorescent OLEDs are scarcely described in literature. By attaching substituted

phenyl rings to the central phosphazene ring materials with very high triplet energies were obtained. The substituents were either linked by phosphorous-oxygen bonds to yield phenoxy substituted derivatives or by phosphorus-carbon bonds to yield phenyl substituted derivatives. Due to the non-conjugated linkage to the cyclic phosphazene ring the conjugation within the molecules is extremely confined. The phenoxy substituted cyclic phosphazenes were synthesised by nucleophilic substitution of chlorine atoms in hexachlorocyclotriphosphazene with phenolate groups while the phenyl substituted cyclic phosphazenes were formed in a cyclocondensation reaction of three equivalents of substituted phosphinic amides. The phenyl substituted cyclic phosphazenes have superior thermal properties compared to the phenoxy substituted derivatives. The detailed results of the phosphazene-based host materials are described in chapter 8.

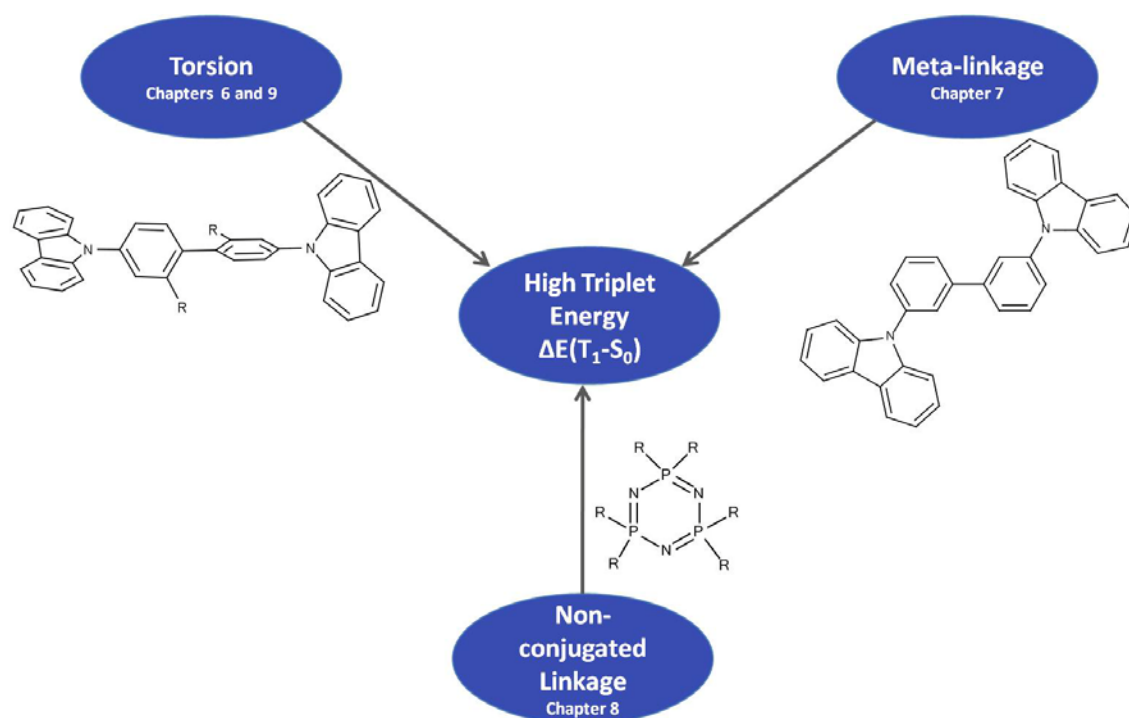


Figure 16. Different synthetic approaches to host materials with high triplet energy $\Delta E(T_1-S_0)$.

In the following the key results of the individual publications are summarised. Detailed descriptions of the synthesis and characterisation of the different classes of host materials are provided in the respective chapters.

4.1 High triplet energy host materials by introducing torsion (Chapters 6 and 9)

In chapter 6 the synthesis and characterisation of six CBP-based host materials with twisted molecular structure is presented. By a systematic variation of the substitution pattern the structure-property relations are investigated. The motivation was to modify the molecular structure and properties of the well-known host material 4,4'-bis(carbazol-9-yl)-2,2'-biphenyl (CBP). Since CBP is a crystalline material we tried to modify the thermal properties of the new host materials. In addition, the low triplet energy limits the use of CBP as host for blue phosphorescent emitters. In order to increase the triplet energy the conjugation of the basic CBP-structure was decreased by introducing torsion. By attaching methyl or trifluoromethyl groups in the 2- and 2'-positions of the central biphenyl unit twisted molecular structures are obtained. In Figure 17 the chemical structures of CBP and the twisted CBP-derivatives CDBP and **7-11** are shown. The numbers of the molecules refer to the numbers in the publication.

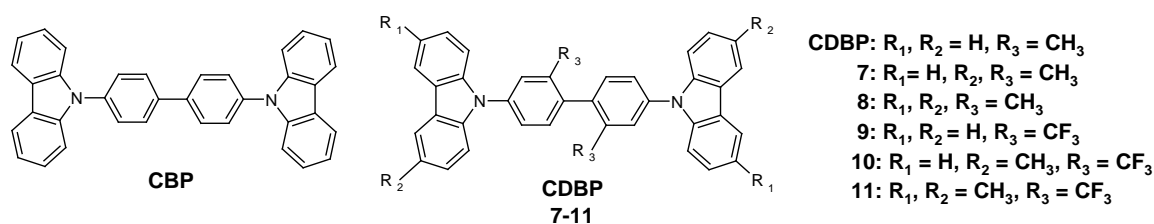


Figure 17. Chemical structures of CBP and the twisted CBP-derivatives CDBP and **7-11**.

The synthesis was carried out by Ullmann-condensation of the 2,2'-methyl or 2,2'-trifluoromethyl substituted 4,4'-diiodobiphenyl units and carbazole units with optional methyl substitution at the 3- and 6-positions. In contrast to the crystalline parent compound CBP, the host materials reveal amorphous behaviour as shown in the DSC traces in Figure 18. By introducing methyl or trifluoromethyl substituents in the 2- and 2'-positions of the biphenyl unit the tendency to form molecular glasses is increased. With increasing methyl substitution at the outer carbazole units high glass transition temperatures up to 121° were obtained.

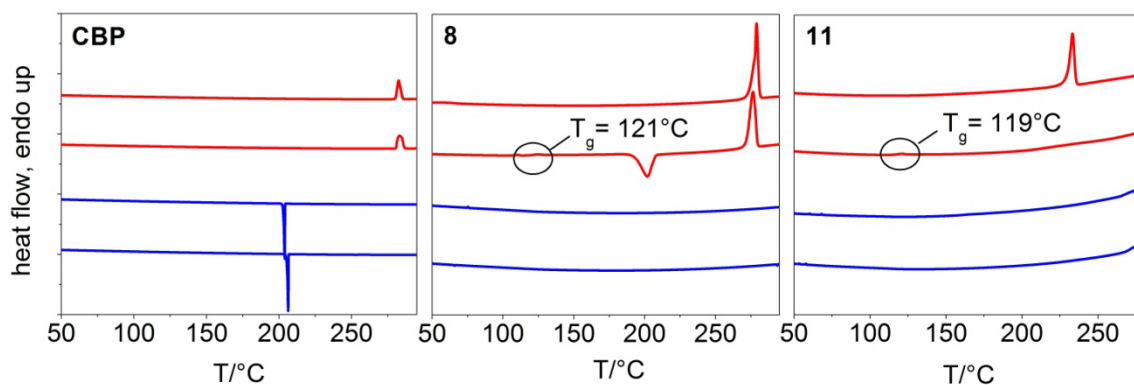


Figure 18. DSC traces of crystalline CBP and the amorphous host materials with methyl (**8**) and trifluoromethyl (**11**) substituents in the 2- and 2'-position of the central biphenyl, respectively. Shown are the first and second heating (red) and cooling (blue) traces at a scan rate 10 K min^{-1} .

The torsion angles obtained by DFT-calculations increases from 33° for the unsubstituted CBP to 82° and 73° for the twisted CH_3 - and CF_3 -substituted derivatives **8** and **11**. Thus, the conjugation is effectively limited. This translates into higher triplet energies which can be extracted from the highest energy peak of low temperature emission spectra shown in Figure 19a.

In a more detailed spectroscopic study (chapter 9) it was found that the monomeric phosphorescence in pure films is superimposed by triplet excimer emission centred at around 2.5-2.6 eV (cf. Figure 19 b and c). This unstructured emission from a sandwich-type carbazole excimer has a much longer radiative lifetime for the more polar CF_3 -substituted series than for the CH_3 -substituted series. Additionally, it was shown that the fluorescence of the polar CF_3 -substituted series is of charge-transfer character causing the observed unstructured and red-shifted fluorescence spectra compared to the CH_3 -substituted series. These findings were supported by DFT-calculations (cf. Figure 19 d and e).

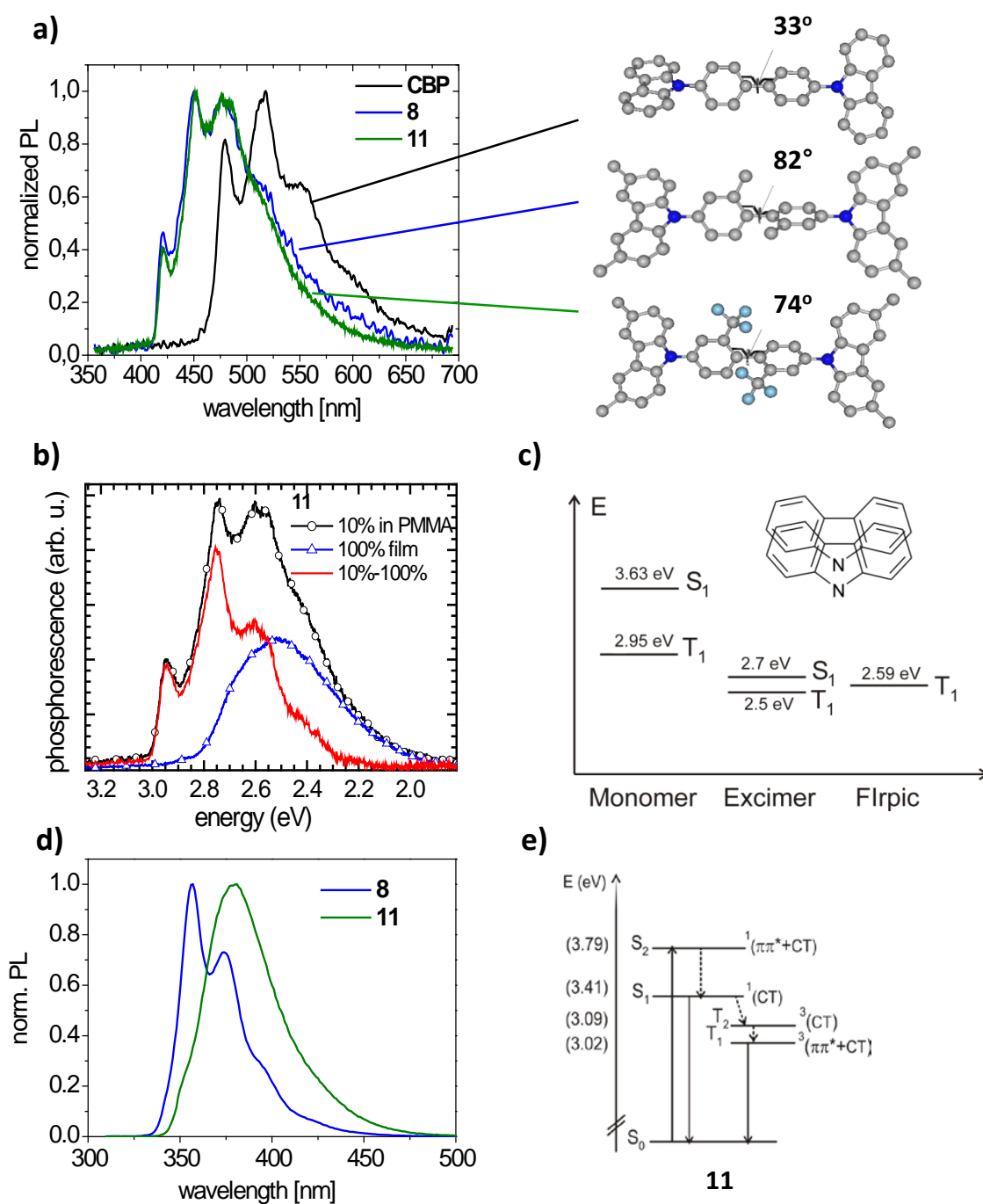


Figure 19. a) Phosphorescence spectra of **CBP**, **8** and **11** in a 10 wt.-% solid solution of PMMA (exc. 355 nm, 10 K), also shown are the geometry optimised molecular structures of the compounds with the torsion angles. b) Phosphorescence of **11** in a pure film (blue), in 10 wt.-% solid solution in PMMA (black) and the difference spectrum (red). c) Energy diagram illustrating the singlet and triplet energy levels for the carbazole monomer, the sandwich-type carbazole excimer and of the emitter Flrpic. d) Fluorescence spectra of **8** and **11** (in cyclohexane, exc. 300 nm). e) Scheme of singlet and triplet energy levels based on DFT-calculations illustrating the charge-transfer character of the fluorescence of **11**. The predominant nature of transition is denoted by charge transfer (CT) or ππ* next to the energy levels.

In addition, by varying the substitution pattern to lower the energy barriers within a device the energy levels can be fine-tuned and adjusted to the neighbouring layer. The effects on electronic properties are summarised in Figure 20. By introducing the electron withdrawing CF_3 -substituents the HOMO level of **9** can be lowered by 0.1 eV compared to the CH_3 -analogue **CDBP**. Another trend to be observed is the increase of the HOMO level with increasing amount of methyl substitution at the carbazole units along the series **CDBP**, **7** to **8** as well as **9**, **10** to **11**. Moreover, the methyl substitution at the electroactive 3- and 6-positions of the carbazole unit prevents dimerisation reactions of oxidized radical cationic states, thus, leading to host materials which are electrochemically stable against oxidation in cyclic voltammetry measurements.

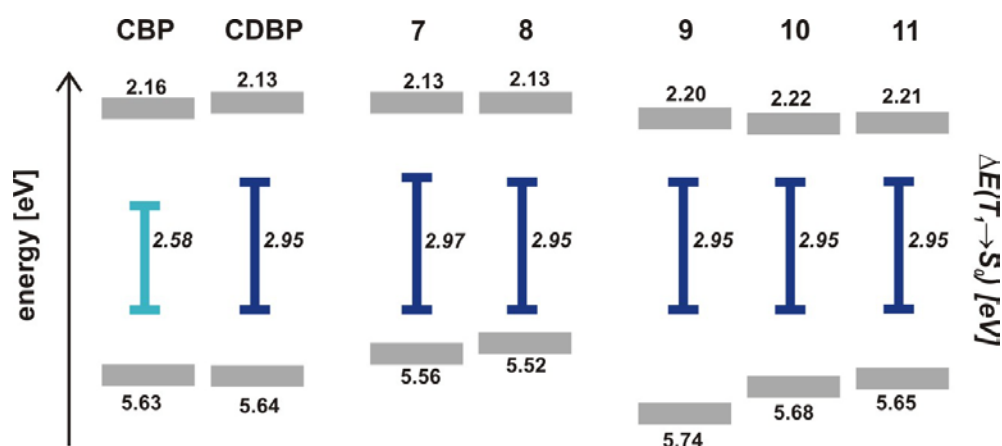


Figure 20. Energy diagram showing the location of the HOMO and LUMO levels of CBP and the twisted CBP-derivatives. The triplet energy of each compound is illustrated as coloured bar.

These results show that the thermal, optical and electronic properties of CBP can be optimised by applying a systematic variation of the substitution pattern of CBP in the 2- and 2'-position of the biphenyl unit and at the 3- and 6-position of the carbazole moieties. In an OLED device (setup: ITO//hole injection layer: PEDOT:PSS//hole transport layer: 35 nm MoO_3 -doped DPBIC//20 nm DPBIC//emission layer: 40 nm **8** doped with 20 % light blue emitter//hole and exciton blocking layer: 2,6-dicarbazolyl-1,5-pyridine (PYD2)⁸⁵//electron transport layer: 50 nm Alq_3 //LiF//100 nm Al) a peak external quantum efficiency of 14.7 % and a high brightness of 61000 cd/m^2 could be achieved. At 1000 cd/m^2 the external quantum efficiency of 14.4 % is still very high.

4.2 High triplet energy host materials by *meta*-linkage (Chapter 7)

This chapter also deals with the synthesis and characterisation of CBP-derivatives. Contrary to the previously presented CBP-derivatives, here the series of CBP-derivatives is characterised by a *meta*-linkage of the carbazole units to the central biphenyl unit which is either unsubstituted (**1** and **2**) or additionally twisted by methyl substituents in the 2- and 2'-positions (**3** and **4**).

Similar to the *para*-linked CBP-derivatives described in chapter 6 the synthesis was carried out by Ullmann-condensation (cf. Figure 21). The dihalogenated biphenyl units were either synthesised in a copper mediated homocoupling of 3-bromo-phenylboronic acid or by iodination of 2,2'-dimethylbiphenyl. This direct iodination of the biphenyl unit with iodine and iodic acid is a specific feature of the synthesis. It yields 5,5'-diiodo-2,2'-dimethylbiphenyl – a simple and versatile building block for the synthesis of molecules with confined conjugation which to the best of our knowledge has not been described in literature before.

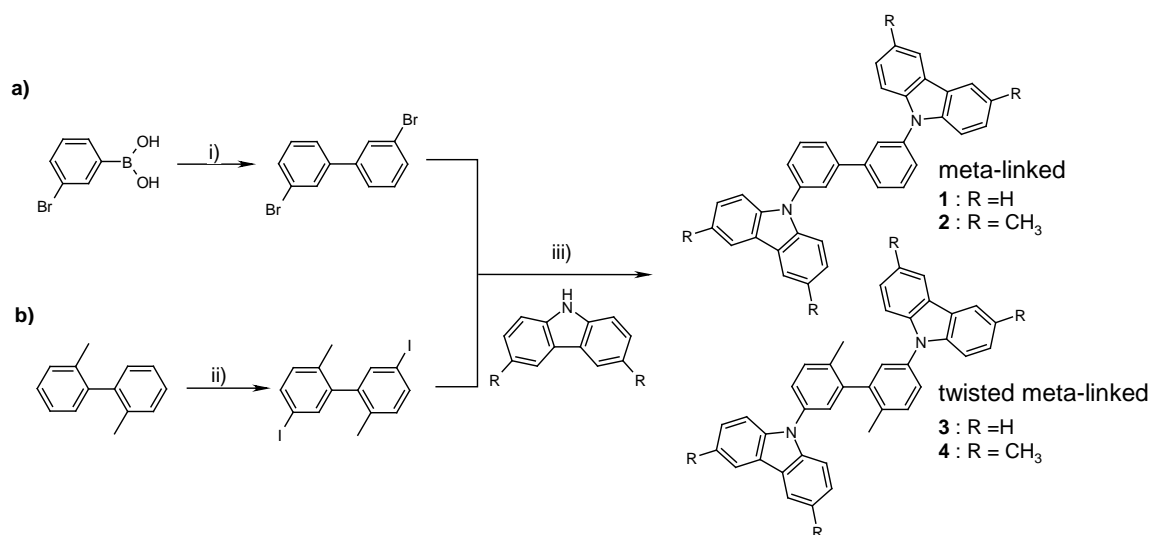


Figure 21. Synthetic routes to **a)** *meta*-linked CBP-derivatives **1** and **2** and **b)** twisted *meta*-linked CBP-derivatives **3** and **4**. Reagents and conditions: i) Cu(OAc)₂, DMF, 100°C, 90 min; ii) I₂, HIO₃, H₂SO₄, H₂O, CCl₄, acetic acid, 80°C, 4 h; iii) Cu, K₂CO₃, 18-crown-6, *o*-dichlorobenzene, reflux, 24 h.

All *meta*-linked CBP-derivatives **1-4** are thermally stable up to at least 315°C. While compound **1** shows crystalline behaviour in the DSC experiment, the introduction of

methyl groups at the carbazole and/or the biphenyl renders **2-4** amorphous materials with the highest T_g of 120°C for derivative **4**.

In the optical analysis the two pairs **1** and **3** and **2** and **4** show very similar absorption and fluorescence spectra since the carbazole chromophore in **1** and **3** and in **2** and **4** are identical. Due to the additional methyl substitution at the 3- and 6-position of the carbazole units the spectra of **2** and **4** are bathochromically shifted by ca. 13 nm compared to **1** and **3**. The *meta*-linkage of the two carbazole units to the biphenyl unit provides effective reduction of conjugation as evident by comparing the triplet energies of CBP, **1** and **3** in Figure 22.

Compared to the *para*-linked CBP, the highest energy peak of the *meta*-linked derivative **1** is considerably blue shifted by 65 nm, which corresponds to an increase of triplet energy of 2.58 eV for CBP to 2.98 eV for **1**. Yet, the additionally introduced torsion into the molecular structure as in **3** does not increase the triplet energy any further.

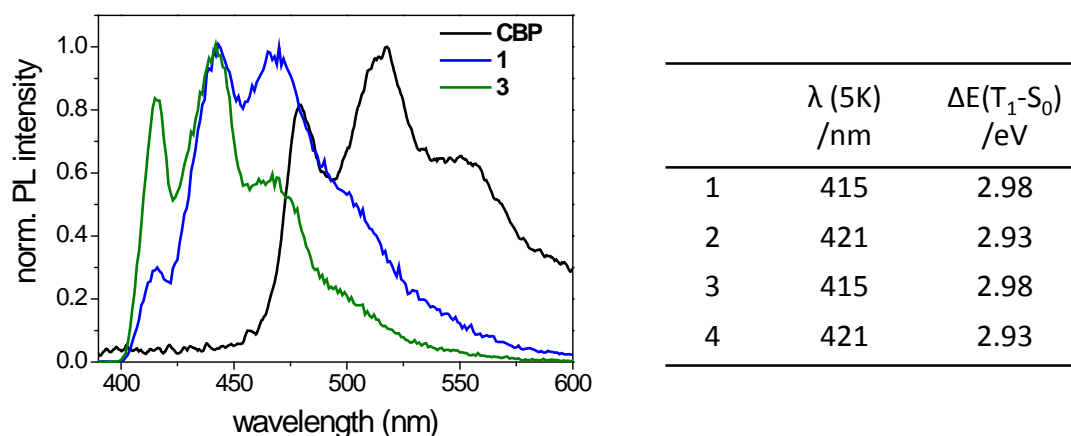


Figure 22. Left: Phosphorescence spectra of the *para*-linked CBP, the *meta*-linked derivative **1** and the twisted *meta*-linked derivative **3** in a 10 wt.-% solid solution of PMMA (exc. 355 nm, 10 K). Right: Triplet energies of the *meta*-linked derivatives **1-4**.

The electrochemical behaviour was investigated by cyclic voltammetry. As already observed in the previous series of carbazole based host materials, methyl protection at the electroactive 3- and 6-positions of carbazole renders the material **2** and **4** stable against oxidation in cyclic voltammetry.

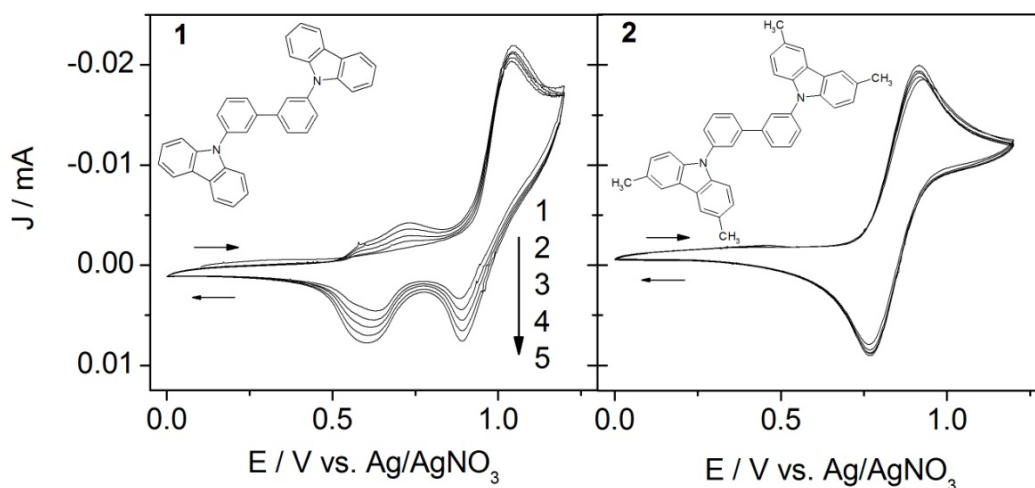


Figure 23. Cyclic voltammograms of **1** and **2** with methyl protection in the electroactive 3- and 6-positions of the carbazole units (five scans, scan rate 50 mV/sec, $2 \cdot 10^{-3}$ M in CH_2Cl_2).

To demonstrate the potential of the *meta*-linked CBP-derivatives OLEDs were fabricated with **1-4** as host materials for the blue phosphorescent emitter Ir(dbfmi). The optimised device structure and the obtained external quantum efficiencies versus luminance are shown in Figure 24 (for molecular structures see chapter 7). A mixed matrix system was chosen to facilitate hole injection from the hole transporting layer DPBIC. The emission layer consists of the hosts **1-4** : DPBIC : Ir(dbfmi) in a ratio of 75 : 20 : 5. Saturated blue emission was obtained with CIE-coordinates of $x = 0.16$ and $y = 0.18$. The host materials **2** and **4** gave significantly lower external quantum efficiencies compared with **1** and **3**. Since the devices employing **2** and **4** with methyl groups at the carbazole units need higher operation voltages compared to **1** and **3** with unsubstituted carbazole units worse transport properties for **2** and **4** are assumed. The highest efficiency was achieved in the case of **3** with an external quantum efficiency of 8.7% and a power efficiency of 10.2 lm W^{-1} (at 100 cd m^{-2}) and 6.1% and 6.0 lm W^{-1} (at 1000 cd m^{-2}), respectively.

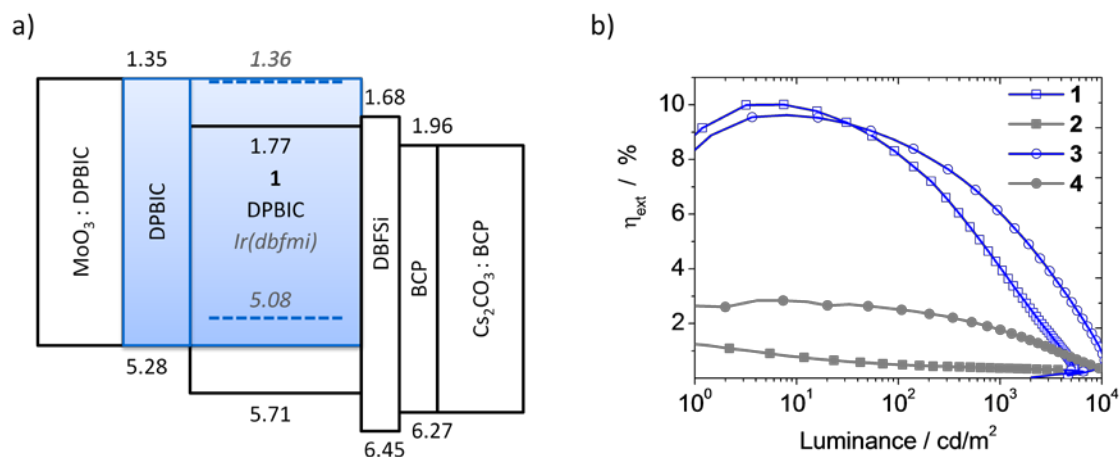


Figure 24. **Left:** Energy level diagram of the OLED device employing **1** as host for Ir(dbfmi); Ionisation potentials and electron affinities are indicated. The dotted lines represent the levels of the emitter Ir(dbfmi). **Right:** External quantum efficiency-luminance characteristics of the devices with **1-4** as host material for Ir(dbfmi).

In summary, the *meta*-linkage is an effective concept in designing host materials with high triplet energy. By selective methyl substitution the thermal properties could be improved.

4.3 High triplet energy host materials by non-conjugated linkage (Chapter 8)

Another approach to host materials with high triplet energy is realised in the class of phosphazenes. Here, especially the cyclotriphosphazenes are considered comprising a six-membered ring of alternating phosphorous and nitrogen atoms with alternating double bonds. Each phosphorous atom bears two substituents, in this case (un)substituted phenyl rings, which are attached via a non-conjugated type of linkage. Two sets of materials were synthesised: in the phenoxy substituted derivatives **OP1-OP3** the substituents are attached via phosphorous-oxygen bonds whereas in the phenyl substituted derivatives **CP1-CP3** phosphorous-carbon bonds are formed (cf. Figure 25).

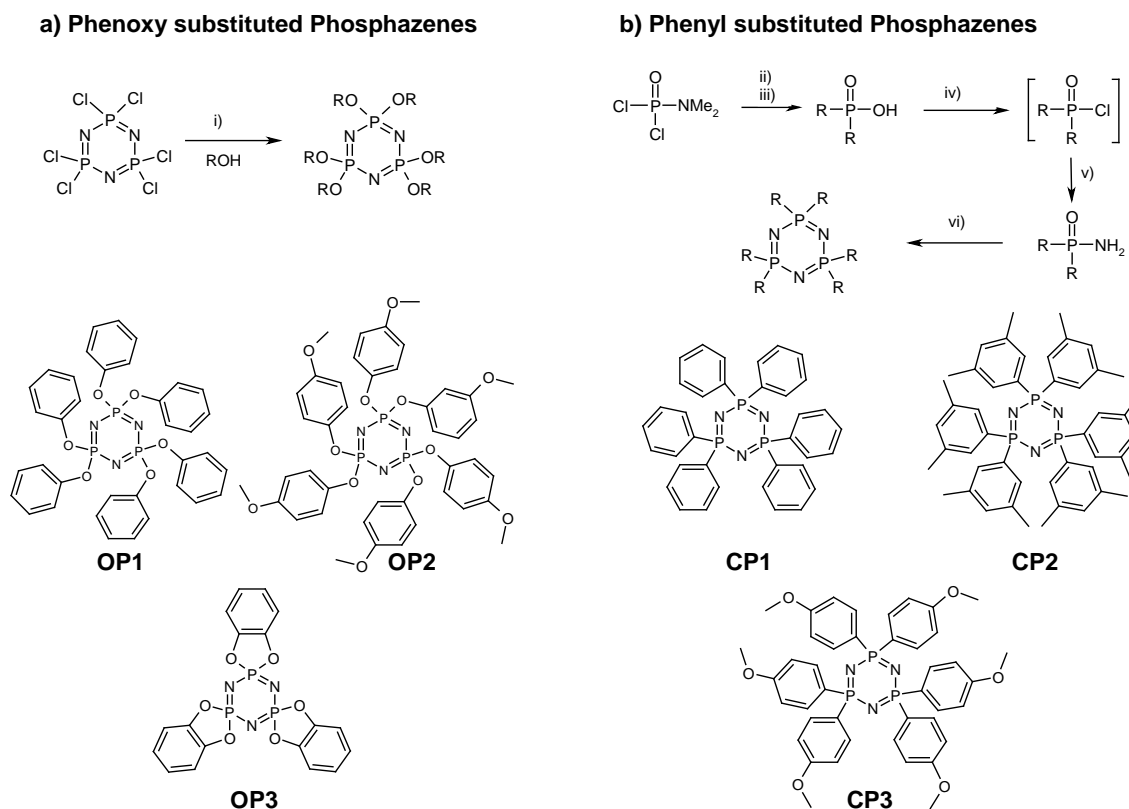


Figure 25. Synthesis and chemical structures of **a)** phenoxy substituted cyclic phosphazenes **OP1-OP3** and **b)** phenyl substituted cyclic phosphazenes **CP1-CP3**. Reagents and conditions: i) NaH, abs. THF, 70°C, 48 h (catechol: RT, 24 h); i) MgRBr, abs. THF, RT, 2 h; ii) conc. HCl, 80°C, 1 h; iii) thionyl chloride, abs. toluene, 55°C, 20 min; iv) NH₃ (g), 0°C, 10 min; v) PPh₃, CCl₄, NEt₃, benzene, dichloromethane, 40°C, 5 - 22 h.

The phenoxy substituted cyclic phosphazenes were prepared by nucleophilic substitution of the six chlorine atoms in hexachlorocyclotriphosphazene with different phenolates as nucleophiles while the phenyl substituted cyclic phosphazenes were formed in a cyclocondensation reaction of three equivalents of substituted phosphinic amides.

In the thermal analysis the higher mobility due to the phosphorous-oxygen linkage causes much lower transition temperatures for the phenoxy substituted than for the phenyl substituted phosphazenes. For example, **OP1** already melts at 116°C. Due to the low T_g s of -12°C and 1°C, films of **OP1** and **OP2** readily crystallise. Using the bifunctional alcohol catechol introduces more rigidity reflected in the higher melting temperature of 251°C for **OP3**. However, **OP3** does not sublime without decomposition. Thus, the phenoxy substituted cyclic phosphazenes are less suited as host materials due to their

thermal properties. In contrast, the phenyl substituted phosphazenes **CP1-CP3** show good thermal stability. Despite their crystalline behaviour in the DSC measurements amorphous films of **CP1-CP3** can be prepared that are morphologically stable for months.

Since the substituents are attached above and below the central ring plane conjugation across the phosphazene ring is prevented. Thus, the host materials reveal very high optical band gaps of more than 4.2 eV and as well very high triplet energies of more than 3.2 eV (see Figure 26).

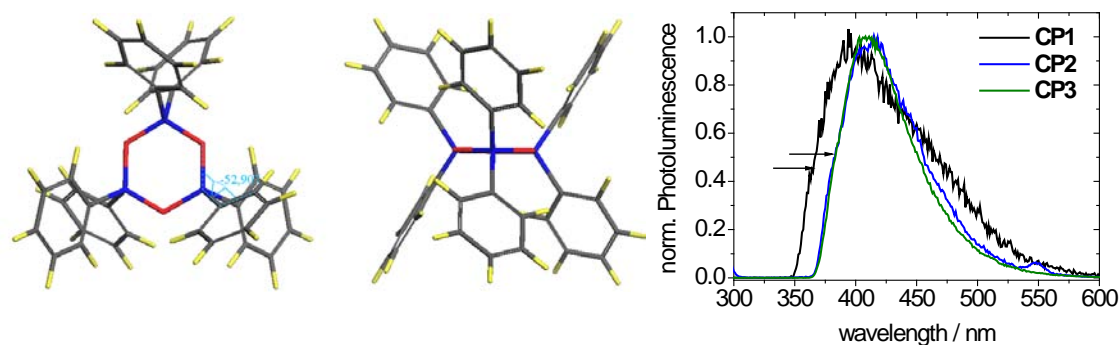


Figure 26. Left: Geometry optimised structure of **CP1**. Right: phosphorescence spectra of **CP1-CP3** (neat films, 5 K); the arrows indicate the small shoulders in the emission spectra taken for the determination of the triplet energy of the compounds.

CP2 shows balanced transport properties for holes and electrons in single carrier devices. In an OLED with the saturated blue emitter Ir(dbmfi) ($\Delta E(T_1-S_0) = 2.75$ eV) a peak luminance of 5000 cd/m^2 was reached at 13.5 V. At 100 cd m^{-2} and 1000 cd m^{-2} the power efficiencies are 4.9 lm W^{-1} and 2.3 lm W^{-1} , respectively.

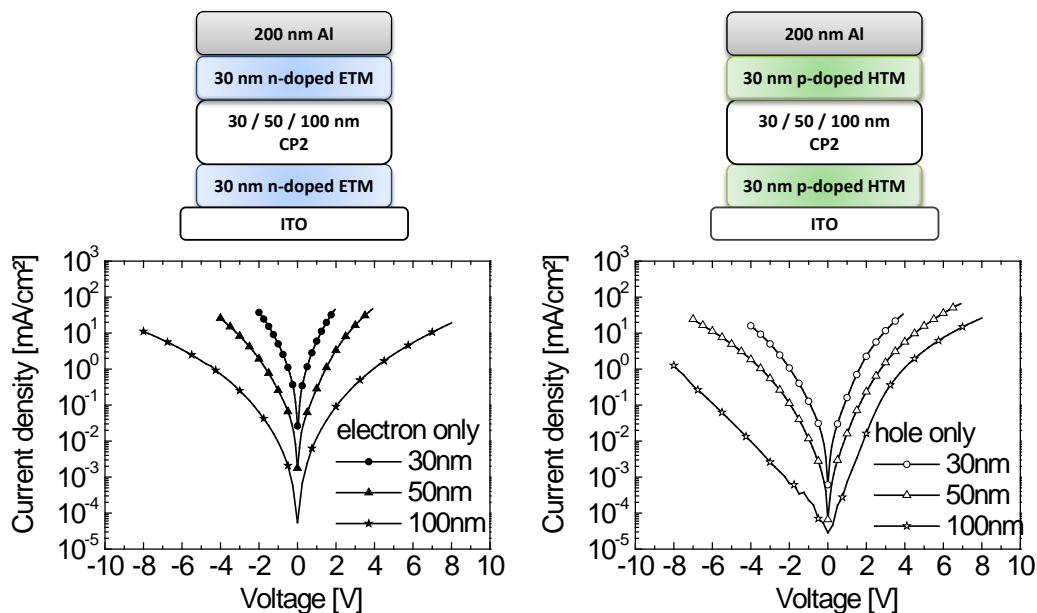


Figure 27. JV-characteristics of CP2 in e-only device (**left**) and h-only device (**right**).

To summarise, phosphazene-based host materials with high triplet energies can be achieved by non-conjugated linkage of the substituents to the central phosphazene ring. It was shown that the phosphazene materials with phenyl substitution have superior properties compared to the materials with phenoxy substitution.

Patent application

In addition to the four publications presented in chapters 6 to 9, one patent was filed during the period of the thesis. The patent (WO 2009153276 A1)¹ was published on December 23, 2009 and deals with “Cyclic phosphazene compounds and the use thereof in organic light-emitting diodes”.

¹ Inventors: Evelyn Fuchs (BASF SE), Oliver Molt (BASF SE), Nicolle Langer (BASF SE), Christian Lennartz (BASF SE), Peter Strohriegl (Universität Bayreuth), Pamela Schrögel (Universität Bayreuth), Applicant: BASF SE.

Individual contributions to joint publications

In the following, the contributions of the individual authors to the papers are specified.

Chapter 6

This work is published in *Journal of Materials Chemistry* (**2011**, 21, 2266) with the title:

“A Series of CBP-Derivatives as Host Materials for Blue Phosphorescent Organic Light-Emitting Diodes”

by **Pamela Schrögel**, Aušra Tomkevičienė, Peter Strohrriegl, Sebastian T. Hoffmann, Anna Köhler and Christian Lennartz.

I synthesised most of the materials for this publication. I characterised all materials, investigated the thermal, optical and electrochemical properties and I wrote the publication.

Aušra Tomkevičienė helped with the synthesis of some of the host materials. Sebastian Hoffmann carried out the low temperature time-gated spectroscopy. Christian Lennartz did the computational calculations. Anna Köhler and Peter Strohrriegl supervised the project and corrected the manuscript.

Chapter 7

This work is accepted by *Organic Electronics* with the title:

“Meta-linked CBP-derivatives As Host Materials For A Blue Iridium Carbene Complex”

by **Pamela Schrögel**, Nicolle Langer, Christian Schildknecht, Gerhard Wagenblast, Christian Lennartz and Peter Strohrriegl.

I synthesized three of the host materials and Nicolle Langer provided one host material for this publication. I characterised all materials, investigated the thermal, optical and electrochemical properties and I wrote the publication.

Gerhard Wagenblast was responsible for the low temperature time-gated spectroscopy. Christian Schildknecht fabricated the OLED devices and Christian Lennartz carried out computational calculations. Peter Strohriegl supervised the project and corrected the manuscript.

Chapter 8

This work is submitted to *Chemistry of Materials* with the title:

“Phosphazene-based Host Materials for the Use in Blue Phosphorescent OLEDs”

by **Pamela Schrögel**, Matthias Hoping, Wolfgang Kowalsky, Arvid Hunze, Herbert Börner, Gerhard Wagenblast, Christian Lennartz and Peter Strohriegl.

I synthesised and characterised all materials for this publication. I investigated the thermal and optical properties and I wrote the publication.

Matthias Hoping fabricated the OLED devices, Arvid Hunze fabricated the single carrier devices and Herbert Börner carried out the ultra-violet photoelectron spectroscopy. Gerhard Wagenblast was responsible for the low temperature time-gated spectroscopy and Christian Lennartz did the computational calculations. Wolfgang Kowalsky and Peter Strohriegl supervised the project and corrected the manuscript.

Chapter 9: Appendix

This work is published in *Journal of Physical Chemistry B* (**2011**, 115, 414) with the title:

“Triplet Excimer Emission in a Series of 4,4’-bis(N-carbazolyl)-2,2’-biphenyl Derivatives”

by Sebastian T. Hoffmann, **Pamela Schrögel**, Michael Rothmann, Rodrigo Albuquerque, Peter Strohriegl and Anna Köhler.

This work appears as appendix since the major work concerning optical spectroscopy was carried out by Sebastian Hoffmann. Sebastian Hoffmann wrote the publication.

I synthesised the materials which were investigated in this study. I was involved in scientific discussion and corrected the manuscript. Rodrigo Albuquerque assisted in the computational calculations and Michael Rothmann was involved in scientific discussions. Peter Strohriegl and Anna Köhler supervised the project and corrected the manuscript.

5 References

- 1 J. Johnson, *Chem. Eng. News* **2007**, 85 (49), 46.
- 2 EU Commission Regulation (EC) No 244/2009 of 18 March 2009: Ecodesign requirements for non-directional household lamps.
- 3 http://www.osram.com/osram_com/News/Business_Financial_Press/2010/101001_OLED.html (date: March 08, 2011)
- 4 <http://ge.geglobalresearch.com/blog/a-glimpse-into-the-future-of-lighting/> (date: March 08, 2011)
- 5 J. Kido, K. Hongawa, K. Okuyama, K. Nagai, *Appl. Phys. Lett.* **1994**, 64, 815.
- 6 http://www.osram.com/osram_com/LED/OLED_Lighting/ORBEOS_Products/index.html (date: March 08, 2011)
- 7 http://www.osram.com/osram_com/LED/OLED_Lighting/index.html (date: March 08, 2011)
- 8 http://www.newscenter.philips.com/de_de/standard/news/lighting/20100716_LumibladeCreativeLab_fuer_OLED-Beleuchtungstechnologie.wpd (date: March 08, 2011)
- 9 S. Reineke, F. Linder, G. Schwartz, N. Seidler, K. Walzer, B. Lüssem, K. Leo, *Nature* **2009**, 459, 234.
- 10 W. Brütting, in: *Physics of Organic Semiconductors*, W. Brütting (Ed.), Wiley-VCH Verlag, Weinheim, **2005**.
- 11 D. Hertel, H. Bässler, in: *Organic Light-Emitting Devices*, K. Müllen (Ed.), U. Scherf (Ed.), Wiley-VCH Verlag, Weinheim, **2006**.
- 12 A. Köhler, H. Bässler, *Mater. Sci. Eng. R* **2009**, 66, 71.
- 13 M. Sauer (Ed.), J. Hofkens (Ed.), J. Enderlein (Ed.), *Handbook of Fluorescence Spectroscopy and Imaging*, Wiley-VCH Verlag, Weinheim, **2011**.
- 14 M. Pope, H. P. Kallmann, P. Magnante, *J. Chem. Phys.* **1963**, 38, 2042.
- 15 J. H. Burroughes, D. D. C. Bradley, A. R. Brown, R. N. Marks, K. Mackay, R. H. Friend, P. L. Burns, A. B. Holmes, *Nature* **1990**, 347, 539.
- 16 S. L. M. van Mensfoort, V. Shabro, R. J. de Vries, R. A. J. Janssen, R. Coehoorn, *J. Appl. Phys.* **2010**, 107, 113710.

- 17 Nüesch, L. J. Rothberg, E. W. Forsythe, Q. T. Le, Y. Gao, *Appl. Phys. Lett.* **1999**, *74*, 880.
- 18 I. G. Hill, A. Kahn, *J. Appl. Phys.* **1998**, *84*, 5583.
- 19 T.M. Brown, J.S. Kim, R.H. Friend, F. Cacialli, R. Daik, W.J. Feast F., *Synth. Met.* **2000**, *111-112*, 285.
- 20 M. Stößel, J. Staudigel, F. Steuber, J. Blässing , J. Simmerer, A. Winnacker, H. Neuner, D. Metzdorf, H.-H. Johannes, W. Kowalsky, *Synth. Met.* **2000**, *111-112*, 19.
- 21 G. Parthasarathy, C. Shen, A. Kahn, S. R. Forrest, *J. Appl. Phys.* **2001**, *89*, 4986.
- 22 L. S. Hung, C. W. Tang, M. G. Mason, *Appl. Phys. Lett.* **1997**, *70*, 152.
- 23 M. Pfeiffer, S. R. Forrest, K. Leo, M. E. Thompson, *Adv. Mater.* **2002**, *14*, 1633.
- 24 M. Pfeiffer, K. Leo, X. Zhou, J. S. Huang, M. Hofmann, A. Werner, J. Blochwitz-Nimoth, *Org. Electron.* **2003**, *4*, 89.
- 25 K. Walzer, B. Maennig, M. Pfeiffer, K. Leo, *Chem. Rev.* **2007**, *107*, 1233.
- 26 H. Bässler, *Phys. Stat. Sol. (B)* **1981**, *107*, 9.
- 27 H. Bässler, *Phys. Stat. Sol. (B)* **1993**, *175*, 15.
- 28 R. Schmechel, H. von Seggern, *Phys. Stat. Sol. (A)* **2004**, *201*, 1215.
- 29 M. A. Baldo, D. F. O'Brien, Y. You, A. Shoustikov, S. Sibley, M. E. Thompson, S. R. Forrest, *Nature* **1998**, *395*, 151.
- 30 M. A. Baldo, D. F. O'Brien, M. E. Thompson, S. R. Forrest, *Phys. Rev. B* **1999**, *60*, 14422.
- 31 M. C. Gather, A. Köhnen, K. Meerholz, *Adv. Mater.* **2011**, *23*, 233.
- 32 K. T. Kamtekar, A. P. Monkman, M. R. Bryce, *Adv. Mater.* **2010**, *22*, 575.
- 33 T. K. Hatwar, M. E. Kondakova, D. J. Giesen, J. P. Spindler, in: *Organic Electronics: Materials, Processing, Devices and Applications*, F. So (Ed.), CRC Press Taylor and Francis Group, Boca Raton, **2010**.
- 34 C. W. Tang, S. A. VanSlyke, *Appl. Phys. Lett.* **1987**, *51*, 913.
- 35 H. Antoniadis, M. A. Abkowitz, B. R. Hsieh, *Appl. Phys. Lett.* **1994**, *65*, 2030.
- 36 P. Strohriegel, J. V. Grazulevicius, *Adv. Mater.* **2002**, *14*, 1439.
- 37 Y. Shirota, *J. Mater. Chem.* **2000**, *10*, 1.

- 38 A. J. Mäkinen, I. G. Hill, R. Shashidhar, N. Nikolov, Z. H. Kafafi, *Appl. Phys. Lett.* **2001**, *79*, 557.
- 39 M. Stolka, J. F. Yanus, D. M. Pai, *J. Phys. Chem.* **1984**, *88*, 4707.
- 40 K. Naito, A. Miura, *J. Phys. Chem.* **1993**, *97*, 6240.
- 41 B. E. Koene, D. E. Loy, M. E. Thompson, *Chem. Mater.* **1998**, *10*, 2235.
- 42 Z. Deng, S. T. Lee, D. P. Webb, Y. C. Chan and W. A. Gambling, *Synth. Met.* **1999**, *107*, 107.
- 43 L.-B. Lin, R. H. Young, M. G. Mason, S. A. Jenekhe, P. M. Borsenberger, *Appl. Phys. Lett.* **1998**, *72*, 864.
- 44 K. Goushi, R. Kwong, J. J. Brown, H. Sasabe, C. Adachi, *J. Appl. Phys.* **2004**, *95*, 7798.
- 45 Y. Kuwubara, H. Ogawa, H. Inada, N. Noma, Y. Shirota, *Adv. Mater.* **1994**, *6*, 667.
- 46 P. M. Borsenberger, L. Pautmeier, R. Richert, H. Bässler, *J. Chem. Phys.* **1991**, *94*, 8276.
- 47 J. Y. Shen, C. Y. Lee, T.-H. Huang, J. T. Lin, Y.-T. Tao, C.-H. Chien, C. Tsai, *J. Mater. Chem.* **2005**, *15*, 2455.
- 48 G. G. Malliaras, Y. Shen, D. H. Dunlap, *Appl. Phys. Lett.* **2001**, *79*, 2582.
- 49 S. Barth, P. Müller, H. Riel, P. F. Seidler, W. Rieß, H. Vestweber, H. Bässler, *J. Appl. Phys.* **2001**, *89*, 3711.
- 50 T. Yasuda, Y. Yamaguchi, D.-C. Zou, T. Tsutsui, *Jpn. J. Appl. Phys. Part 1* **2002**, *41*, 5626.
- 51 V. I. Adamoich, S. R. Cordero, P. I. Djurovich, A. Tamayo, M. E. Thompson, B. W. D'Andrade, S. R. Forrest, *Org. Electron.* **2003**, *4*, 77.
- 52 K. A. Higginson, X.-M. Zhang, F. Papadimitrakopoulos, *Chem. Mater.* **1998**, *10*, 1017.
- 53 M. Jandke, P. Strohriegl, S. Berleb, E. Werner, W. Brütting, *Macromolecules* **1998**, *31*, 6434.
- 54 M. Redecker, D. D. C. Bradley, M. Jandke, P. Strohriegl, *Appl. Phys. Lett.* **1999**, *75*, 109.
- 55 R. A. Klenkler, H. Aziz, A. Tran, Z. D. Popovic, G. Xu, *Org. Electron.* **2008**, *9*, 285.

- 56 M. E. Kondakova, T. D. Pawlik, R. H. Young, D. J. Giesen, D. Y. Kondakov, C. T.
Brown, J. C. Deaton, J. R. Lenhard, K. P. Klubek, *J. Appl. Phys.*, **2008**, *104*, 094501.
- 57 S.-J. Su, T. Chiba, T. Takeda, J. Kido, *Adv. Mater.* **2008**, *20*, 2125.
- 58 D. B. Papkovsky, *Sensors and Actuators B* **1995**, *29*, 213.
- 59 M. A. Baldo, C. Adachi, S. R. Forrest, *Phys. Rev. B* **2000**, *62*, 10967.
- 60 M. A. Baldo, S. Lamansky, P. E. Burrows, M. E. Thompson, S. R. Forrest, *Appl.*
Phys. Lett. **1999**, *75*, 4.
- 61 K. A. King, P. J. Spellane, R. J. Watts, *J. Am. Chem. Soc.* **1985**, *107*, 1431.
- 62 C. H. Yang, C. C. Tai, I. W. Sun, *J. Mater. Chem.* **2004**, *14*, 947.
- 63 C. Adachi, R. C. Kwong, P. Djurovich, V. Adamovich, M. A. Baldo, M. E.
Thompson, S. R. Forrest, *Appl. Phys. Lett.* **2001**, *79*, 2082.
- 64 L. Xiao, Z. Chen, B. Qu, J. Luo, S. Kong, Q. Gong, J. Kido, *Adv. Mater.* **2011**, *23*,
926.
- 65 G. N. Lewis, M. Kasha, *J. Am. Chem. Soc.* **1944**, *66*, 2100. D. F. Evans, *J. Chem. Soc.*
1957, 1351.
- 66 A. van Dijken, K. Brunner, H. Börner, B. M. W. Langeveld, in: Highly efficient
OLEDs with Phosphorescent Materials, H. Yersin, Wiley VCH Verlag, Weinheim,
2008.
- 67 J. E. Adams, W. W. Mantulin, J. R. Huber, *J. Am. Chem. Soc.* **1973**, *95*, 5477.
- 68 C. Adachi, R. Kwong, S. R. Forrest, *Org. Electron.* **2001**, *2*, 37.
- 69 D. Tanaka, H. Sasabe, X.J. Li, S. J. Su, T. Takeda, J. Kido, *Jpn. J. Appl. Phys.* **2007**,
46, L10.
- 70 S. Tokito, T. Iijima, Y. Suzuri, H. Kita, T. Tsuzuki, F. Sato, *Appl. Phys. Lett.* **2003**, *83*,
569.
- 71 I. Tanaka, Y. Tabata, S. Tokito, *Chem. Phys. Lett.* **2004**, *400*, 86.
- 72 J. He, H. Liu, Y. Dai, X. Ou, J. Wang, S. Tao, X. Zhang, P. Wang, D. Ma, *J. Phys.*
Chem. C **2009**, *113*, 6761.
- 73 V. Adamovich, J. Brooks, A. Tamayo, A. M. Alexander, P. I. Djurovich, B. W.
D'Andrade, C. Adachi, S. R. Forrest, M. E. Thompson, *New J. Chem.* **2002**, *26*,
1171.

- 74 R. J. Holmes, S. R. Forrest, Y.-J. Tung, R. C. Kwong, J. J. Brown, S. Garon, M. E. Thompson, *Appl. Phys. Lett.* **2003**, *82*, 2422.
- 75 M.-F. Wu, S.-J. Yeh, C.-T. Chen, H. Murayama, T. Tsuboi, W.-S. Li, I. Chao, S.-W. Liu, J.-K. Wang, *Adv. Funct. Mater.* **2007**, *17*, 1887.
- 76 M.-H Tsai, H.-W. Lin, H.-C. Su, T.-H. Ke, C.-C. Wu, F.-C. Fang, Y.-L. Liao, K.-T. Wong, C.-I. Wu, *Adv. Mater.* **2006**, *18*, 1216.
- 77 S.-Y. Takizawa, V. A. Montes, P. Anzenbacher, *Chem. Mater.* **2009**, *21*, 2452.
- 78 H. Inomata, K. Goushi, T. Masuko, T. Konno, T. Imai, H. Sasabe, J. J. Brown, C. Adachi, *Chem. Mater.* **2004**, *16*, 1285.
- 79 M. M. Rothmann, S. Haneder, E. Da Como, C. Lennartz, C. Schildknecht, P. Strohhriegl, *Chem. Mater.* **2010**, *22*, 2403.
- 80 S.-J. Su, H. Sasabe, T. Takeda, J. Kido, *Chem. Mater.* **2008**, *20*, 1691.
- 81 S. O. Jeon, K. S. Yook, C. W. Joo, J. Y. Lee, *Adv. Mater.* **2010**, *22*, 1872.
- 82 X. Ren, J. Li, R. J. Holmes, P. I. Djurovich, S. R. Forrest, M. E. Thompson, *Chem. Mater.* **2004**, *16*, 4743.
- 83 R. J. Holmes, B. W. D'Andrade, S. R. Forrest, X. Ren, J. Li, M. E. Thompson, *Appl. Phys. Lett.* **2003**, *83*, 3818.
- 84 J.-J. Lin, W.-S. Liao, H.-J. Huang, F.-I. Wu, C.-H. Cheng, *Adv. Funct. Mater.* **2008**, *18*, 485.
- 85 E. L. Williams, K. Haavisto, J. Li, G. E. Jabbour, *Adv. Mater.* **2007**, *19*, 197.

6 A Series of CBP-derivatives as Host Materials for Blue Phosphorescent Organic Light-emitting Diodes

Pamela Schrögel,^a Aušra Tomkevičienė,^{†a} Peter Strohriegl,^{*a} Sebastian T. Hoffmann,^b

Anna Köhler,^b Christian Lennartz^c

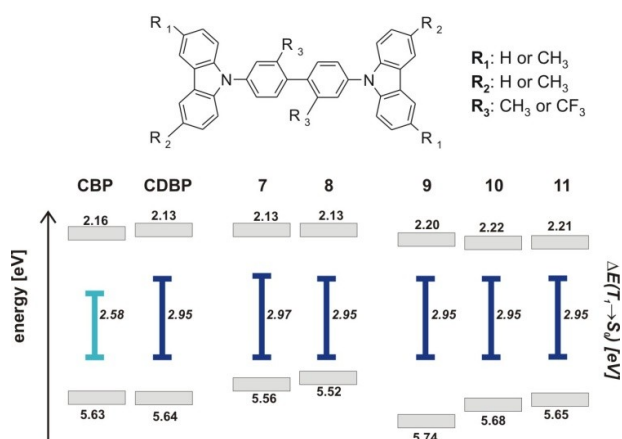
^aLehrstuhl Makromolekulare Chemie I, Universität Bayreuth, 95440 Bayreuth, Germany,

^bLehrstuhl Experimentalphysik II, Universität Bayreuth, 95440 Bayreuth, Germany,

^cBASF SE, 67056 Ludwigshafen, Germany

[†] Current address: Kaunas University of Technology, Department of Organic Technology,
Radvilenu pl. 19, LT-50254 Kaunas, Lithuania

*Corresponding author: peter.strohriegl@uni-bayreuth.de



published in *Journal of Materials Chemistry* **2011**, *21*, 2266-2273.

Reproduced by permission of The Royal Society of Chemistry

doi.org/10.1039/c0jm03321a

Abstract

We report a series of **CBP**-derivatives with superior thermal and electronic properties for the use as host materials for blue electrophosphorescent organic light emitting diodes. We applied a systematic variation of the substitution pattern in the 2- and 2'-position of the biphenyl unit and the 3- and 6-positions of the carbazole moieties. In contrast to the crystalline parent compound **CBP**, all methyl and trifluoromethyl substituted derivatives show amorphous behaviour. Substitution in the 2- and 2'-position of the biphenyl causes a twisting of the phenyl rings. Hence, the degree of conjugation of the molecules is limited which leads to enlarged triplet energies of approximately 2.95 eV compared to 2.58 eV for **CBP**. The methyl substitution at the active 3- and 6-positions of the pendant carbazole units yields materials with an electrochemically stable behavior against oxidation.

Keywords

CBP, blue phosphorescent OLEDs, carbazole, host materials, electrochemical stability.

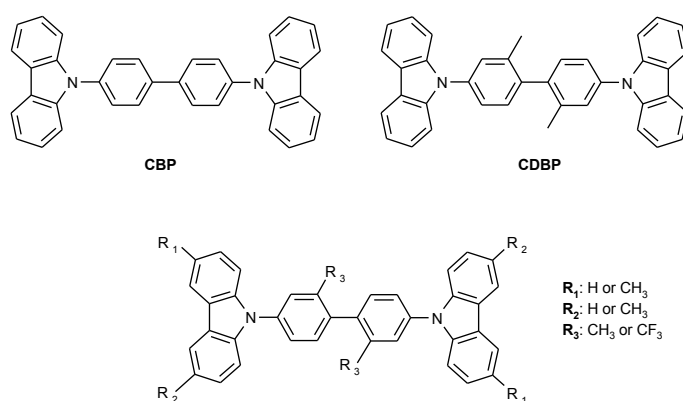
Introduction

Recent developments of efficient emitters for organic light emitting diodes (OLEDs) are often focused on phosphorescent transition metal complexes. Due to elementary spin statistics 75 % triplet excitons and 25 % singlet excitons are formed on initial charge recombination. By fast intersystem crossing all singlet excitons will be efficiently converted to the triplet state. Hence, with these phosphorescent emitters the theoretical limit of the internal quantum efficiency is 100%.^{1,2,3} Due to concentration quenching effects phosphorescent materials show a loss in efficiency if the neat material is used in OLEDs. To avoid self quenching it is necessary to dope the emitters into an appropriate host. It is essential that the triplet energy ($\Delta E T_1-S_0$) of the host is higher than that of the emitter in order to prevent energy back transfer from the phosphorescent guest to the host. 4,4'-Bis(9-carbazolyl)-biphenyl (**CBP**) is a widely used matrix material for phosphorescent emitters. Due to its triplet energy $\Delta E (T_1-S_0)$ of 2.55 eV⁴, CBP is a suitable matrix for green phosphorescent emitters like tris(2-phenylpyridine)iridium(III) Ir(ppy)₃.^{3,5} Blue emitting materials such as the commonly used bis(4,6-difluorophenyl)-pyridinato-*N,C2*picolate-iridium(III) Irpic ($\Delta E (T_1-S_0) = 2.62$ eV⁶) require hosts with higher triplet energies. The key to such materials is to confine the conjugated system in the host molecules. In *N,N'*-dicarbazolyl-3,5-benzene (mCP) this is accomplished by exchanging the biphenyl group by a single benzene unit in combination with *meta* conjugation instead of *para* which leads to a triplet energy of approximately 2.90 eV.^{7,8} Another approach to enlarge the triplet energy of **CBP** based materials comprises the attachment of two methyl groups in the 2- and 2'-position of the central biphenyl which leads to 4,4'-bis(9-carbazolyl)-2,2'-dimethylbiphenyl (**CDBP**) with a triplet energy of 2.79 eV.^{4,9,10} Over the years many different carbazole based host materials have been described.^{11,12,13} Ma *et al.* recently described a series of non-conjugated carbazole host materials where the linkage groups between two carbazole moieties were varied. This leads to a loss of conjugation in the molecules and high triplet energies.¹⁴

Another crucial requirement for the successful operation of OLEDs is the ability of the materials to form stable amorphous films.¹⁵ This property guarantees that the emitter is uniformly diluted in the host to minimize the effect of concentration quenching. In

addition, the absence of grain boundaries, which may act as trap states, makes the use of organic glasses as OLED materials advantageous.^{16,17} The glass transition temperature of materials for OLED applications is ideally above 100°C. In general, the introduction of bulky substituents hinders packing of the molecules and leads to an amorphous behavior of the material. On the other hand, detrimental effects on the charge carrier transport properties are observed. 9-(4-tert-Butylphenyl)-3,6-bis(triphenylsilyl)-carbazole (CzSi), for example, combines appropriate thermal properties with a confined conjugated system; however, the hole mobility of $5 \times 10^{-5} \text{ cm}^2/\text{V}\cdot\text{s}$ is rather low.¹⁸ By exchanging the triphenylsilyl groups by trityl groups the hole mobility rises by one order of magnitude to $5 \times 10^{-4} \text{ cm}^2/\text{V}\cdot\text{s}$. However, this material shows a stronger efficiency roll off at higher current densities than CzSi.¹⁹

We have prepared a series of **CBP** derivatives in which the substitution pattern in both the 2- and 2'-positions of the biphenyl unit and in the 3- and 6-positions of the carbazole unit has been systematically varied (Scheme 1). The attachment of the methyl and trifluoromethyl groups in these positions leads to amorphous materials with large triplet energies making them suitable as hosts for blue phosphorescent emitters.



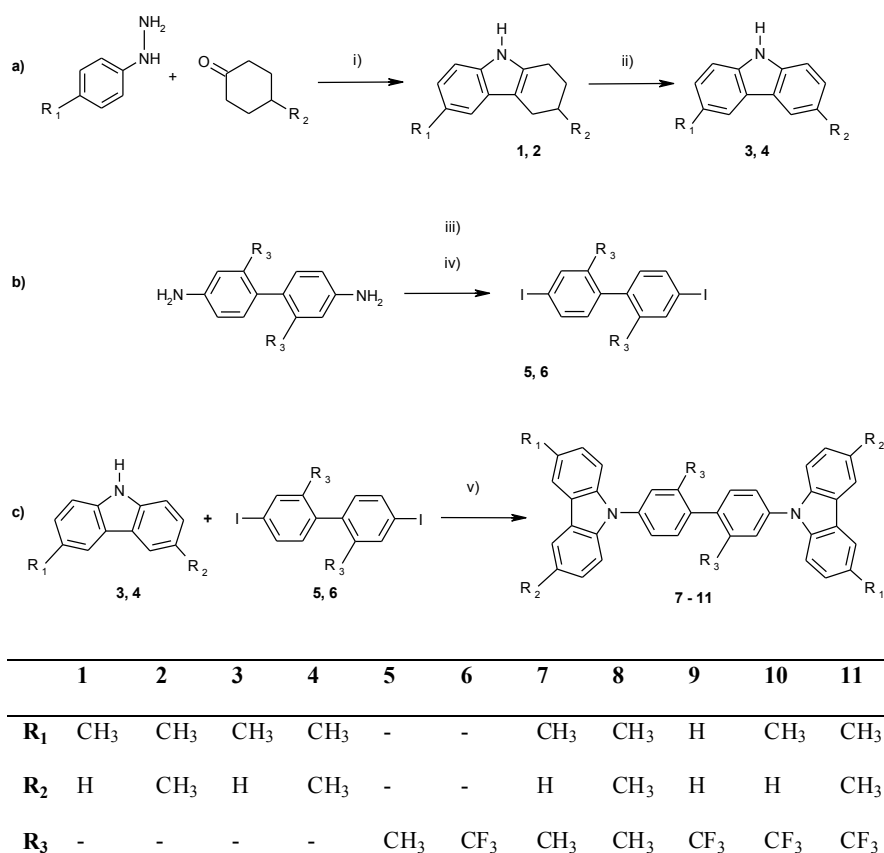
Scheme 1. Chemical structures of the substituted 4,4'-bis(9-carbazolyl)-biphenyls.

In this work we report the synthesis of five amorphous derivatives of **CBP** together with their thermal and optical properties. The energy levels have been measured by cyclic voltammetry and absorption measurements. Furthermore, a detailed cyclic voltammetry study of the materials gives insight into the electrochemical stability of the **CBP** derivatives. In addition, DFT calculations were carried out to obtain the ground state geometries of the CBP derivatives.

Results and Discussion

Synthesis

In a two step synthesis 3-methylcarbazole **3** and 3,6-dimethylcarbazole **4** were prepared from 4-methyl-phenylhydrazine and cyclohexanone or 4-methyl-cyclohexanone as the starting materials in a *Borsche* reaction (Scheme 2a). The first step yields the 1,2,3,4-tetrahydrocarbazoles **1** and **2** which are subsequently dehydrogenated with palladium on activated charcoal.^{20,21}



Scheme 2. Synthetic routes to **a)** methyl substituted carbazoles **b)** tilted biphenyls and **c)** methyl substituted CBP derivatives. Reagents and conditions: i) acetic acid, 80°C, 30 min; ii) Pd(C), 1,2,4-trimethylbenzene, 170°C, 6 h; iii) H₂O, HCl, NaNO₂, 0-5°C; iv) I₂, NaI, dichloromethane, r.t., 24 h; v) Cu, K₂CO₃, 18-crown-6, *o*-dichlorobenzene, reflux, 24 h.

The synthesis of the diiodobiphenyls is shown in Scheme 2b. 4,4'-Diiodo-2,2'-dimethylbiphenyl **5** and 4,4'-diiodo-2,2'-bis(trifluoromethyl)biphenyl **6** were prepared by diazotation of the corresponding diamine and subsequent reaction with sodium iodide.²² The carbazole containing host materials **7-11** were prepared via the Ullmann coupling

reaction of diiodo compounds **5** or **6** with carbazole or the methylcarbazoles **3** and **4**, respectively (Scheme 2c). Mass spectrometry, $^1\text{H-NMR}$ spectroscopy and $^{13}\text{C-NMR}$ spectroscopy were used to identify the materials and the data are given in the experimental part. The purity of the materials was monitored by SEC measurements.

Thermal properties

The thermal properties of the newly synthesised compounds were examined by thermogravimetric analysis (TGA) and differential scanning calorimetry (DSC) in a nitrogen atmosphere at a scanning rate of 10 K min^{-1} . All materials reveal high thermal stabilities, with an onset of weight loss at temperatures (T_D) exceeding 310°C , as determined by TGA measurements (Table 1).

In

Figure 1, the DSC thermograms of **CBP**, the methyl substituted compound **8** and the trifluoromethyl derivative **11** are presented. The parent compound CBP shows a crystalline behaviour in the DSC. The melting is observed at 285°C and upon cooling the material crystallises at 183°C . In contrast, compound **8** exhibits a melting peak at 277°C . In the cooling cycle no crystallisation is observed as the material solidifies in an amorphous phase. In the second heating curve the glass transition is observed at 121°C followed by a recrystallisation at 200°C . The CF_3 -substituted derivative **11** remains in the amorphous phase after the first melting at 233°C . In the second heating only the glass transition at 119°C is observed.

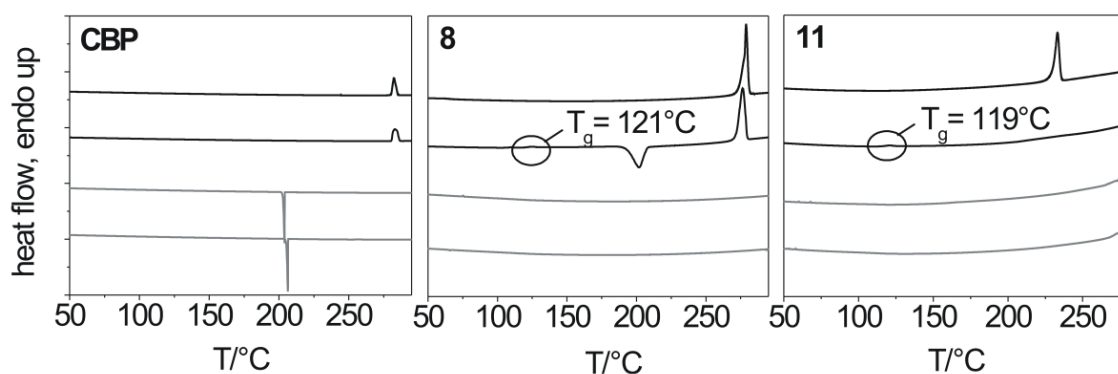


Figure 1. DSC traces of carbazole based compounds **CBP**, **8**, and **11** at a scan rate of 10 K min^{-1} , N_2 atmosphere. Shown are from top to bottom: the first heating (black), second heating (black), first cooling (grey) and second cooling (grey) traces.

These results show that by the introduction of additional methyl- and trifluoromethyl groups into the basic **CBP** structure the thermal properties are improved. While the parent compound **CBP** is highly crystalline, all **CBP** derivatives **7-11** reveal high glass transition temperatures ranging from 94 to 121°C and all materials remain amorphous upon cooling (Table 1). For OLED applications materials with high glass transition temperatures ($T_g \sim 100^\circ\text{C}$) are advantageous for the operational stability of the device. In an morphologically stable amorphous host material the emitter molecules are homogenously diluted which prevents concentration quenching. The melting, crystallization and glass transition temperatures of all derivatives are summarised in Table 1.

Table 1. Thermal properties of the carbazole-substituted biphenyls **CBP**, **CDBP**, and **7-11**.^d

	$T_g / ^\circ\text{C}$	$T_m / ^\circ\text{C}$	$T_{cr} / ^\circ\text{C}$	$T_{ID}^a / ^\circ\text{C}$
CBP	--	283	205	365
CDBP	94	--	--	310
7	106	--	--	310
8	121	277	200 ^c	312
9	100	232	--	310
10	105	210 ^b	--	337
11	119	233 ^b	--	333

^a T_{ID} is the temperature at which an initial loss of mass was observed in a thermogravimetric experiment with a heating rate of 10 K min^{-1} in a nitrogen atmosphere.

^b Observed only in the first heating scan.

^c Observed during the heating scan.

^d T_g : glass-transition temperatures, T_m : melting temperatures, T_{cr} : crystallization temperatures and T_{ID} : initial decomposition temperatures.

Optical properties

The compounds **CBP**, **CDBP** and **7-11** were analyzed by UV/Vis, fluorescence and phosphorescence spectroscopy. In addition, the molecular structures of all compounds were simulated via DFT-calculations to facilitate the interpretation of the experimental results. The geometry optimized structures of **CBP**, **8**, and **11** are visualized in Figure 2. Due to the steric demand of the substituents at the 2- and 2'-positions at the biphenyl

unit, **8** and **11** reveal twisted molecular structures with torsion angles between the two phenyl rings of the biphenyl unit of 82° and 74° which are significantly higher compared to the more planar **CBP** (33°).

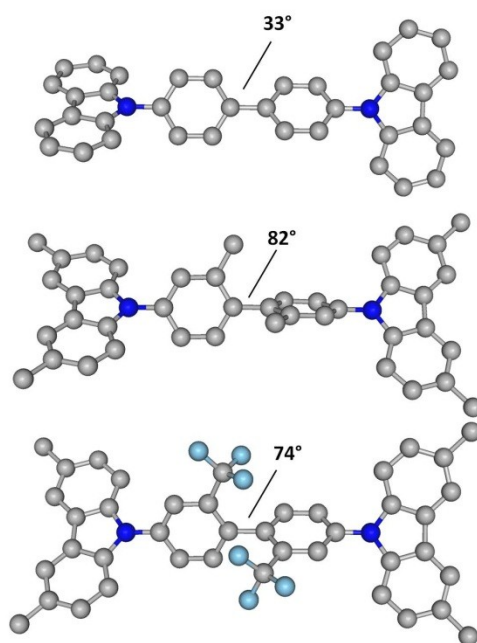


Figure 2. Geometry optimized structures of **CBP**, **8**, and **11** (top to bottom) with different torsion angles.

Figure 3 displays the room temperature absorption and fluorescence spectra taken from 10^{-5} M cyclohexane solutions together with the phosphorescence spectra obtained from 10 wt% solid solutions of **CBP**, **8**, and **11** in PMMA at 10 K. In order to understand how the substitutions affect the excited states of these compounds, we first consider the effect of the methyl substitution at the central biphenyl unit by comparing **CBP** and **8**. For **8**, the first and second absorption are at 351 nm and 300 nm which can both be assigned to the absorption of the 3,6-dimethylcarbazole units. In the case of **CBP**, the features associated with transitions localized on the carbazole are still present at 339 nm and 290 nm. The observed bathochromic shift of approximately 10 nm in compound **8** is caused by the additional methyl groups at the carbazole units. In **CBP** however, there is an additional broad absorption centred at about 320 nm. This feature is likely to be associated with transitions between orbitals that involve the central biphenyl unit of the molecule. In the fluorescence spectra, in contrast, **CBP** and **8** show very similar vibrational structures with a strong maximum at about 355 nm for both compounds. We

now consider how changing the substituents on the central biphenyl unit from methyl to trifluoromethyl affects the optical transitions. While **8** shows the signature of the carbazole-based transitions in the absorption and fluorescence spectra, **11** has an additional contribution to the absorption, centred at about 325 nm. As for **CBP**, we consider the additional absorption to involve the central biphenyl unit. The main difference of compound **11** compared to **CBP** and **8** is the observed featureless fluorescence centered at 410 nm. The broad bathochromically shifted fluorescence is clearly not due to transitions localized on the carbazole. The absence of vibrational fine structure rather points to a charge-transfer type transition, for example from the carbazole moiety to the central, trifluoromethyl substituted biphenyl rings.

For applications of compound **7-11** as host materials for blue phosphorescent emitters the triplet energies are of major interest. In the phosphorescence spectra of compound **8** and **11**, we observe two sharp peaks at 420 nm and at 450 nm as well as a broad peak centred at 480 nm. On the contrary, the emission of **CBP** is bathochromically shifted by 60 nm. As a result, **8** and **11** reveal a triplet energy of approximately 2.95 eV (420 nm), significantly higher than that of **CBP** of 2.58 eV (480 nm). Apparently, the conjugation between the two phenyl rings is interrupted by introducing CH₃ and CF₃ substituents at the 2- and 2'-positions of the central biphenyl leading to higher triplet energies.

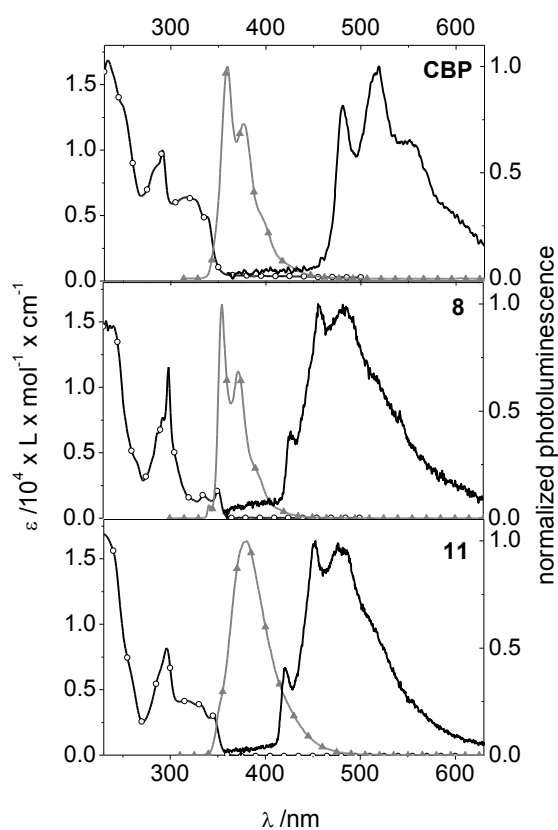


Figure 3. Comparison of the absorption (dark grey with circles), fluorescence (light grey with triangles) and phosphorescence (black) spectra of **CBP**, **8**, and **11**. Absorption and fluorescence were taken in 10^{-5} M cyclohexane solutions at 300 K, phosphorescence was measured in 10 wt% solid solutions in PMMA at 10 K.

All results of the photophysical investigations of compounds **CBP**, **CDBP**, and **7-11** are summarized in Table 2. With increasing CH_3 -content on the pendant carbazole units in the series **CDBP**, **7**, and **8** as well as in the series of **9**, **10**, and **11** a small bathochromic shift is noticeable in both the absorption and fluorescence spectra. We attribute this to the electron donating effect of the CH_3 -units. All compounds which are twisted by substituents at the central biphenyl show triplet energies of approximately 2.95 eV. These high triplet energies of the materials **CDBP** and **7-11** make them suitable host materials for deep blue phosphorescent emitters. It should be noted that the triplet energies of **CBP** and **CDBP** are slightly higher than in neat films reported by Tokito *et al.*^{4,9,10} as in our case the phosphorescence spectroscopy was carried out in 10 wt-% solid solutions of PMMA.

Table 2. Optical properties of **CBP**, **CDBP** and the **CBP**-derivatives **7-11**.

	λ_{EA}^a /nm	λ_{EA}^b /nm	λ_{em}^{RT} ^c	λ_{em}^{10K} ^d	$\Delta E(S_0-S_1)^e$	$\Delta E(T_1-S_0)$
	solution	film	/nm	/nm	/eV	/eV
CBP	350	357	356, 374	477	3.47	2.58
CDBP	346	353	342, 358	419	3.51	2.95
7	353	361	349, 366	417	3.43	2.97
8	357	365	355, 372	421	3.39	2.95
9	343	350	368	419	3.54	2.95
10	350	358	373	419	3.46	2.95
11	353	360	379	420	3.44	2.95

^a Edge of absorption measured in 10^{-5} M cyclohexane solutions at room temperature.

^b Edge of absorption measured on neat films at room temperature.

^c Wavelengths of the intensity maxima of the fluorescence at 300 nm excitation of 10^{-5} M cyclohexane solutions at room temperature.

^d Wavelength of the highest energy maximum measured on film samples of 10 wt-% compound in PMMA at 10 K.

^e The optical band gap was determined from the UV/Vis absorption onset of neat films.

Cyclic voltammetry

The electrochemical behaviour of the **CBP**-derivatives was studied by cyclic voltammetry in a conventional three-electrode cell using a platinum working electrode, a platinum wire counter electrode, and a Ag/AgNO₃ reference electrode. In particular, the oxidation processes were investigated in dichloromethane solutions. The HOMO levels of the compounds were estimated from the half-wave potential of the first oxidation relative to ferrocene. The LUMO levels were calculated by adding the optical band gap to the HOMO levels. Table 3 lists the values for the HOMO and LUMO levels. In the CV-experiments **CBP** and **CDBP** show very similar HOMO levels of 5.63 eV and 5.64 eV. This observation is not surprising as in both molecules the HOMO is mainly located on the electron rich carbazole units. In the case of the methyl substitution in the 3- and 6-positions of the carbazole units the additional *+I*-effect on the carbazole shifts the HOMO levels to slightly higher values. The HOMO level is 5.56 eV for compound **7**

and 5.52 eV for compound **8**. In the case of the compounds **9-11** the strong $-I$ -effect of the trifluoromethyl substituents causes a decrease of the HOMO level of approximately 0.1 eV (5.74 eV for **9**) in comparison with **CDBP** (5.64 eV). By the subsequent introduction of methyl groups at the carbazole moieties in compounds **10** and **11** the HOMO level rises again to 5.68 eV and 5.65 eV, respectively. In contrast, the LUMO levels of all compounds are less affected by the introduction of the substituents on the carbazole units. However, in compounds **9-11** the trifluoromethyl substitution at the biphenyl lowers the LUMO level slightly by approximately 8 meV compared to compounds **CDBP**, **7**, and **8**.

Table 3. Experimentally determined energy levels of the **CBP** derivatives.

	HOMO ^a /eV	LUMO ^b /eV
CBP	5.63	2.16
CDBP	5.64	2.13
7	5.56	2.13
8	5.52	2.13
9	5.74	2.20
10	5.68	2.22
11	5.65	2.21

^a Estimated from the half-wave potential of the first oxidation in the cyclic voltammetry measurements.

^b Estimated from the HOMO values and the optical band gap.

These considerations show that the energy levels of the **CBP** derivatives can be fine-tuned to some extent by the variation of the substitution pattern at the connecting biphenyl moiety as well as at the pendant carbazoles. Especially, the HOMO levels can be varied as can be seen in Figure 4. Thus, with these slight variations in the molecular structure the energy levels of the different layers in an OLED can be adjusted to each other in order to minimize energy barriers within the device.

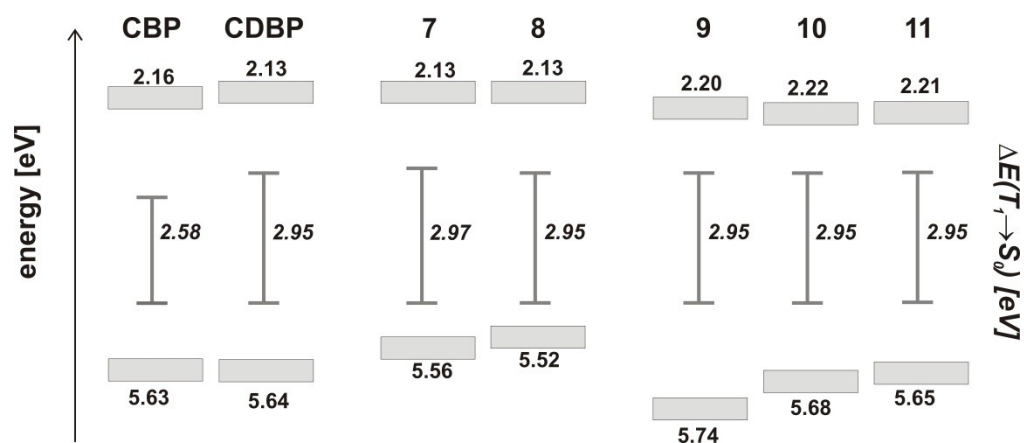


Figure 4. Energy diagram showing the location of the HOMO and LUMO levels of the different **CBP**-derivatives. The solid line displays the position of the triplet energies $\Delta E(T_1-S_0)$.

Cyclic voltammetry experiments with repeated cycles give an insight into the electrochemical stability of the **CBP** derivatives. As radical cations and anions are involved in charge transport processes the electrochemical stability of the materials used in electroluminescent devices contributes to the overall stability of the device. Figure 5 shows the cyclic voltammograms with five repeated oxidation cycles of **CBP**, **7**, and **8** in 2×10^{-3} M dichloromethane solutions.

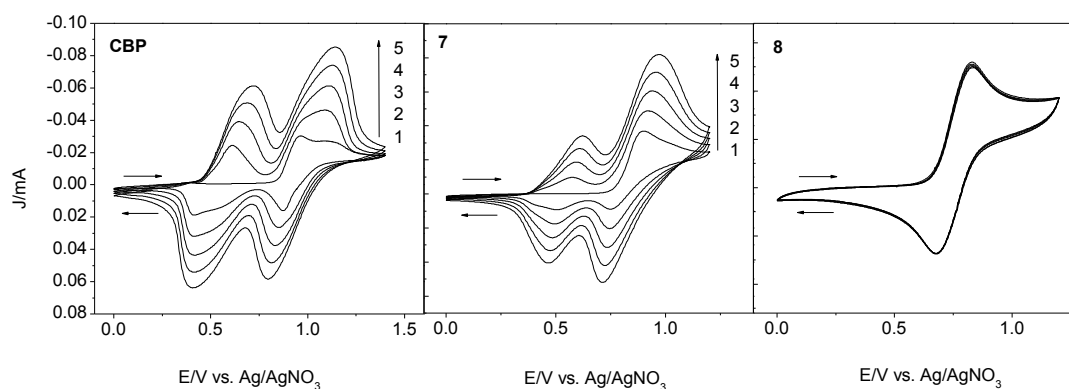


Figure 5. Cyclic voltammograms of **CBP**, **7**, and **8** (five scans, scan rate 50 mV/sec, 2×10^{-3} M in CH_2Cl_2).

CBP reveals an irreversible oxidation behaviour as here oligomerisation reactions of the oxidised species can take place at the active 3- and 6-positions of the carbazole units. This kind of dimerisation is known from triphenylamine and *N*-phenylcarbazole. The

mechanism is shown in Figure 6.^{23,24} In the first step the molecule is oxidised at the electron lone pair of the nitrogen atom and a radical cation is formed. The radical stabilises into the 3-position of the carbazole where recombination of two radical molecules takes place under elimination of two protons.

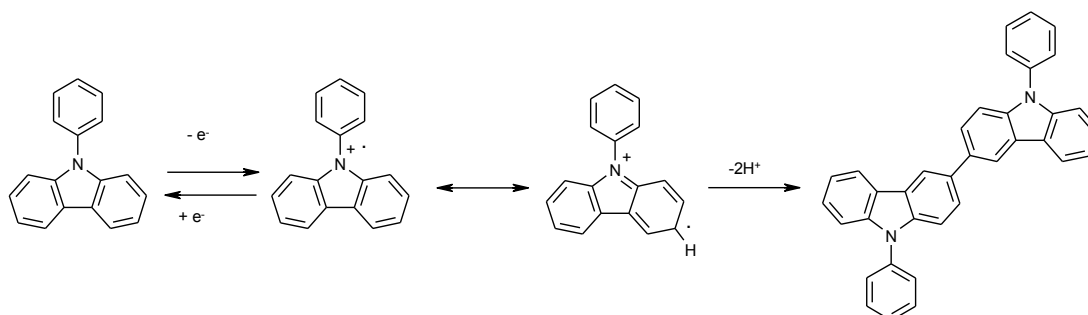


Figure 6. Formation of the radical cation of *N*-phenylcarbazole upon oxidation and subsequent dimerisation at the active 3-position.

The oligomeric species are oxidised more easily, *i.e.* at lower voltages. In the cyclic voltammogram the emerging signal at 0.6 V to 0.7 V is assigned to the oxidation of the newly formed oligomeric species. The electrochemical behaviour of **7** is very similar to **CBP**. However, the signal between 0.4 V and 0.6 V indicating the coupling of two carbazole units is growing more slowly compared with **CBP**, as in compound **7** oligomerisation can occur only at the unblocked 6-positions. In contrast, compound **8** reveals a fully reversible oxidation behaviour which can be attributed to the complete blocking of the active 3- and 6-positions of the carbazole units.

Experimental Section

Materials

All chemicals and reagents were used as received from commercial sources without further purification. 2,2'-Bis(trifluoromethyl)benzidine was synthesised according to a procedure described by Rogers *et al.*²⁵ The solvents for reactions and purification were all distilled before use.

Characterisation

^1H - and ^{13}C -NMR spectra were recorded with a Bruker AC 300 (300 MHz, 75 MHz) and CDCl_3 as solvent. All data are given as chemical shifts δ (ppm) downfield from $\text{Si}(\text{CH}_3)_4$. For optical measurements, 10^{-5} M cyclohexane solutions of the materials as well as thin films on quartz substrates were prepared. Both, neat films and films with 10 wt% of the compound in poly(methylmethacrylate) were prepared by spincoating. The UV/VIS spectra were measured in solution and on neat films with a Hitachi U-3000 spectrometer. Fluorescence spectra in solution were obtained from a Shimadzu spectrofluorophotometer RF-5301PC using excitation at 300 nm. The phosphorescence spectra were taken with the thin film samples mounted in a continuous flow helium cryostat. The temperature was controlled with an Oxford Intelligent temperature controller-4 (ITC-502). Excitation was provided by a pulsed, frequency-tripled NdYAG laser at 355 nm (3.49 eV) (Spectron SL401). This wavelength corresponds to the red tail of the first absorption band in our compounds. The duration of the laser pulses was 6 ns and the laser was operated at a repetition rate of 10 Hz by a self made electronic delay generator. The light emitted by the sample was dispersed and subsequently detected by a time gated intensified CCD camera (Andor iStar DH734-18F-9AM). The measurements were taken with a delay time of 500 ns and a gate width of 60 ms. The measurements were carried out at an excitation density of about $250 \mu\text{Jcm}^{-2} \text{pulse}^{-1}$ on films of about 150 nm thickness as determined by a Dektak profilometer. To increase the signal-to-noise-ratio, all spectra were obtained by averaging over 2000 laser shots. For differential scanning calorimetry measurements (DSC) a Diamond DSC apparatus from Perkin Elmer was used (heating/cooling rate 10 K min^{-1}). Thermogravimetric analysis (TGA) was performed on a Mettler Toledo TGA/SDTA815e machine at a heating rate of 10 K min^{-1} in a nitrogen atmosphere. Cyclic voltammetry measurements were carried out in absolute solvents measuring at a platinum working electrode versus a Ag/AgNO_3 reference electrode. Each measurement was calibrated against an internal standard (ferrocene/ferrocenium redox system). The purity of the target compounds was checked with a Waters size exclusion chromatography system (SEC) for oligomers (analytical columns: crosslinked polystyrene gel (Polymer Laboratories), length: $2 \times 60 \text{ cm}$, width: 0.8

cm, particle size: 5 μm , pore size 100 \AA , eluent THF (0.5 mL min^{-1} , 80 bar), polystyrene standard).

Calculations

Geometries were optimized using the BP86-functional^{26,27} in combination with a split-valence basis set (SV(P)) including polarization functions on all heavy atoms.²⁸ All calculations were carried out with the turbomole program package.²⁹

Synthetic procedures

General procedure for the preparation of methyl substituted carbazoles

3-Methyl-6,7,8,9-tetrahydro-5H-carbazole (1). 3-Methylphenylhydrazine hydrochloride (10.0 g, 63 mmol) was added to a solution of cyclohexanone (6.2 g, 63 mmol) in acetic acid (30 mL) under an argon atmosphere over a period of one hour. After stirring at 80°C for half an hour the reaction mixture was extracted with dichloromethane and washed several times with 5 % aqueous sodium hydrogen carbonate solution to neutralise the acetic acid. After drying the organic layer over anhydrous sodium sulphate the solvent was evaporated. Yield: 9.25 g (79 %). EI-MS m/z : 185 (95, M^+).

3,6-Dimethyl-6,7,8,9-tetrahydro-5H-carbazole (2). Compound **2** was prepared according to the procedure described for **1**. Yield: 93 %.

3-Methylcarbazole (3). To 9.25 g (50 mmol) of 3-methyl-6,7,8,9-tetrahydro-5H-carbazole (**1**) in 30 mL of 1,2,4-trimethylbenzene was added 10 % palladium on activated charcoal (2.66 g, 25 mmol). The mixture was refluxed for 6 h. In order to remove the catalyst the mixture was diluted with dichloromethane and filtered over neutral aluminium oxide. After the removal of dichloromethane, hexane was added and the product was obtained as white precipitate. Yield: (88 %). EI-MS m/z : 181 (100, M^+). $^1\text{H-NMR}$ (300 MHz, CDCl_3), δ (ppm): 8.06 (dd, 1H), 7.94 (s, 1H, NH), 7.90 (ds, 1H), 7.41 (m, 2H), 7.35 (d, 1 H), 7.27-7.21 (m, 2H), 2.55 (s, 3H). $^{13}\text{C-NMR}$ (75 MHz, CDCl_3), δ (ppm): 139.82, 137.71, 137.26, 128.75, 127.18, 125.65, 123.14, 120.26, 120.24, 119.22, 110.55, 110.24, 21.44.

3,6-Dimethylcarbazole (4). Compound **4** was prepared according to the procedure given for **3**. Yield: (86 %). EI-MS m/z : 195 (100, M^+). $^1\text{H NMR}$ (300 MHz, CDCl_3), δ (ppm):

7.85 (m, 2H), 7.84 (s, 1H, NH), 7.31 (d, 2H), 7.24 (dd, 2H), 2.55 (s, 6H). $^{13}\text{C-NMR}$ (75 MHz, CDCl_3), δ (ppm): 138.07, 128.48, 126.99, 123.41, 120.18, 110.22, 21.44.

General procedure for the preparation of substituted biphenyls

4,4'-Diiodo-2,2'-dimethylbiphenyl (5). 2,2'-Dimethylbenzidine dihydrochloride (14.3 g, 50 mmol) was suspended in 125 mL of water and 15 mL of conc. hydrochloric acid and the suspension was cooled to 0-5°C. A solution of sodium nitrite (7.18 g, 100 mmol) in 20 mL of water was added drop wise. The resulting cold tetrazonium salt solution was added slowly to a well-stirred solution of iodine (30.5 g, 120 mmol) and sodium iodide (30.0 g, 200 mmol) in 50 mL of water and 100 mL of dichloromethane at a temperature below 5°C. The mixture was stirred for 24 h at room temperature and the excess of iodine was removed by the addition of a sodium thiosulfate solution. The product was extracted with dichloromethane and washed several times with water. After drying the organic layer over anhydrous sodium sulphate, the solvent was evaporated and the residue was purified by column chromatography on silica gel with hexane as eluent to afford compound **5**. Yield: 16.6 g (76 %). EI-MS m/z : 434 (100, M^+). $^1\text{H-NMR}$ (300 MHz, CDCl_3), δ (ppm): 7.63 (d, 2H), 7.55 (dd, 2H), 6.79 (d, 2H). 1.98 (s, 6H). $^{13}\text{C-NMR}$ (75 MHz, CDCl_3), δ (ppm): 139.99, 138.75, 138.22, 134.81, 130.87, 93.13, 19.47.

4,4'-Diiodo-2,2'-bis(trifluoromethyl)biphenyl (6). Compound **6** was prepared according to the procedure given for **5**. Yield: 1.91 g (75 %). EI-MS m/z : 542 (100, M^+). $^1\text{H-NMR}$ (300 MHz, CDCl_3), δ (ppm): 8.07 (d, 2H), 7.89 (dd, 2H), 6.99 (d, 2H). $^{13}\text{C-NMR}$ (75 MHz, CDCl_3), δ (ppm): 139.97, 135.88, 135.06, 132.86, 130.32 (q, 2J (C-F) = 30.8 Hz), 122.56 (q, 1J (C-F) = 273.0 Hz), 93.55.

General procedure for the Ullmann condensation

4,4'-Bis(3-methylcarbazolyl)-2,2'-dimethylbiphenyl (7). 4,4'-Diiodo-2,2'-dimethylbiphenyl (**5**) (1 g, 2.3 mmol), 3-methylcarbazole (**3**) (1.0 g, 5.52 mmol), potassium carbonate (2.5 g, 18.4 mmol), copper powder (0.58 g, 9.2 mmol) and 18-crown-6 (0.12 mg, 0.46 mmol) were refluxed in 15 mL of *o*-dichlorobenzene in an argon atmosphere for 24 h. Copper and inorganic salts were filtered off and the solvent was evaporated. Column chromatography on silica gel with hexane/tetrahydrofurane (20 : 1) as eluent yielded

0.72 g (58 %) of **7** as white solid. EI-MS m/z : 540 (100, M^+). $^1\text{H-NMR}$ (300 MHz, CDCl_3), δ (ppm): 8.14 (d, 4H), 7.97 (m, 4H), 7.55-7.43 (m, 12H), 7.32-7.27 (m, 4H), 2.58 (s, 6H), 2.29 (s, 6H). $^{13}\text{C-NMR}$ (75 MHz, CDCl_3), δ (ppm): 141.11, 139.83, 139.23, 137.88, 137.11, 130.78, 129.31, 128.19, 127.24, 125.76, 124.16, 123.57, 123.30, 120.28, 119.72, 109.88, 109.65, 21.45, 20.17. T_m : $-\text{°C}$; T_g : 106°C.

4,4'-Bis(9-carbazolyl)-2,2'-dimethylbiphenyl (**CDBP**), 4,4'-bis(3,6-dimethylcarbazolyl)-2,2'-dimethylbiphenyl (**8**), 4,4'-bis(9-carbazolyl)-2,2'-bis(trifluoromethyl)biphenyl (**9**),³⁰ 4,4'-bis(3-methylcarbazolyl)-2,2'-bis(trifluoromethyl)biphenyl (**10**), and 4,4'-bis(3,6-dimethylcarbazolyl)-2,2'-bis(trifluoromethyl)biphenyl (**11**) were prepared according to the procedure given for **7**.

4,4'-Bis(9-carbazolyl)-2,2'-dimethylbiphenyl (**CDBP**). Yield: 0.59 g (50 %). EI-MS m/z : 512 (100, M^+). $^1\text{H-NMR}$ (300 MHz, CDCl_3), δ (ppm): 8.20 (d, 4H), 7.58-7.45 (m, 14H), 7.36-7.31 (m, 4H), 2.31 (s, 6H). $^{13}\text{C-NMR}$ (75 MHz, CDCl_3), δ (ppm): 140.96, 140.01, 137.95, 136.92, 130.81, 128.36, 125.94, 124.34, 123.42, 120.36, 119.94, 109.94, 20.17. T_m : $-\text{°C}$; T_g : 94°C.

4,4'-Bis(3,6-dimethylcarbazolyl)-2,2'-dimethylbiphenyl (**8**). Yield: 0.7 g (50 %). EI-MS m/z : 568 (100, M^+). $^1\text{H-NMR}$ (300 MHz, CDCl_3), δ (ppm): 7.93 (ds, 4H), 7.52-7.40 (m, 10H), 7.26 (dd, 4H), 2.57 (s, 12H), 2.28 (s, 6H). $^{13}\text{C-NMR}$ (75 MHz, CDCl_3), δ (ppm): 139.64, 139.40, 137.82, 137.32, 130.75, 129.06, 128.01, 127.07, 123.98, 123.46, 120.22, 109.60, 21.45, 20.19. T_m : 277°C; T_g : 121°C.

4,4'-Bis(9-carbazolyl)-2,2'-bis(trifluoromethyl)biphenyl (**9**). Yield: 0.71 g (62 %). EI-MS m/z : 620 (100, M^+). $^1\text{H-NMR}$ (300 MHz, CDCl_3), δ (ppm): 8.20 (d, 4H), 8.09 (d, 2H), 7.93 (dd, 2H), 7.71 (d, 2H), 7.55-7.48 (m, 8H), 7.40-7.35 (m, 4H). $^{13}\text{C-NMR}$ (75 MHz, CDCl_3), δ (ppm): 140.41, 138.33, 135.32, 133.49, 133.41, 130.90 (q, 2J (C-F) = 31.5 Hz), 129.15, 126.48, 124.68, 123.83, 123.44 (q, 1J (C-F) = 272.3 Hz), 120.76, 120.60, 109.50. T_m : 232°C; T_g : 100°C.

4,4'-Bis(3-methylcarbazolyl)-2,2'-bis(trifluoromethyl)biphenyl (**10**). Yield: 0.8 g (55 %). EI-MS m/z : 648 (100, M^+). $^1\text{H-NMR}$ (300 MHz, CDCl_3) δ (ppm): 8.15 (d, 2H), 8.07 (d, 2H), 7.99 (m, 2H), 7.86 (dd, 2H), 7.68 (d, 2H), 7.54-7.30 (m, 10H), 2.60 (s, 6H). $^{13}\text{C-NMR}$ (75 MHz, CDCl_3), δ (ppm): 140.56, 138.66, 138.51, 135.10, 133.37, 130.82 (q, 2J (C-F) =

30.8 Hz), 130.22, 128.90, 127.63, 126.20, 124.48, 123.99, 123.74, 123.46 (q, 1J (C-F) = 273.8 Hz), 120.56, 120.50, 109.45, 109.22, 21.43. T_m : 210°C; T_g : 105°C.

4,4'-Bis(3,6-dimethylcarbazolyl)-2,2'-bis(trifluoromethyl)biphenyl (11). Yield: 1.4 g (56 %). EI-MS m/z : 676 (100, M^+). 1H -NMR (300 MHz, $CDCl_3$), δ (ppm): 8.05 (d, 2H), 7.95 (m, 4H), 7.85 (dd, 2H), 7.66 (d, 2H), 7.42 (d, 4H), 7.30 (dd, 4H), 2.59 (s, 12H). ^{13}C -NMR (75 MHz, $CDCl_3$), δ (ppm): 138.82, 138.71, 134.87, 133.34, 130.75 (q, 2J (C-F) = 30.8 Hz), 130.00, 128.66, 127.46, 124.25, 123.91, 123.50 (q, 1J (C-F) = 272.3 Hz), 120.46, 109.18, 21.43. T_m : 233°C; T_g : 119°C.

Conclusions

We have described a number of **CBP** derivatives in which the substitution in the 2- and 2'-position of the biphenyl and in the 3- and 6-position of the carbazole unit is systematically varied. This substitution of the parent crystalline **CBP** leads to the materials **7-11** which have a much lower tendency to crystallise. Their glass transition temperatures range from 94 – 121°C. The highest glass transition temperatures were determined for 3,6-dimethylcarbazole bearing derivatives **8** and **11** with 121°C and 119°C, respectively.

The main effect of the methyl substitution in 2- and 2'-position of the biphenyl unit is a twisting of the two central phenyl rings. Due to this electronic decoupling, the conjugation length in the molecule is limited which causes an increase of the triplet energy ΔE (T_1-S_0) from 2.58 eV for **CBP** to 2.95 – 2.97 eV for **7-11**.

Fine-tuning of the energy levels, especially the HOMO levels, can be achieved by a suitable choice of substitution pattern of the **CBP** derivatives. Cyclic voltammetry with repeated cycles shows that by introducing substituents at the 3- and 6-positions of the pendant carbazole units the oxidation to the radical cation becomes fully reversible and thus electrochemical stable host materials are accessible.

Acknowledgements

The authors thank Irene Bauer and Dr Michael Rothmann for the help during synthesis and characterisation of the novel CBP derivatives. We also thank Dr. Ingo Münster, Dr. Evelyn Fuchs and Dr. Nicolle Langer for fruitful discussions. Financial support from the BMBF project TOPAS 2012 (FKZ 13N 10447) is gratefully acknowledged. P.S. thanks the Universität Bayern e.V. for a grant.

References

- ¹ M. A. Baldo, D. F. O'Brian, Y. You, A. Shoustikov, S. Sibley, M. E. Thompson, S. R. Forrest, *Nature (London)*, 1998, **395**, 151-154.
- ² D. F. O'Brian, M. A. Baldo, M. E. Thompson, and S. R. Forrest, *Appl. Phys. Lett.*, 1999, **74**, 4, 442-444.
- ³ M. A. Baldo, S. Lamansky, P. E. Burrows, M. E. Thompson, and S. R. Forrest, *Appl. Phys. Lett.*, 1999, **75**, 4-6.
- ⁴ S. Tokito, T. Iijima, T. Tsuzuki, F. Sato, *Appl. Phys. Lett.*, 2003, **83**, 2459-2461.
- ⁵ C. Adachi, M. A. Baldo, M. E. Thompson, S. R. Forrest, *J. Appl. Phys.*, 2001, **90**, 5048-5051.
- ⁶ S. Lamansky, P. Djurovich, D. Murphy, F. A. Razzaq, C. Adachi, P.E. Burrows, S. R. Forrest, M. E. Thompson, *J. Am. Chem. Soc.*, 2001, **123**, 4304-4312.
- ⁷ V. Adamovich, J. Brooks, A. Tamayo, A. M. Alexander, P. Djurovich, B.W. D'Andrade, C. Adachi, S. R. Forrest, M. E. Thompson, *New J. Chem.*, 2002, **26**, 1171-1178.
- ⁸ R. J. Holmes, S. R. Forrest, Y. J. Tung, R. C. Kwong, J. J. Brown, S. Garon, M. E. Thompson, *Appl. Phys. Lett.*, 2003, **82**, 2422-2424.
- ⁹ S. Tokito, T. Iijima, Y. Suzuri, H. Kita, T. Tsuzuki, F. Sato, *Appl. Phys. Lett.*, 2003, **83**, 569-571.
- ¹⁰ I. Tanaka, Y. Tabata, and S. Tokito, *Chem. Phys. Lett.*, 2004, **400**, 86-89.
- ¹¹ G. Lei, L. Wang, Y. Qiu, *Appl. Phys. Lett.*, 2004, **85**, 5403-5405.
- ¹² E. L. Williams, K. Haavisto, J. Li, G. E. Jabbour, *Adv. Mater.*, 2007, **19**, 197-202.

- 13 S.-J. Su, H. Sasabe, T. Takeda, J. Kido, *Chem. Mater.*, 2008, **20**, 1691-1693.
- 14 J. He, H. Lui, X. Dai, X. Ou, J. Wang, S. Tao, X. Zhang, P. Wang, D. Ma, *J. Phys. Chem. C*, 2009, **113**, 6761-6767.
- 15 P. Strohhriegl, J. V. Grazulevicius, *Adv. Mater.*, 2002, **14**, 1439-1452.
- 16 Y. Shirota, *J. Mater. Chem.*, 2000, **10**, 1-25.
- 17 R. Schmechel, H. Von Seggern, *Phys. Status Solidi A*, 2004, **201**, 1215-1235.
- 18 M.-H Tsai, H.-W. Lin, H.-C. Su, T.-H. Ke, C.-C. Wu, F.-C. Fang, Y.-L. Liao, K.-T. Wong, C.-I. Wu, *Adv. Mater.*, 2006, **18**, 1216-1220.
- 19 M.-H. Tsai, T.-H. Ke, H.-W. Lin, C.-C. Wu, S.-F. Chiu, F.-C. Fang, Y.-L. Liao, K.-T. Wong, Y.-H. Chen, C.-I. Wu, *Appl. Mater. Interf.*, 2009, **1**, 567-574.
- 20 M. Kuroki, Y. Tsunashima, *J. Heterocyclic Chem.*, 1981, **18**, 709-714.
- 21 E. C. Horning, M.G. Horning, G. N. Walker, *J. Am. Chem. Soc.* 1948, **70**, 3935-3936.
- 22 H.-W. Schmidt, D. Guo, *Makromol. Chem.*, 1988, **189**, 2029-2037.
- 23 J. F. Ambrose, R. F. Nelson, *J. Electrochem. Soc.*, 1968, **115**(11), 1159-1164.
- 24 J. F. Ambrose, L. L. Carpenter, R. F. Nelson, *J. Electrochem. Soc.*, 1975, **122**(7), 876-894.
- 25 H. G. Rogers, R. A. Gaudiana, W. C. Hollinsed, P. S. Kalyanaraman, J. S. Manello, C. McGowan, R. A. Minns, R. Sahatjian, *Macromolecules*, 1985, **18**, 1058-1068.
- 26 J. P Perdew, W. Yue, *Phys. Rev. B: Condens. Matter Mater. Phys.*, 1986, **33**, 8800-8802.
- 27 A. D. Becke, *Phys. Rev. A: At., Mol., Opt. Phys.*, 1988, **36**, 3098-3100.
- 28 A. Schäfer, H. Horn, R. Ahlrichs, *J. Chem. Phys.*, 1992, **97**, 2571-2577.
- 29 R. Ahlrichs, M. Bär, M. Häser, H. Horn, C. Kölmel, *Chem. Phys. Lett.*, 1989, **162**, 165-169.
- 30 Z. Ge, T. Hayakawa, S. Ando, M. Ueda, T. Akiike, H. Miyamoto, T. Kajita, M. Kakimoto, *Chem. Lett.*, 2008, **37**(3), 294-295.

7 Meta-linked CBP-Derivatives As Host Materials For A Blue Iridium Carbene Complex

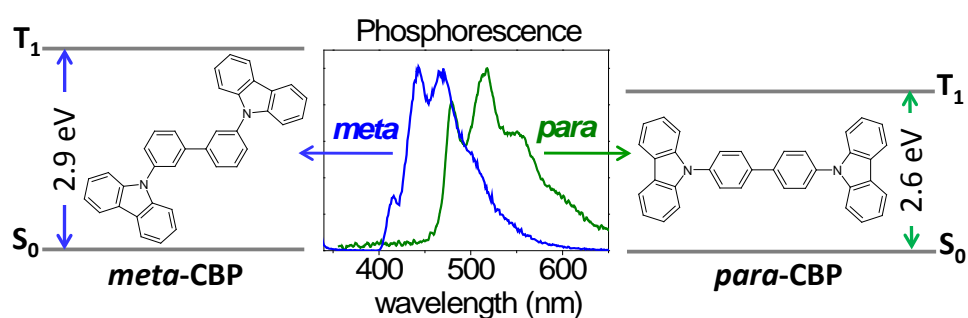
By Pamela Schrögel,^a Nicolle Langer,^b Christian Schildknecht,^b Gerhard Wagenblast,^b

Christian Lennartz,^b Peter Strohriegl^{*,a}

^aLehrstuhl Makromolekulare Chemie I, Universität Bayreuth,
D-95440 Bayreuth, Germany

^bBASF SE, D-67056 Ludwigshafen, Germany

*Corresponding author: peter.strohriegl@uni-bayreuth.de



This manuscript has been accepted by *Organic Electronics* in a slightly revised version.

Abstract

We present four derivatives of 4,4'-bis(9-carbazolyl)biphenyl (CBP) for the use as host materials in blue phosphorescent organic light emitting diodes. By replacing the *para*-linkage by a *meta*-linkage of the carbazole substituents at the central biphenyl unit materials with improved thermal and optical properties are obtained. The triplet energy of the *meta*-linked host materials is significantly increased to more than 2.90 eV compared to 2.58 eV for the *para*-linked CBP. Moreover, selective methyl substitution of the basic *meta*-CBP structure leads to materials with high glass transition temperatures up to 120°C and electrochemical stability of the oxidised species against dimerisation. In a comparative investigation the *meta*-CBP derivatives are employed in an OLED as host materials for the blue phosphorescent emitter *mer*-tris(*N*-dibenzofuranyl-*N'*-methylimidazole)iridium (III) (Ir(dbfmi)).

Keywords

CBP-derivatives, electroluminescence, blue phosphorescent OLEDs

Introduction

The presentation of OLEDs based on the electrophosphorescence was a breakthrough in device performance. With the introduction of phosphorescent emitters both the electrogenerated singlet and triplet excitons contribute to the emission of light. The fast intersystem crossing efficiently converts singlet excitons to the triplet state leading to a theoretical internal quantum efficiency of 100%.^{1,2,3} To avoid self-quenching the emitter has to be doped into an appropriate host material.⁴ For an efficient exothermic energy transfer from the host to the guest molecules, the triplet energy of the host must be higher compared to the emitter. In the case of blue emitters the host's energy gap between the singlet ground state (S_0) and the first excited triplet state (T_1) has to be at least 2.8 eV. To obtain high triplet energies for the host materials the conjugation of the materials must be limited. This requirement makes the development of host material for blue triplet emitters particularly challenging because lowering the conjugation, i.e. increasing the singlet and triplet energies may negatively affect the charge transport properties.⁵

Many organic compounds used as host materials for phosphorescent emitters are based on carbazole.^{6,7,8} One reason is the high intrinsic triplet energy of carbazole of 3.0 eV.⁹ The most prominent example for a carbazole based host material is 4,4'-bis(9-carbazolyl)-biphenyl (CBP) where the N-atoms of the carbazole units are connected with a biphenyl unit at the 4,4'-positions. The molecular structure allows for an extended conjugation of the carbazole units over the biphenyl structure leading to a decrease in triplet energy to around 2.56 eV.¹⁰ If the conjugation between the constituting units in carbazole derivatives is minimised the triplet energy can be maintained at a high level. Many approaches to confine the conjugated system in carbazole derivatives have been described in literature. One way to minimise the conjugation in carbazole based host materials introduced by Tokito et al. is to attach two methyl groups in the 2,2'-positions of the central biphenyl in CBP leading to the host material 4,4'-bis(9-carbazolyl)-2,2'-dimethylbiphenyl (CDBP).^{11,12} Due to the steric hindrance the biphenyl is forced into a tilted conformation which reduces the conjugation in the molecule and concomitantly enlarges the triplet energy to 2.79 eV. We recently reported a series of CBP-based materials with high triplet energies using a similar concept by introducing methyl and

trifluoromethyl substituents in the 2,2'-positions of the central biphenyl unit.^{13,14} Another design concept is to choose different linkers between the carbazole units such as a single phenyl ring instead of biphenyl in N,N'-dicarbazolyl-3,5-benzene (mCP)^{15,16} or non-conjugated units as, for example, an aliphatic cyclohexyl ring or an oxygen-bridge.¹⁷ In mCP another effect reduces the conjugation: instead of the *para*-connection, the two carbazole moieties are *meta*-linked over the phenyl ring.^{18,19} A major drawback of mCP however is its high crystallinity. Matrix materials with carbazole units linked to a biphenyl in the 3,3'-positions have been described in a patent of Adachi and Forrest²⁰ and a number of following patents. In the scientific literature *meta*-linked CBP derivatives are to the best of our knowledge only reported in a theoretical study about heterofluorene linker groups between the two carbazoles as alternatives to biphenyl.²¹ Besides the high triplet energy a host material has to reveal a stable amorphous phase at device operating temperatures.²² This ensures homogeneous mixing of the emitter within the matrix material and minimises the effects of concentration quenching. In addition the use of organic glasses in OLEDs helps to avoid grain boundaries which may act as trap states.^{23,24} Organic glasses can be obtained by avoiding strong intermolecular forces like hydrogen bonding or π - π stacking between the molecules. A very common design concept for molecular glasses is the space-filling star-shaped topology, as in the well-known hole transporting organic glass 4,4',4''-tris(carbazol-9-yl)triphenylamine (TCTA).²⁵ Furthermore, the introduction of bulky substituents leads to a larger intermolecular distance and a hindrance in packing and therefore to amorphous behaviour. For example, in 9-(4-tert-butylphenyl)-3,6-bis(triphenylsilyl)-carbazole (CzSi)²⁶ and 3,5-di(*N*-carbazolyl)tetraphenylsilane (SimCP)²⁷ packing of the molecules is avoided by introducing bulky triphenylsilyl groups. However, the separation of the conducting units usually leads to a decrease in charge carrier mobility.

In this work we describe the preparation, the thermal and optical characterisation along with the OLED application of four *meta*-linked **CBP**-derivatives. Materials revealing high triplet energies and amorphous behaviour with high glass transition temperatures are achieved by attaching the carbazole units at the *meta*-position of the phenyl rings of the biphenyl moiety in combination with a selective methyl substitution at the *meta*-**CBP** structure. Cyclic voltammetry studies and a comparative OLED device study employing

the new materials as host for a blue phosphorescent emitter are also presented. The molecular structures of the host materials **1-4** are depicted in Figure 1.

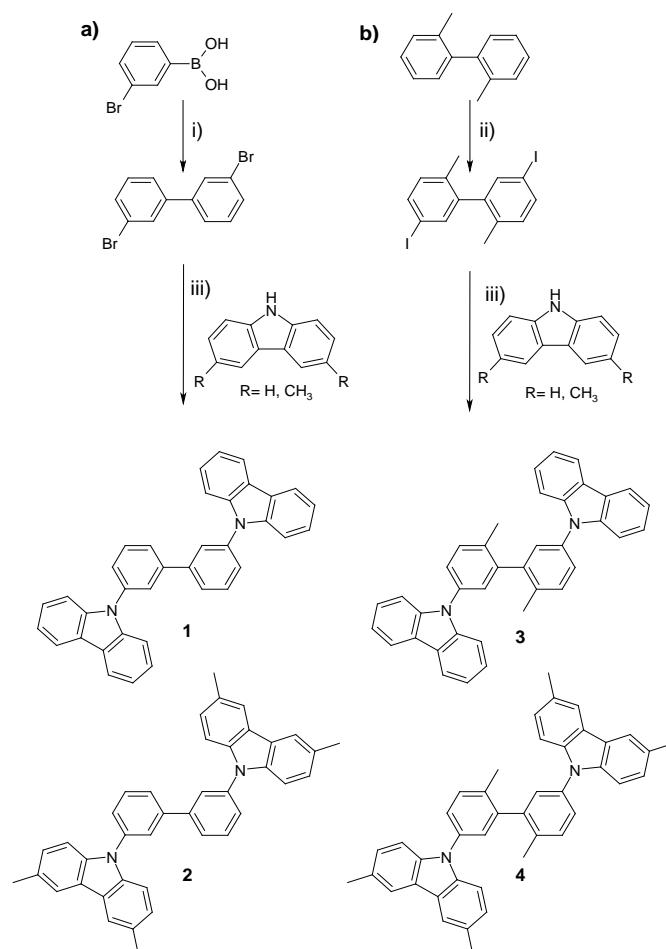


Figure 1. Chemical structures and synthetic routes to **a)** *meta*-linked CBP derivatives **1** and **2** and **b)** twisted *meta*-linked CBP derivatives **3** and **4**. Reagents and conditions: i) $\text{Cu}(\text{OAc})_2$, DMF, 100°C , 90 min; ii) I_2 , HIO_3 , H_2SO_4 , H_2O , CCl_4 , acetic acid, 80°C , 18 h; iii) Cu , K_2CO_3 , 18-crown-6, *o*-dichlorobenzene, reflux, 24 h.

2. Results and Discussion

2.1. Synthesis

In Figure 1a the synthetic route to the *meta*-linked CBP derivatives **1** and **2** is depicted. In a copper-mediated homocoupling reaction 3-bromophenylboronic acid reacts to 3,3'-dibromobiphenyl.²⁸ An Ullmann-type reaction of dibromobiphenyl with carbazole or 3,6-dimethylcarbazole¹³ yields the host materials.

To obtain the twisted *meta*-linked CBP-derivatives **3** and **4**, first, 5,5'-diiodo-2,2'-dimethyl-biphenyl was prepared by direct iodination²⁹ of 2,2'-dimethylbiphenyl with

iodine and iodic acid in acetic acid (Figure 1b). Via 2D ^1H -NMR experiments (see Supplementary Information) the selective iodination at the 5- and 5'-positions of the biphenyl could be confirmed. Here, the inductive effect of the methyl groups in the 2- and 2'-positions of the biphenyl increases the electron density in the 5- and 5'-positions and favours the electrophilic attack of I^+ . We consider this 5,5'-diiodo-2,2'-dimethylbiphenyl unit as a versatile building block for the synthesis of materials with confined conjugation which, to the best of our knowledge, has not been described in the literature before. The tilted *meta*-linked CBP derivatives **3** and **4** were prepared via the Ullmann-type reaction of 5,5'-diiodo-2,2'-dimethylbiphenyl with carbazole or 3,6-dimethylcarbazole.¹³

Mass spectrometry, ^1H - and ^{13}C -NMR spectroscopy were used to identify the materials. The data are given in the experimental part. All materials were purified by repeated zone sublimation.

2.2 Thermal properties

We examined the thermal properties of the *meta*-linked CBP derivatives **1-4** by thermal gravimetric analysis (TGA) and differential scanning calorimetry (DSC) in nitrogen atmosphere at a scanning rate of 10 K min^{-1} . All results are summarised in Table 1.

Table 1. Thermal properties of CBP and the *meta*-linked host materials **1-4**.

	$T_g / ^\circ\text{C}$	$T_m / ^\circ\text{C}$	$T_{cr} / ^\circ\text{C}$	$T_{ID}^a / ^\circ\text{C}$
CBP	--	283	205 ^b	365
1	--	271	191 ^b	315
2	107	270	184 ^c	349
3	108	237	176 ^c	319
4	120	212	--	319

T_g : glass-transition temperature, T_m : melting temperature, T_{cr} : crystallization temperature and T_{ID} : initial decomposition temperature.

[a] T_{ID} is the temperature at which an initial mass loss was observed in a thermogravimetric experiment with a heating rate of 10 K min^{-1} in a nitrogen atmosphere.

[b] Observed during cooling scan.

[c] Observed only during the heating scan.

Both the *para*-linked CBP and the *meta*-linked **1** show crystalline behaviour in the DSC experiment. For the *meta*-derivative **1** the melting and the crystallisation are observed at around 10°C lower temperatures than for CBP. Methyl substitution at the pendant carbazoles in **2** leads to a material with a much lower tendency to crystallise. The glass transition of **2** is observed at 107°C and the recrystallisation is observed at a high temperature of 184°C. In compound **3** the introduction of methyl groups only at the central biphenyl unit leads to nearly the same glass transition temperature of 109°C and nearly the same recrystallisation temperature of 176°C. The biphenyl substitution in combination with the methyl substitution at the carbazoles increases the T_g even to 120°C for compound **4**. Moreover, for compound **4** crystallisation is observed neither in the cooling nor in the heating cycle which renders **4** the derivative of the series with the highest tendency to form a molecular glass. This thermal investigation shows that the introduction of additional methyl groups at the central biphenyl and/or the adjacent carbazole moieties of the *meta*-linked molecular structure has beneficial effects on the thermal properties, i.e. amorphous materials with high T_g s in the range of 107°C to 120°C are obtained.

2.3 Optical properties

The room temperature UV/Vis absorption and fluorescence spectra of 10^{-5} M cyclohexane solutions of **1-4** are depicted on top of Figure 2. Compounds **1** and **3** as well as compounds **2** and **4** show very similar spectra. In each compound the absorption and photoluminescence behaviour is dominated by optical transitions localised on the carbazole units. Since the chromophor in compounds **1** and **3** and in compounds **2** and **4** are identical it is not surprising that these two pairs of materials show nearly the same absorption and fluorescence spectra. For compound **2** and **4** the additional methyl substituents on the chromophor 3,6-dimethylcarbazole cause a bathochromic shift of 13 nm in the absorption and emission spectra compared to compounds **1** and **3**.

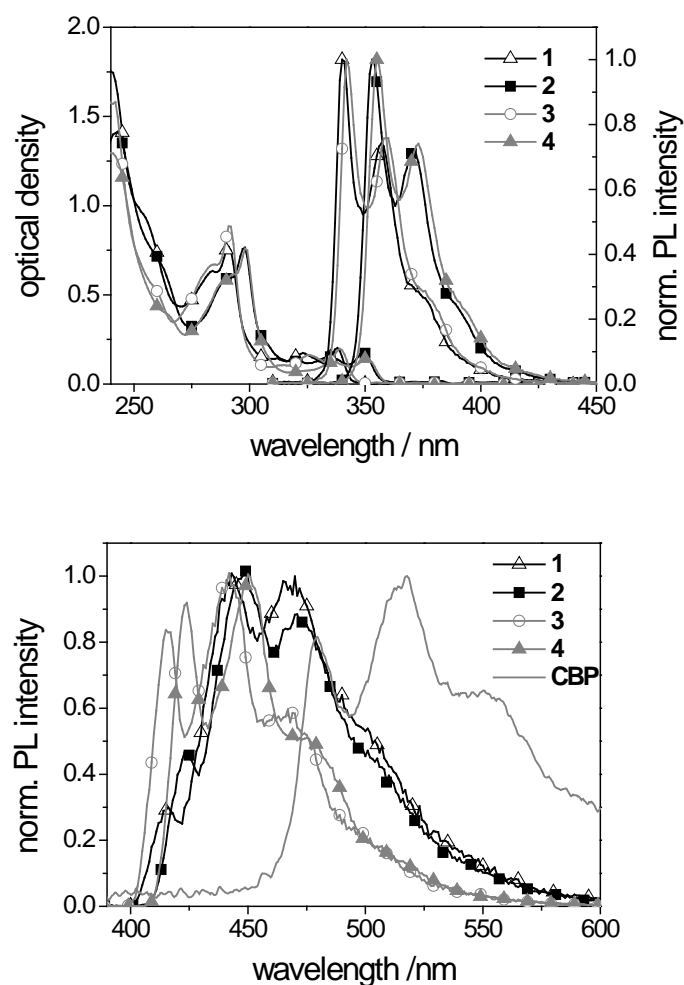


Figure 1. Top: Absorption and fluorescence spectra of **1-4** taken in 10^{-5} M solutions in cyclohexane at 300 K. Bottom: Normalised phosphorescence spectra of CBP and **1-4** measured in 2 wt% solid solution of the compounds in PMMA at 5K.

As a prerequisite for the application of **1-4** as host materials, their triplet energy has to be higher compared to that of the blue phosphorescent emitter. By measuring phosphorescence at low temperatures the triplet energies can be experimentally determined as the highest energy peak of luminescence.

In order to understand how the *meta*-linkage of the carbazole units affects the triplet energy we compare the phosphorescence spectra of the *para*-linked **CBP** and the *meta*-linked derivative **1-4**. The most striking difference in the normalised spectra (see Figure 2, bottom) is the remarkable blue shift in phosphorescence of **1-4** compared with **CBP**. The emission of **1**, for example, is shifted to lower wavelengths by 65 nm compared with **CBP**, corresponding to triplet energies of 2.98 eV for **1** and 2.58 eV for **CBP**. This is a

proof of the design concept of *meta*-connection to achieve high triplet energies. In fact, the methyl substitution at the central biphenyl moiety is expected to lead to even higher triplet energies by introducing torsion between the phenyl rings of the biphenyl unit as is well known from CDBP. However, in the case of the *meta*-linked host materials the additional twisted molecular structure has only minor effects on the emission characteristics. Similar to the emission at room temperature, compounds **1** and **3** and compounds **2** and **4** reveal the highest energy peaks at the same wavelength, while the shape of the phosphorescence spectra is different. In the case of the twisted methyl substituted biphenyl containing compounds **3** and **4** the 0-0 transition is more pronounced and the width of the spectra is smaller than for **1** and **2**. As an effect of the methyl substitution at the 3- and 6-position of the carbazole units we observe again a small bathochromic shift of ca. 10 nm for compounds **2** and **4** compared to **1** and **3**. All results of the photo physical investigations of CBP and the *meta*-linked matrix materials **1-4** are summarised in Table 2.

Table 2. Optical properties and energy levels of CBP and the *meta*-linked host materials **1-4**.

	λ_{EA}^a	λ_{EA}^b	$\lambda_{em}^{RT,c}$	$\lambda_{em}^{5K,d}$	$\lambda_{em}^{5K,e}$	HOMO	LUMO	HOMO ^g	LUMO ^h
	[nm]	[nm]	[nm]	[nm]	[nm]	[eV]	[eV]	[eV]	[eV]
	solution	film	solution	film	film	calculated		experimental	
CBP	350	357	356, 374	484	477	-5.58	-1.78	-5.63	-2.16
1	344	354	340, 357	421	415	-5.71	-1.77	-5.65	-2.15
2	357	365	353, 370	452 ^f	421	-5.48	-1.71	-5.56	-2.17
3	346	354	342, 359	423	415	-5.64	-1.51	-5.65	-2.16
4	358	369	355, 373	431	421	-5.44	-1.47	-5.53	-2.17

[a] Absorption edge measured in 10^{-5} M cyclohexane solutions at room temperature.

[b] Absorption edge measured on neat films at room temperature.

[c] Wavelengths of the intensity maxima of the fluorescence at 300 nm excitation of 10^{-5} M cyclohexane solutions at room temperature.

[d] Measured on film samples (100%) at 5 K.

[e] Measured in 2 wt-% PMMA at 5 K.

[f] No 0-0 transition is observed.

[g] Estimated from the half-wave potential of the first oxidation in the cyclic voltammetry experiment.

[h] Estimated from the HOMO values and the optical band gap (determined from the UV/Vis absorption onset of neat films).

2.4 Cyclic voltammetry

The electrochemical behaviour of **1-4** was investigated by cyclic voltammetry in a conventional three-electrode setup using a platinum working electrode, a platinum wire as counter electrode, and a Ag/AgNO₃ reference electrode. Particularly, the oxidation behaviour of **1-4** in dichloromethane solutions was studied. From the half-wave potential of the first oxidation relative to ferrocene the HOMO value of the compounds can be deduced. By adding the optical band gap to the HOMO value the LUMO value can be estimated. As the cyclic voltammetry is measured in solution and not in the solid state the values of HOMO and LUMO may differ from the solid state values in an OLED. Both the experimentally received and the calculated values for the energy levels of CBP and of **1-4** are listed in Table 2. The *meta*-linked compounds **1** and **3** with unsubstituted carbazole units reveal almost the same energy levels as for CBP. In contrast, **2** and **4** show ca. 10 mV higher HOMO levels which can be attributed to the inductive effect of the additional methyl groups in the 3- and 6-positions of the carbazole units. The cyclic voltammetry experiments show that the behaviour upon oxidation is clearly dominated by the molecules' site with the highest electron density, i.e. the carbazole moieties. Contrary to the theoretical expectations, the substitution on the central biphenyl unit does not affect the HOMO levels and fairly no effects of the different substitution pattern on the LUMO levels are observed.

Charge transport processes in organic semiconductors involve the formation of radical anions and cations. Thus, investigations of the electrochemical stability can give information about the stability of the materials in OLED devices. To evaluate the electrochemical stability of the materials we carried out multicycle experiments. The cyclic voltammograms showing five repeated oxidation cycles of **1** and **2** in $2 \cdot 10^{-3}$ M dichloromethane solutions are given as Supplementary Information. In the case of **1**, the oxidation cycles are not reproducible. After the first reduction into the uncharged molecule at 0.88 V an additional reduction at around 0.59 V is observed. The latter can be attributed to new oligomeric species formed during dimerisation reactions at the active 3- and 6-positions of the carbazole units after the first oxidation of the molecule.^{30,31} As the oligomeric species is oxidised more easily the corresponding oxidation process takes place at a lower voltage of around 0.70 V. In contrast, **2** reveals a

fully reversible oxidation behaviour. The methyl substitution at the adjacent carbazole units blocks the electroactive 3- and 6-positions and renders the oxidised species stable against dimerisation in solution. The same stability of the radical cations was also found for compound **4** in contrast to **3**.

2.5 Phosphorescent Organic Light-Emitting Diodes

To demonstrate the potential of **1-4** as host materials for blue phosphorescent emitters OLEDs were fabricated. First, we tested the materials in the setup shown in Figure 3. On top of the ITO glass substrate poly(3,4-ethylene-dioxy-thiophene):poly(styrene-sulfonate) (PEDOT:PSS) was applied by spin coating as hole injection layer followed by 10 nm DPBIC p-doped with molybdenum(VI) oxide as hole transporting layer. An additional 10 nm thick layer of DPBIC followed as exciton and electron blocker. The 20 nm emission layer consisted of 5 % Ir(dbfmi) doped into the *meta*-linked CBP host materials. 10 nm of the host material were deposited as hole and exciton blocking layer followed by 20 nm of caesium carbonate doped 2,9-dimethyl-4,7-diphenyl-1,10-phenanthroline (BCP) as electron transporting layer. As cathode 1 nm Cs₂CO₃ and 100 nm aluminium were deposited.

The turn-on voltage at 1 cd m⁻² of 4.5 V is quite high and luminances of 100 cd m⁻² and 1000 cd m⁻² are achieved at voltages of 5.6 V and 6.8 V, respectively. In some cases we observed a small contribution of the hole transporting material DPBIC to the emission. This indicates that the exciton formation is shifted towards the hole conducting layer. We attribute this to the high energy barrier for hole injection from the DPBIC into the emission layer causing as well the high turn-on voltage. In contrast, electrons do not have to overcome major energy barriers.

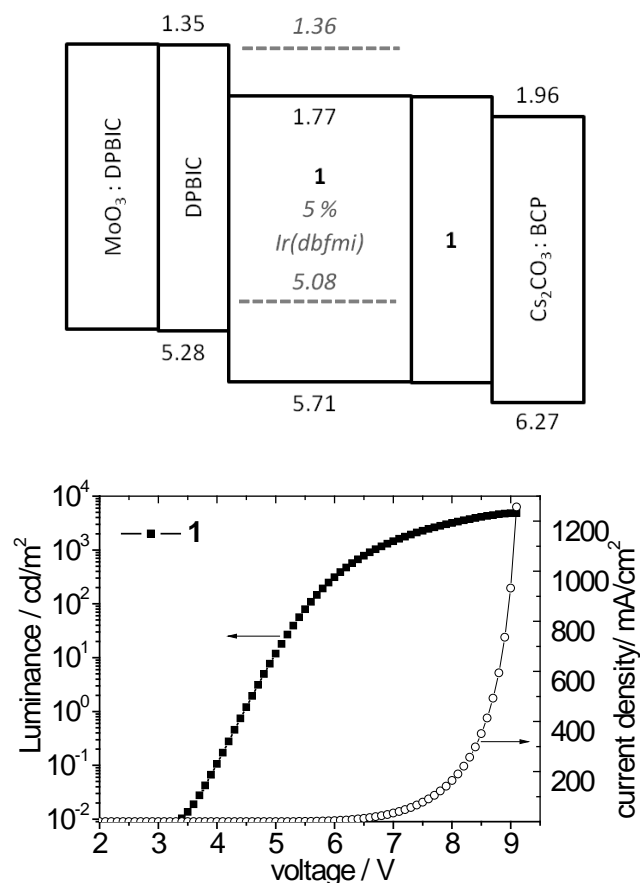


Figure 2. Top: Energy level diagram of the OLED device employing **1** as host for Ir(dbfmi); Ionisation potentials and electron affinities obtained from calculations are indicated. The grey dotted lines represent the levels of the emitter Ir(dbfmi). **Bottom:** Luminance-voltage plot (filled symbols) and current density-voltage characteristic (open symbols).

To improve the hole injection into the emission layer we coevaporated the hole transporting DPBIC into the emission layer providing a barrier free path for holes. The optimised device setup and the molecular structures of the materials used are shown on top of Figure 4. 10 nm molybdenum(VI) oxide doped DPBIC as hole transporting layer and an additional 10 nm thick layer of DPBIC were used as exciton and electron blocker. The 20 nm thick emission layer comprises a mixed matrix system of the carbazole containing host materials **1-4** with DPBIC and the blue emitter Ir(dbfmi) in the ratio 75 : 20 : 5. 2,8-bis(triphenylsilyl)-dibenzofuran (DBFSi) (5 nm) was used as exciton and hole blocking material followed by 5 nm BCP and 40 nm BCP n-doped with Cs₂CO₃. As cathode 1 nm Cs₂CO₃ and 100 nm aluminium were deposited.

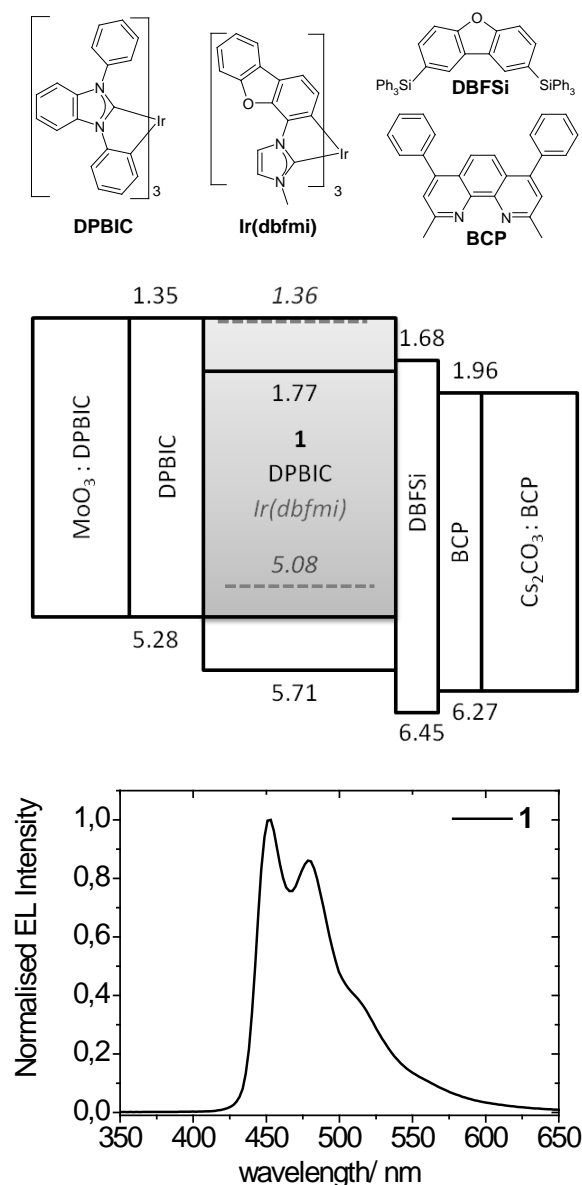


Figure 3. Top: Energy level diagram of the optimised OLED device employing **1** as host for Ir(dbfmi) with chemical structures of the materials used; Ionisation potentials and electron affinities obtained from calculations are indicated. The grey dotted lines represent the levels of the emitter Ir(dbfmi). **Bottom:** Electroluminescence spectrum of the devices with **1** as host material for Ir(dbfmi). CIE coordinates: $x = 0.16$, $y = 0.18$.

In the electroluminescence spectrum of the optimised device setup the pure emission of the phosphor Ir(dbfmi) can be observed with CIE-coordinates of $x = 0.16$ and $y = 0.18$ (Figure 4, bottom). By decreasing the hole injection barrier in the mixed matrix system the exciton formation zone could be successfully separated from the hole transporting layer. Moreover, the applied voltages at 100 and 1000 cd m^{-2} could be significantly lowered, to 3.5 V and 4.4 V, respectively, in the case of host **1** (see Figure 5).

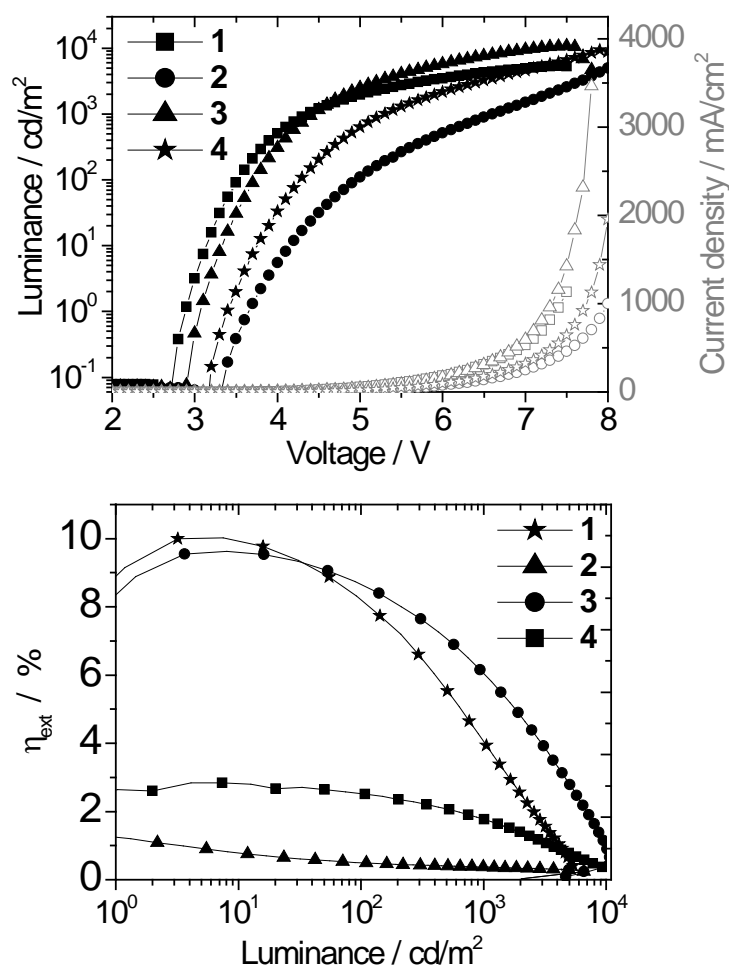


Figure 4. Top: Luminance-voltage curves (black filled symbols) and current density-voltage characteristics (grey open symbols) of the optimised device setup. **Bottom:** External quantum efficiency-luminance curves of the devices with **1-4** as host material for Ir(dbfmi).

Peak luminances are 5300 cd m⁻² for **1**, 5000 cd m⁻² for **2**, 10800 cd m⁻² for **3** and 9300 cd m⁻² for **4**. For hosts **1** and **3** higher luminances are reached at lower voltages than for **2** and **4**. Comparing the efficiencies of the four *meta*-linked CBP-derivatives **1-4**, the compounds **2** and **4** with methyl substituents at the 3- and 6-positions of the carbazole units show significantly lower efficiencies than **1** and **3**. As evident from the current density-voltage-plot in Figure 5, higher operation voltages are needed in the devices employing the host materials **2** and **4**. We assume that the transport properties of **2** and **4** with methyl substituents at the carbazole units are worse compared to **1** and **3** with unsubstituted carbazole units. In contrast, **1** and **3** give similar performances with slightly better values for **3** at higher luminances. The highest efficiency was achieved for

3 with an external quantum efficiency of 8.7 % and a power efficiency of 10.2 lm W⁻¹ at 100 cd m⁻² rolling to 6.1 % and 6.0 lm W⁻¹ at 1000 cd m⁻², respectively. All performance data are summarised in Table 3.

Table 3. Performance data at 100 cd m⁻² and 1000 cd m⁻² using **1-4** as host materials for the blue emitter Ir(dbmfi).

	at 100 cd m ⁻²				at 1000 cd m ⁻²			
	Voltage	η_c	η_p	η_{ext}	Voltage	η_c	η_p	η_{ext}
	[V]	[cd A ⁻¹]	[lm W ⁻¹]	[%]	[V]	[cd A ⁻¹]	[lm W ⁻¹]	[%]
1	3.5	11.5	10.2	8.2	4.4	5.7	4.1	4.1
2	4.9	0.9	0.6	0.5	6.6	0.6	0.3	0.4
3	3.7	12.2	10.2	8.7	4.4	8.5	6.0	6.1
4	4.3	4.5	3.3	2.6	5.3	3.1	1.9	1.8

η_c : current efficiency; η_p : power efficiency; η_{ext} : external quantum efficiency.

The large differences in device performance as evident from Table 3 are quite surprising as the chemical structures of all hosts **1-4** are very similar. These findings show that each combination of emitter and host needs to be chosen very carefully as the host-emitter-system is very sensitive to even small structural variations which may change the charge-carrier balance in the device or the chemical compatibility of host and emitter. Both effects in conjunction with the relatively long triplet lifetime of Ir(dbmfi) of ~20 μsec ⁴¹ could negatively influence the device performance.

3. Experimental

Materials. All chemicals and reagents were used as received from commercial sources without further purification. The solvents for reactions and purification were all distilled before use.

Characterization. ¹H- and ¹³C-NMR spectra were recorded with a Bruker AC 300 (300 MHz, 75 MHz) and CDCl₃ as solvent. All data are given as chemical shifts δ (ppm) downfield from Si(CH₃)₄. For optical measurements, 10⁻⁵ M cyclohexane (Ultrasolv®)

solutions of the materials as well as thin films on quartz substrates were prepared by spincoating. The UV/VIS spectra were measured in solution and on neat films with a Hitachi U-3000 spectrometer. Fluorescence spectra in solution were obtained from a Shimadzu spectrofluorophotometer RF-5301PC using excitation at 300 nm. Phosphorescence spectra of thin films have been measured at 5 K (Helium cryostat Optistat CF from Oxford Instruments) applying the technique of time-gated spectroscopy (with fluorescence and phosphorescence lifetime spectrometer FLSP 920 from Edinburgh Instruments). For differential scanning calorimetry measurements (DSC) a Diamond DSC apparatus from Perkin Elmer was used (heating/cooling rate 10 K/min, nitrogen). Thermogravimetric analysis (TGA) was performed on a Mettler Toledo TGA/SDTA815e machine at a heating rate of 10 K/min under nitrogen. Cyclic voltammetry measurements were carried out in absolute solvents measuring at a platinum working electrode versus a Ag/AgNO₃ reference electrode. Each measurement was calibrated against an internal standard (ferrocene/ferrocenium redox system). The purity of the target compounds was checked with a Waters size exclusion chromatography system (SEC) for oligomers (analytical columns: crosslinked polystyrene gel (Polymer Laboratories), length: 2×60 cm, width: 0.8 cm, particle size: 5 μm, pore size 100 Å, eluent THF (0.5 mL/min, 80 bar), polystyrene standard).

Computational Methods. The transport levels of the materials used were determined via density functional calculations. For the ionisation potential and the electron affinity first the geometry of the neutral as well as the charged states were optimised using the BP86-functional^{32,33} in combination with a split-valence basis set (SV(P)) including polarization functions on all heavy atoms³⁴. For iridium an effective core potential was employed.³⁵ For the energetics we performed single point calculations at the optimised geometries using the same functional in combination with a TZVP-basis set.³⁶ To account for dielectric solid state effects a UPS/IEPS-calibrated version of the conductor like screening model (COSMO)³⁷ was used in conjunction with these single point calculations. All calculations were carried out with the turbomole program package.³⁸

Synthetic Procedures. The synthesis of tris[(3-phenyl-1*H*-benzimidazol-1-yl-2(3*H*)-yliden-1,2-phenylene]-iridium (DPBIC),³⁹ 2,8-bis(triphenylsilyl)-dibenzofuran (DBFSi)⁴⁰, *mer*-tris(*N*-dibenzofuranyl-*N'*-methylimidazole)-iridium (III) (Ir(dbfmi))^{40,41} and 3,6-dimethyl-carbazole¹³ is described in literature.

3,3'-Dibromobiphenyl was synthesized according to a procedure reported by Demir et al.²⁸ Yield: 43 %. EI-MS *m/z*: 312 (100, M⁺), 232 (5), 152 (95). ¹H-NMR (300 MHz, CDCl₃), δ (ppm): 7.70 (dd, 2H), 7.52-7.46 (m, 4H), 7.31 (dd, 2H). ¹³C-NMR (75 MHz, CDCl₃), δ (ppm): 142.11, 131.16, 130.74, 130.50, 126.09, 123.33.

5,5'-Diiodo-2,2'-dimethylbiphenyl. 2,2'-Dimethylbiphenyl (9.9 g, 54 mmol) in 120 mL of acetic acid and 5.5 mL of water were heated to 90°C to get a clear solution. After the addition of iodine (10.9 g, 43 mmol), iodic acid (5.7 g, 32 mmol), 5.5 mL of sulphuric acid and 5.5 mL of tetrachloromethane the solution was stirred at 80 °C for 18 h. The excess of iodine was removed by adding a solution of sodium hydrogen sulphide. The product was extracted with dichloromethane and washed several times with water. After drying the organic layer over anhydrous sodium sulfate, the solvent was evaporated. The resulting yellowish oily product was recrystallized from ethyl acetate to yield 6.9 g (16 mmol, 30 %) of a white solid. EI-MS *m/z*: 434 (100, M⁺), 180 (50), 165 (47). ¹H-NMR (300 MHz, CDCl₃), δ (ppm): 7.58 (dd, 2H), 7.42 (ds, 2H), 7.00 (d, 2H). 1.99 (s, 6H). ¹³C-NMR (75 MHz, CDCl₃), δ (ppm): 142.30, 137.65, 136.56, 135.48, 131.83, 90.41, 19.38.

General procedure for the Ullmann- type reaction:

Dihalogenobiphenyl (2.3 mmol), carbazole (5.06 mmol), potassium carbonate (2.5 g, 18.4 mmol), copper powder (0.58 g, 9.2 mmol) and 18-crown-6 (0.12 mg, 0.46 mmol) were refluxed in 15 mL of *o*-dichlorobenzene in an argon atmosphere for 24 h. Copper and inorganic salts were filtered off and the solvent was evaporated. Column chromatography on silica gel with mixtures of hexane/tetrahydrofurane as eluent yielded the products **1** – **4** as white solids.

3,3'-Bis(carbazolyl)biphenyl (1). Yield: 47 %. EI-MS *m/z*: 484 (100, M⁺), 316 (10), 234 (39). ¹H-NMR (300 MHz, CDCl₃), δ (ppm): 8.17 (d, 4 H), 7.88 (m, 2H), 7.75 (dt, 2H), 7.70 (dd, 2 H), 7.60 (dt, 2H), 7.51 (d, 4H), 7.43 (dt, 4H), 7.31 (dt, 4H). (¹³C-NMR (75 MHz,

CDCl₃), δ (ppm): 142.42, 141.19, 138.82, 130.84, 126.80, 126.52, 126.39, 126.10, 123.79, 120.71, 120.40, 110.08.

3,3'-Bis(3,6-dimethylcarbazolyl)biphenyl (2). Yield: 55 %. EI-MS m/z : 540 (100, M⁺), 345 (5), 270 (24). ¹H-NMR (300 MHz, CDCl₃), δ (ppm): 7.92 (m, 4H), 7.86 (m, 2H), 7.70 (dt, 2H), 7.66 (dd, 2H), 7.57 (dt, 2H), 7.38 (d, 4H), 7.24 (dd, 4H), 2.56 (s, 3H). ¹³C-NMR (75 MHz, CDCl₃), δ (ppm): 142.38, 139.63, 139.24, 130.70, 129.55, 127.52, 126.41, 126.05, 125.76, 123.84, 120.56, 109.75, 21.74.

3,3'-Bis(carbazolyl)-6,6'-dimethylbiphenyl (3). Yield: 50 %. EI-MS m/z : 512 (100, M⁺), 329 (8), 257 (17), 166 (12). ¹H-NMR (300 MHz, CDCl₃), δ (ppm): 8.15 (d, 4H), 7.55-7.39 (m, 14H), 7.32-7.26 (m, 4H), 2.33 (s, 6H). ¹³C-NMR (75 MHz, CDCl₃), δ (ppm): 142.51 141.25 135.65, 135.46, 131.85, 127.96 126.45, 126.26, 123.67, 120.65, 120.20, 110.09, 20.11.

3,3'-Bis(3,6-dimethylcarbazolyl)-6,6'-dimethylbiphenyl (4). Yield: 55 %. EI-MS m/z : 568 (100, M⁺), 358 (15), 284 (29), 192 (24). ¹H-NMR (300 MHz, CDCl₃), δ (ppm): 7.90 (s, 4H), 7.52-7.45 (m, 4H), 7.41-7.38 (m, 4H), 7.33 (d, 4H), 7.21(d, 4H), 2.55 (s, 12H), 2.30 (s, 6H). ¹³C-NMR (75 MHz, CDCl₃), δ (ppm): 142.47, 139.72, 136.06, 134.98, 131.70, 129.30, 127.69, 127.39, 126.10, 123.70, 120.49, 109.74, 21.73, 20.06.

OLED fabrication. The organic layers were deposited by thermal evaporation in high vacuum (<10⁻⁶ mbar) onto indium-tin-oxide (ITO, 10 ohm/square) precoated glass substrates. Prior to use the ITO glass was degreased using organic solvents and cleaned using an UV-ozon oven for 30 minutes. The organic layers and the metal cathode were evaporated without breaking the vacuum. The current density-luminance-voltage (J-L-V) characteristics of the OLEDs were measured by a Keithley source meter 2400 and a Konica Minolta CS-200, respectively. EL spectra were taken by a CCD spectral analyser by Zeiss. EQEs were calculated from the luminance, current density, and EL spectrum, assuming a Lambertian distribution.

4. Conclusions

We have described a series of CBP derivatives with a *meta*-linkage of the carbazole moieties to the central biphenyl unit. By selective methyl substitution at two sites of the basic *meta*-CBP structure, the 3- and 6-position of the pendant carbazoles and at the 6- and 6'-position of the biphenyl unit, the tendency to crystallise could be lowered. Glass transition temperatures in the range of 107°C to 120°C were achieved. The *meta*-linkage reduces the conjugation of the molecules effectively, leading to high triplet energies in the range of 2.93 eV to 2.98 eV compared with 2.58 eV for CBP. Here, the additional twist by the methyl substitution at the biphenyl unit does not increase the triplet energy any further, but narrows the phosphorescence spectra of **3** and **4** compared with **1** and **2**. Introducing methyl groups at the 3- and 6-position of the pendant carbazole units in the matrix materials **2** and **4** leads to electrochemical stability of the oxidised species in cyclic voltammetry. The highest efficiencies were achieved with the twisted *meta*-linked derivative **3** giving external quantum efficiencies of 8.7 % and 6.1 % and power efficiencies of 10.2 lm W⁻¹ and 6.0 lm W⁻¹ at 100 cd m⁻² and 1000 cd m⁻², respectively. These first results show that *meta*-linked CPB-derivatives are suited host materials for blue emitters with saturated blue phosphorescence at 450 nm.

Acknowledgement

We thank Irene Bauer for the help during synthesis and characterisation of the host materials and Christian Bonsignore and Mustapha Al-Helwi for their support during the device fabrication and characterisation. We also thank Dr. Ingo Münster, Dr. Evelyn Fuchs and Dr. Soichi Watanabe for scientific discussions. Financial support from the BMBF project TOPAS 2012 (FKZ 13N 10447) is gratefully acknowledged. P.S. thanks the Universität Bayern e.V. for a grant. Supporting Information is available online from Wiley InterScience or from the author.

References

- ¹ M. A. Baldo, D. F. O'Brian, Y. You, A. Shoustikov, S. Sibley, M. E. Thompson, S. R. Forrest, *Nature (London, U. K.)* **1998**, *395*, 151-154.
- ² D. F. O'Brian, M. A. Baldo, M. E. Thompson, and S. R. Forrest, *Appl. Phys. Lett.* **1999**, *74* (4), 442-444.
- ³ M. A. Baldo, S. Lamansky, P. E. Burrows, M. E. Thompson, S. R. Forrest, *Appl. Phys. Lett.* **1999**, *75*, 4-6.
- ⁴ C. Adachi, M. A. Baldo, M. E. Thompson, S. R. Forrest, *J. Appl. Phys.* **2001**, *90*, 5048-5051.
- ⁵ A. B. Padmaperuma, L. S. Sapochak, P. E. Burrows, *Chem. Mater.* **2006**, *18*, 2389-2396.
- ⁶ P.-I. Shih, C.-L. Chiang, A. K. Dixit, C.-K. Chen, M.-C. Yuan, R.-Y. Lee, C.-T. Chen, E. W.-G. Diau, C.-F. Shu, *Org. Lett.* **2006**, *8*, 2799-2802.
- ⁷ M.-H. Tsai, Y.-H. Hong, C.-H. Chang, H.-C. Su, C.-C. Wu, A. Matoliukstyte, J. Simokaitiene, S. Grigalevicius, J. V. Grazulevicius, C.-P. Hsu, *Adv. Mater.* **2007**, *19*, 862-866.
- ⁸ H. Fukagawa, K. Watanabe, T. Tsuzuki, S. Tokito, *Appl. Phys. Lett.* **2008**, *93*, 133312-133314.
- ⁹ J. E. Adams, W. W. Mantulin, J. R. Huber, *J. Am. Chem. Soc.* **1973**, *95*, 5477-5481.
- ¹⁰ R. J. Holmes, S. R. Forrest, Y. J. Tung, R. C. Kwong, J. J. Brown, S. Garon, M. E. Thompson, *Appl. Phys. Lett.* **2003**, *82*, 2422-2424.
- ¹¹ S. Tokito, T. Iijima, Y. Suzuri, H. Kita, T. Tsuzuki, F. Sato, *Appl. Phys. Lett.* **2003**, *82*, 569-571.
- ¹² I. Tanaka, Y. Tabata, and S. Tokito, *Chem. Phys. Lett.* **2004**, *400*, 86-89.
- ¹³ P. Schrögel, A. Tomkevičienė, P. Strohriegl, S. T. Hoffmann, A. Köhler, C. Lennartz, *J. Mater. Chem.* **2011**, *21*, 2266-2273.
- ¹⁴ S. T. Hoffmann, P. Schrögel, M. Rothmann, R. Q. Albuquerque, P. Strohriegl, A. Köhler, *J. Phys. Chem. B* **2011**, *115* (3), 414-421.

- 15 V. Adamovich, J. Brooks, A. Tamayo, A. M. Alexander, P. Djurovich, B.W.
D'Andrade, C. Adachi, S. R. Forrest, M. E. Thompson, *New J. Chem.* **2002**, *26*,
1171-1178.
- 16 R. J. Holmes, S. R. Forrest, Y. J. Tung, R. C. Kwong, J. J. Brown, S. Garon, M. E.
Thompson, *Appl. Phys. Lett.* **2003**, *82*, 2422-2424.
- 17 J. He, H. Lui, X. Dai, X. Ou, J. Wang, S. Tao, X. Zhang, P. Wang, D. Ma, *J. Phys.*
Chem. C **2009**, *113*, 6761-6767.
- 18 S.-J. Su, T. Chiba, T. Takeda, J. Kido, *Adv. Mater.* **2008**, *20*, 2125-2130.
- 19 S.-J. Su, C. Cai, J. Kido, *Chem. Mater.* **2011**, *23* (2), 274-284.
- 20 C. Adachi, S. R. Forrest, US Patent 2002, 6 458 475.
- 21 J. Yin, S.-L. Zhang, R.-F. Chen, Q.-D. Ling, W. Huang, *Phys. Chem. Chem. Phys.*
2010, *12*, 15448-15458.
- 22 P. Strohriegel, J. V. Grazulevicius, *Adv. Mater.* **2002**, *14*, 1439-1452.
- 23 Y. Shirota, *J. Mater. Chem.* **2000**, *10*, 1-25.
- 24 R. Schmechel, H. Von Seggern, *Phys. Stat. Sol. (A)* **2004**, *201*, 1215-1235.
- 25 Y. Kuwabara, H. Ogawa, H. Inada, N. Noma, Y. Shirota, *Adv. Mater.* **2004**, *6*, 677-
679.
- 26 M.-H Tsai, H.-W. Lin, H.-C. Su, T.-H. Ke, C.-C. Wu, F.-C. Fang, Y.-L. Liao, K.-T. Wong,
C.-I. Wu, *Adv. Mater.* **2006**, *18*, 1216-1220.
- 27 M.-F. Wu, S.-J. Yeh, C.-T. Chen, H. Murayama, T. Tsuboi, W.-S. Li, I. Chao, S.-W. Liu,
J.-K. Wang, *Adv. Funct. Mater.* **2007**, *17*, 1887-1895.
- 28 A. S. Demir, Ö. Reis, M. Emrullahoglu, *J. Org. Chem.* **2003**, *68*, 10130-10134.
- 29 H. O. Wirth, O. Königstein, W. Kern, *Lieb. Ann. Chem.* **1960**, *634*, 84-104.
- 30 J. F. Ambrose, R. F. Nelson, *J. Electrochem. Soc.* **1968**, *115* (11), 1159-1164.
- 31 J. F. Ambrose, L. L. Carpenter, R. F. Nelson, *J. Electrochem. Soc.* **1975**, *122* (7),
876-894.
- 32 J. P. Perdew, W. Yue, *Phys. Rev. B: Condens. Matter Mater. Phys.* **1986**, *33*, 8800-
8802.
- 33 A. D. Becke, *Phys. Rev. A: At., Mol., Opt. Phys.* **1988**, *36*, 3098-3100.
- 34 A. Schäfer, H. Horn, R. Ahlrichs, *J. Chem. Phys.* **1992**, *97*, 2571-2577.

- ³⁵ D. Andrae, U. Häußermann, M. Dolg, H. Stoll, H. Preuss, *Theor. Chim. Acta* **1990**, *77*, 123-141.
- ³⁶ A. Schäfer, C. Huber, R. Ahlrichs, *J. Chem. Phys.* **1994**, *100*, 5829-5835.
- ³⁷ A. Klamt, *J. Phys. Chem.* **1995**, *99*, 2224-2235.
- ³⁸ R. Ahlrichs, M. Bär, M. Häser, H. Horn, C. Kölmel, *Chem. Phys. Lett.* **1989**, *162*, 165-169.
- ³⁹ M. Bold, C. Lennartz, M. Prinz, H.-W. Schmidt, M. Thelakkat, M. Bäte, C. Neuber, W. Kowalsky, C. Schildknecht, H.-H. Johannes, WO Patent 2005, 019373.
- ⁴⁰ N. Langer, K. Kahle, C. Lennartz, O. Molt, E. Fuchs, J. Rudolph, C. Schildknecht, S. Watanabe, G. Wagenblast, WO Patent 2009, 003898.
- ⁴¹ H. Sasabe, J. Takamatsu, T. Motoyama, S. Watanabe, G. Wagenblast, N. Langer, O. Molt, E. Fuchs, C. Lennartz, J. Kido, *Adv. Mater.* **2010**, *22*, 5003-5007.

Supporting Information for:

Meta-linked CBP-Derivatives As Host Materials

For A Blue Iridium Carbene Complex

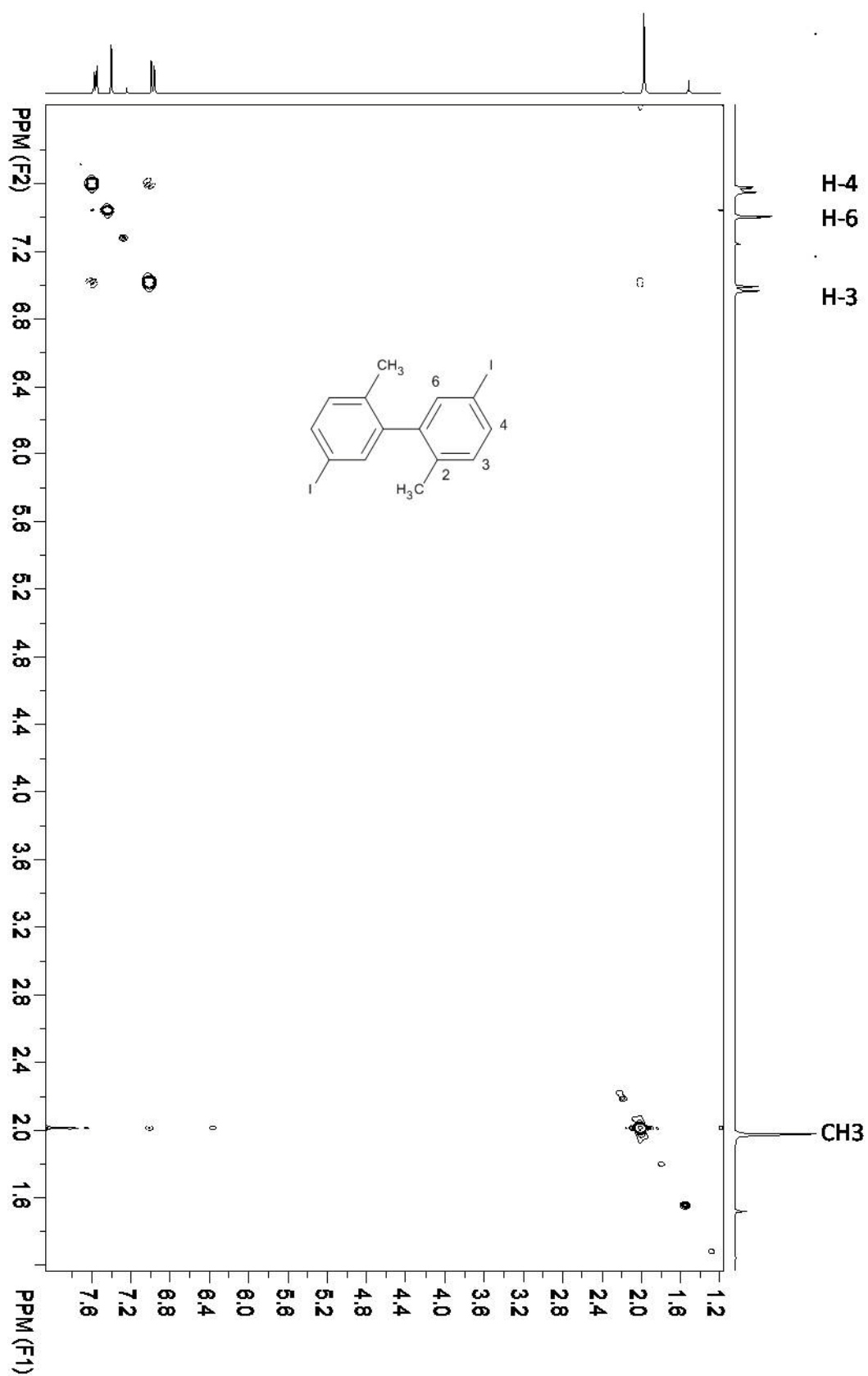
By *Pamela Schrögel,^a Nicolle Langer,^b Christian Schildknecht,^b Gerhard Wagenblast,^b
Christian Lennartz,^b Peter Strohriegl^{*a}*

^aLehrstuhl Makromolekulare Chemie I, Universität Bayreuth,
D-95440 Bayreuth, Germany
BASF SE, D-67056 Ludwigshafen, Germany

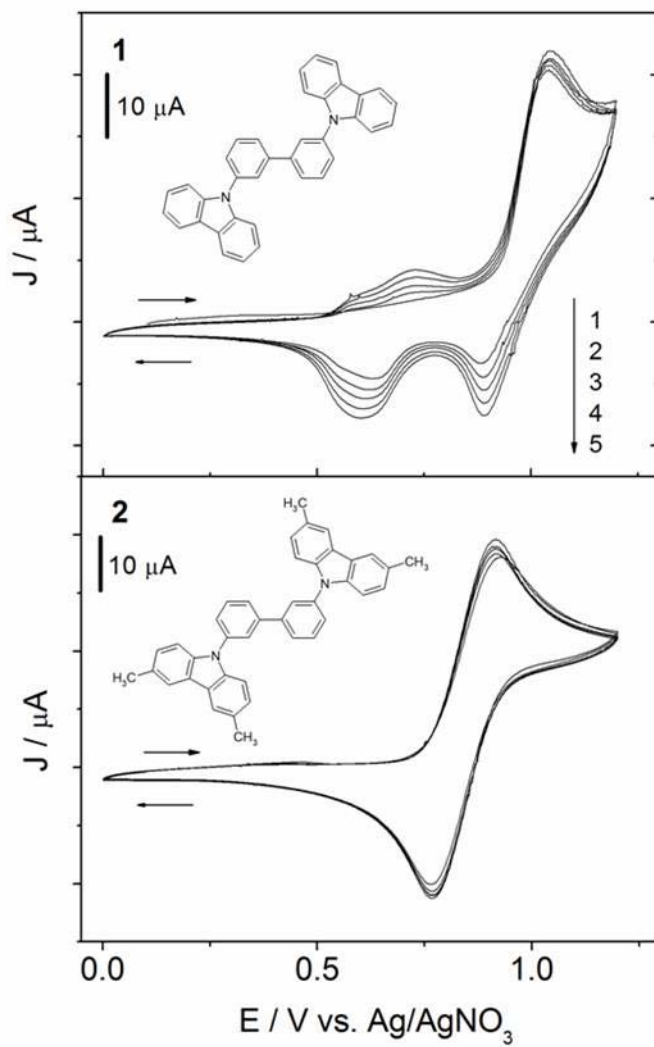
*Corresponding author: peter.strohriegl@uni-bayreuth.de

This manuscript has been accepted by *Organic Electronics* in a slightly revised version.

A: 2D 1H-NMR of 5,5'-diiodo -2,2'-dimethyl-biphenyl



B: Cyclic voltammograms of 1 and 2 (five scans, 50 mV/sec scan rate, 2×10^{-3} M in CH_2Cl_2):



8 Phosphazene-based Host Materials for the Use in Blue Phosphorescent Organic Light-emitting Diodes

Pamela Schrögel,^a Matthias Hopping,^b Wolfgang Kowalsky,^b Arvid Hunze,^c

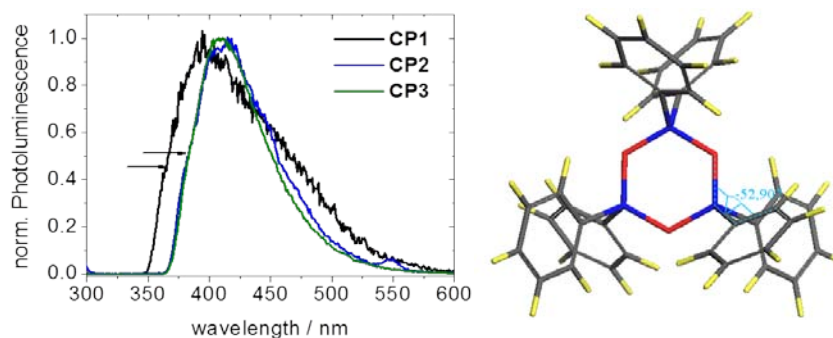
Gerhard Wagenblast,^d Christian Lennartz,^d Peter Strohriegl^{*a}

^a Lehrstuhl Makromolekulare Chemie I, Universität Bayreuth, 95440 Bayreuth, Germany,

^b Institut für Hochfrequenztechnik, TU Braunschweig, D-38023 Braunschweig,

^c Siemens AG, D-91050 Erlangen, Germany, ^d BASF SE, D-67056 Ludwigshafen, Germany

*Corresponding author: peter.strohriegl@uni-bayreuth.de



This manuscript has been submitted to *Chemistry of Materials*
in a slightly revised version.

Abstract

We present a series of low molecular weight materials based on cyclic phosphazenes for the use as host materials in blue phosphorescent organic light-emitting diodes. Substituted phenyl rings are attached to the central phosphazene ring either via phosphorus-oxygen bonds to yield phenoxy substituted derivatives or via direct phosphorus-carbon bonds to yield phenyl substituted derivatives. The phenoxy substituted cyclic phosphazenes were prepared by nucleophilic substitution of the six chlorine atoms in hexachlorocyclotriphosphazene with phenoxy groups whereas the phenyl substituted cyclic phosphazenes were formed in a cyclocondensation reaction of three equivalents of substituted phosphinic amides. The phenyl substitution leads to materials with superior thermal properties compared to the phenoxy substitution. Due to the non-conjugated linkage to the phosphazene core the host materials have very high triplet energies of more than 3 eV. In an OLED device using one compound as host for the saturated blue phosphorescent emitter Ir(dbfmi) a peak power efficiency of 7.6 lm W^{-1} and a peak luminance of 5000 cd m^{-2} was achieved.

Keywords

electroluminescence, OLED, blue phosphorescence

Introduction

Since the first efficient multi-layer organic light-emitting diode (OLED) was invented by Tang and van Slyke in 1987, great advances have been made by extensive development of new OLED materials and sophisticated device setups.^{1,2,3} Nowadays, OLEDs are attracting attention because of their capability to realize full color displays and large area lighting with high power-efficiency and freedom of design. The key to high efficiencies was the discovery of phosphorescent emitters based on organo-transition metal complexes that are able to harvest both electrogenerated singlet and triplet excitons for light emission. Therefore, the theoretical limit of the internal quantum efficiency reaches 100%.⁴ In general, the triplet emitters have to be embedded into a host to avoid concentration quenching.⁵ It is essential that the triplet energy of the host is larger compared to the triplet emitter to prevent energy back transfer from the emitter to the host and to confine triplet excitons on the emitter molecules. This restriction becomes particularly challenging when host materials for deep blue phosphors are in the focus of interest, where host triplet energies larger than 3.0 eV are required. Among the commonly used class of carbazole based host materials, the substituted N-phenylcarbazole 9-(4-tert-butylphenyl)-3,6-di-triphenylsilyl-carbazole (CzSi, $E(T_1-S_0) = 3.02$ eV)⁶ and 1,4-bis(4-(carbazol-9-yl)phenyl)cyclohexane (CBPCH, $E(T_1-S_0) = 3.01$ eV)⁷, for example, show triplet energies close to their intrinsic limit of 3 eV.⁸ To provide host materials with even larger triplet band gaps the conjugation of the host molecules must be extremely confined which limits the choice of possible building blocks. Organosilane compounds have been presented as materials with ultra high band gaps (UGH) and successfully employed in OLEDs as host materials for blue phosphors.^{9,10,11,12}

Besides organosilane compounds, several phosphorus containing host materials, such as phosphine oxides^{13,14,15} have been introduced as promising candidates with high triplet energies. Another class of phosphorus containing materials interesting for the use in organic electroluminescent devices are cyclic phosphazenes. The planar non-conjugated 6-membered ring consisting of alternating P- and N-atoms reveals high chemical and thermal stability and exhibits two bonding sites for substituents on each P-atom. Solution-processible dendrimers with various emitters attached to a cyclic phosphazene

core have already been reported. Via oxygen-phosphorus bonds emitting fluorescent pyrene units or phosphorescent iridium complexes were attached to the phosphazene core and rigid spherical molecules with high glass transition temperatures were obtained.^{16,17,18} Very recently, the same research group presented phenoxy-carbazole and pyridin-oxy-carbazole functionalized cyclic phosphazene materials and their use as host materials for the greenish-blue triplet emitter Flrpic and the green triplet emitter Ir(mppy)₃ in solution processible OLED devices.¹⁹ However, due to their high molecular weight these dendrimers are not suitable for an OLED-fabrication by thermal evaporation.

In this study we present a series of vacuum processible new phosphazene based host materials for saturated blue phosphorescent emitters. In these materials substituted phenyl rings were either attached via phosphorus-oxygen-bonds (phenoxy substituted cyclic phosphazenes) or via phosphorus-carbon-bonds (phenyl substituted cyclic phosphazenes). We present the synthesis of symmetrically substituted organocyclotriphosphazenes along with their thermal and optical properties. The energy levels of the compounds were calculated by density functional theory (DFT) and experimentally determined by ultraviolet photoelectron spectroscopy. To demonstrate the potential as host material for blue phosphorescent emitters an OLED device employing an organocyclotriphosphazene host has been made. In Figure 1 the molecular structures of the organocyclotriphosphazenes are depicted.

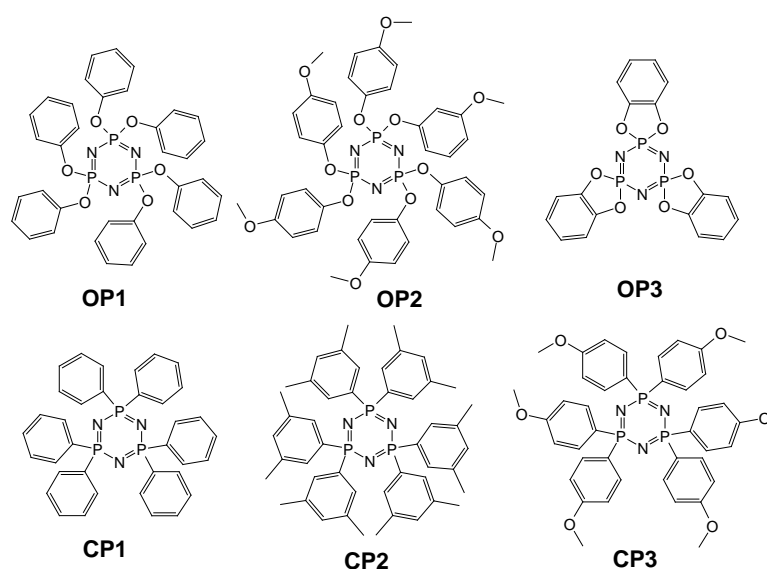


Figure 1. Molecular structures of the cyclic phosphazenes **OP1-OP3** with phenoxy substitution (**top**) and **CP1-CP3** with phenyl substitution (**bottom**).

Experimental Section

Materials

All chemicals and reagents were used as received from commercial sources without further purification. All solvents for reactions and purifications were distilled once, except tetrahydrofuran (THF) which was additionally distilled over potassium.

Characterization

^1H - and ^{13}C -NMR spectra were recorded with a Bruker AC 250 (250 MHz) and CDCl_3 as solvent. All data are given as chemical shifts δ (ppm) downfield from $\text{Si}(\text{CH}_3)_4$. Mass spectra were taken on a Finnigan Mat 8500, Mat 112 S Varian machine using EI-ionization. For optical measurements, 10^{-5} M cyclohexane (Uvasol[®], Merck) solutions of the materials as well as spin coated thin films on quartz substrates were prepared. The UV/VIS spectra were measured in solution and on neat films with a Hitachi U-3000 spectrometer. Fluorescence spectra were measured on a Shimadzu spectrofluorophotometer RF-5301PC using excitation at 220 nm. Phosphorescence spectra of thin films have been measured at 5 K (Helium cryostat Optistat CF from Oxford Instruments) applying the technique of time-gated spectroscopy (with fluorescence and phosphorescence lifetime spectrometer FLSP 920 from Edinburgh Instruments). The photoluminescence quantum yield (η_{PL}) of the 8 % Ir(dbfmi)-doped films of **CP1-CP3** was measured under N_2 flow using an integrating sphere excited at 355 nm with a multichannel spectrometer as the optical detector. Thermogravimetric analysis (TGA) was performed on a Mettler Toledo TGA/SDTA815e machine at a heating rate of 10 K min^{-1} in a nitrogen atmosphere. For differential scanning calorimetry measurements (DSC) a Diamond DSC apparatus from Perkin Elmer was used (heating/cooling rate 10 K min^{-1}). The purity of the target compounds was checked with a Waters size exclusion chromatography system (SEC) for oligomers (analytical columns: cross-linked polystyrene gel (Polymer Laboratories), length: $2 \times 60 \text{ cm}$, width: 0.8 cm , particle size: $5 \mu\text{m}$, pore size 100 \AA , eluent THF (0.5 mL min^{-1} , 80 bar), polystyrene standard). For the fabrication of OLEDs the organic layers were deposited by thermal evaporation in high vacuum ($< 10^{-6} \text{ mbar}$) onto indium-tin-oxide (ITO, 10 ohm/square) pre-coated glass substrates. The organic layers and the metal cathode were evaporated without breaking the vacuum.

Computational Methods

The transport levels of the materials used were determined via density functional calculations. For the ionization potential and the electron affinity first the geometry of the neutral as well as the charged states were optimized using the BP86-functional^{20,21} in combination with a split-valence basis set (SV(P)) including polarization functions on all heavy atoms²². For iridium an effective core potential was employed.²³ For the energetics we performed single point calculations at the optimized geometries using the same functional in combination with a TZVP-basis set.²⁴ To account for dielectric solid state effects a UPS/IEPS-calibrated version of the conductor like screening model (COSMO)²⁵ was used in conjunction with these single point calculations. All calculations were carried out with the turbomole program package.²⁶

Synthetic procedures

The synthesis of tris[(3-phenyl-1H-benzimidazol-1-yl)2(3H)-yliden-1,2-phenylene]iridium (DPBIC),³⁶ 2,8-bis(triphenylsilyl)-dibenzofuran (DBFSi)³⁷ and *mer*-tris(*N*-dibenzofuranyl-*N'*-methylimidazole)iridium (III) (Ir(dbfmi))^{37,27} is described in literature.

General procedure for the synthesis of phenoxy substituted phosphazenes.

The cyclotriphosphazenes **OP1-OP3** were prepared similar to a procedure described in reference [28].

*Hexakisphenoxy*cyclotriphosphazene (**OP1**). A suspension of sodium phenolate was prepared by adding sodium hydride (0.55 g, 23 mmol) to phenole (2.16 g, 23 mmol) dissolved in 40 mL of dry THF under argon. Hexachlorocyclotriphosphazene (1.0 g, 2.88 mmol) dissolved in 10 mL of dry THF was added drop wise via syringe and the mixture was stirred under reflux for two days. After removal of the solvent under reduced pressure the residue was stirred in water for 1 hour. The white solid was washed with methanol to remove the excess of phenole. Yield: 1.69 g (85%). EI-MS *m/z*: 693 (M^+ , 71), 599 (100), 505 (34). ¹H-NMR (250 MHz, CDCl₃), δ (ppm): 7.21-7.08 (m, 18H), 6.93 (d, 12H).

*Hexakis(4-methoxyphenoxy)*cyclotriphosphazene (**OP2**) was synthesized according to the route described above. The reaction time was 24 h. Yield: 0.62 g (49%). EI-MS *m/z*: 873

(M^+ , 100), 749 (78), 626 (8). $^1\text{H-NMR}$ (250 MHz, CDCl_3), δ (ppm): 6.83 (m, 12 H), 6.67 (m, 12H), 3.79 (s, 18H).

Tris(phenylenedioxy)cyclotriphosphazene (OP3). 15 mL of dry THF were added to sodium hydride (1 g, 41.4 mmol) under argon. Catechol (1.9 g, 17.3 mmol) dissolved in 15 mL of dry THF was added dropwise to the NaH solution. After stirring for 90 min at room temperature, the blue mixture was transferred into a dropping funnel and added dropwise to a solution of hexachlorocyclotriphosphazene (2.0 g, 5.75 mmol) dissolved in 10 mL of dry THF. After stirring at room temperature for 24 h, the same purification procedure as described above was used. Yield: 1.88 g (71 %). EI-MS m/z : 459 (M^+ , 100), 351 (12). $^1\text{H-NMR}$ (250 MHz, CDCl_3), δ (ppm): 7.12-7.00 (m, 24 H).

General procedure for the synthesis of phenyl substituted phosphazenes.

Bis(3,5-dimethylphenyl)phosphinic acid (PAc2). 1-Bromo-3,5-dimethylbenzene (13.63 g, 71.44 mmol) was added dropwise to magnesium chips (1.74 g, 71.44 mmol) in absolute THF (80 mL) at room temperature. Once the magnesium was completely dissolved (2 h), a solution of N,N-dimethyl-phosphoryl dichloride $\text{N}(\text{Me})_2\text{P}(\text{O})\text{Cl}_2$ (4.33 mL, 35.72 mmol) in absolute THF (10 mL) was added dropwise by syringe. After 2h the mixture was poured into an ice-cooled solution of NH_4Cl (30 g) in water (500 mL) for the separation of the formed salt. In a distillation setup with Vigreux column the THF was distilled off and the residue was treated with conc. HCl (75 mL) at 80°C . The resulting white solid was dissolved in aqueous NaOH (5.4 g, 300 mL H_2O), and the aqueous layer was twice extracted with ether. The clear aqueous layer was again acidified by the addition of conc. HCl to precipitate the phosphinic acid **PAc2** as white solid. Yield: 6.81 g (70 %). EI-MS m/z : 274 (M^+ , 100), 259 (39), 136 (5). $^1\text{H-NMR}$ (250 MHz, CDCl_3), δ (ppm): 11.35 (s, 1H, OH), 7.35 (d, 4H), 7.11 (s, 2H), 2.28 (m, 12H).

Bis(4-methoxyphenyl)phosphinic acid (PAc3). The same synthetic procedure as described above was used. Yield: 54 % (5.36 g). EI-MS m/z : 278 (M^+ , 100), 263 (19), 247 (8), 107 (15). $^1\text{H-NMR}$ (250 MHz, CDCl_3), δ (ppm): 7.77 (br s, 1H, OH), 7.62 (dd, 4H), 6.83 (dd, 4H), 3.79 (m, 6H).

Bis(3,5-dimethylphenyl)phosphinic amide. (PAm2). Distilled thionyl chloride (0.87 mL, 12 mmol) was added dropwise to a suspension of bis(3,5-dimethylphenyl)phosphinic

acid (1 g, 3.65 mmol) in dry toluene (25 mL) at 55-60°C and stirred for 20 min. After the removal of the excess of thionyl chloride by distillation ammonia gas was passed into the clear solution for 10 min at 0°C. In order to separate the NH₄Cl the organic layer was washed with water. Before the extraction with THF the density of the water layer was increased by the addition of sodium chloride. The combined organic layers were dried over Na₂SO₄ and the solvent was removed under reduced pressure. The phosphinic amide **PAm2** was used for the cyclisation reaction without further purification. Yield: 0.98 g (98 %). EI-MS *m/z*: 273 (M⁺, 100), 257 (19). ¹H-NMR (250 MHz, CDCl₃), δ (ppm): 7.53 (d, 4H), 7.11 (s, 2H), 3.01 (br s, 2H, NH₂), 2.32 (m, 12H).

Bis(3,5-dimethylphenyl)phosphinic amide (PAm3). The same synthetic pathway as described above was used. Yield: 90 % (0.89 g). EI-MS *m/z*: 277(M⁺, 100), 170 (45). ¹H-NMR (250 MHz, CDCl₃), δ (ppm):): 7.83 (m, 4H), 6.92 (m, 4H), 3.81 (m, 3H), 3.08 (br s, 2H, NH₂).

Hexaphenylcyclotriphosphazene (CP1). A suspension of diphenylphosphinic amide (2.0 g, 9.22 mmol), triphenylphosphine (2.9 g, 11.1 mmol), carbon tetrachloride (0.89 mL, 9.22 mmol) and triethylamine (1.3 mL, 9.22 mmol) in dry dichloromethane (25 mL) was refluxed for 5 h. The solvent was removed under reduced pressure. Liquid chromatography on silica gel with hexane:THF mixtures as eluent gave the product as yellowish solid. Yield: 65 % (1.2 g). EI-MS *m/z*: 597 (M⁺, 100), 520 (74), 299 (12), 260 (18), 77 (5). ¹H-NMR (250 MHz, CDCl₃), δ (ppm): 7.76 (dd, 12H), 7.30 (m, 18H). ¹³C-NMR (CDCl₃), δ (ppm): 138.55 (dt, C_{p-bound}), 130.86 (ps d, C_{meta}), 130.44 (m, C_{para}), 127.98 (ps d, C_{ortho}). Elemental analysis: Calc.: C: 72.36 %, H: 5.06 %, N: 7.03 %, P: 15.55 %; Found: C: 72.38 %, H: 5.08 %, N: 7.07 %, P: 15.49 %.

Hexa-(3,5-dimethylphenyl)-cyclotriphosphazene (CP2). The same procedure for the synthesis as described for **CP1** was applied except the reaction time was extended to 22 h. Yield: 65 % (1.2 g). EI-MS *m/z*: 765 (M⁺, 100), 660 (45), 382 (10), 105 (10). ¹H-NMR (250 MHz, CDCl₃), δ (ppm): 7.40 (d, 12H), 6.98 (s, 6H), 2.21 (m, 36H). ¹³C-NMR (CDCl₃), δ (ppm): 138.35 (dt, C_{p-bound}), 137.16 (ps d, C_{meta}), 131.97 (d, C_{para}), 128.90 (d, C_{ortho}) 21.34 (s, methyl). Elemental analysis: Calc.: C: 75.27 %, H: 7.11 %, N: 5.49 %, P: 12.13 %; Found: C: 75.14 %, H: 7.04 %, N: 5.54 %, P: 12.18 %.

Hexa-(4-methoxyphenyl)-cyclotriphosphazene (CP3). The same procedure for the synthesis as described for **CP1** was applied but the reaction time was extended to 14 h. Yield: 50 % (520 mg). EI-MS m/z : 777 (M^+ , 99), 670 (45), 388 (22). $^1\text{H-NMR}$ (250 MHz, CDCl_3), δ (ppm): 7.64 (m, 12H), 6.80 (m, 12H), 3.78 (m, 18H). $^{13}\text{C-NMR}$ (CDCl_3), δ (ppm): 161.24 (m, C_{para}), 132.71 (ps d, C_{meta}), 130.84 (dt, $C_{P-bound}$), 113.39 (ps d, C_{ortho}), 55.31 (s, methoxy). Elemental analysis: Calc.: C: 64.86 %, H: 5.44 %, N: 5.40 %, O: 12.34 %, P: 11.95 %; Found: C: 65.28 %, H: 5.44 %, N: 5.76 %, O: 12.69 %, P: 10.81 %.

Results and Discussion

Synthesis

The phenoxy substituted phosphazenes **OP1-OP3** have been prepared by nucleophilic substitution of the six chlorine atoms in hexachlorocyclotriphosphazene (Figure 2a). By treatment of the phenols with sodium hydride phenoxylates are formed which replace the chlorine atoms by nucleophilic substitution. The synthesis of the phenyl substituted derivatives by direct replacement of the six chlorine atoms in hexachlorocyclotriphosphazene is rather difficult. Both an approach by Grignard reaction and by Friedel-Crafts arylation are known to yield mixtures of several substitution products with only small amounts of the hexa-substituted compounds.^{29,30} Therefore, we devised the synthetic route to phenyl substituted organocyclotriphosphazenes as sketched in Figure 2b. In a Grignard reaction two chlorine atoms of dichloro-N,N-dimethylphosphinic amide are replaced by the substituted phenyl rings. Acidic workup yields the phenyl substituted phosphinic acids³¹. After treatment with thionyl chloride the intermediately formed phosphinic acid chlorides are directly converted into the substituted phosphinic amides in an amination reaction with gaseous ammonia. The organophosphazenes **CP1-CP3** are formed in a cyclocondensation reaction described by Appel et al.³² from three equivalents of a phenyl substituted phosphinic amide.

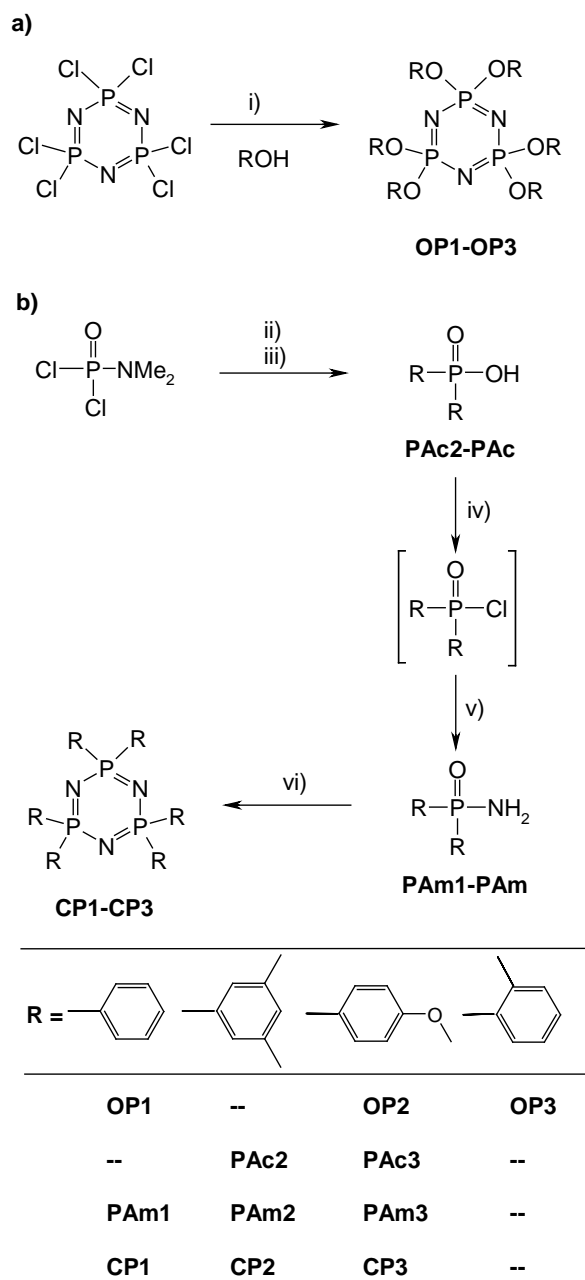


Figure 2. Synthetic route to a) phenoxy substituted cyclic phosphazenes **OP1-OP3** and b) phenyl substituted cyclic phosphazenes **CP1-CP3**. Reagents and conditions: i) NaH, abs. THF, 70°C, 48 h (catechol: RT, 24h); ii) RMgBr, abs. THF, RT, 2h; iii) conc. HCl, 80°C, 1 h; iv) thionyl chloride, abs. toluene, 55°C, 20 min; v) NH₃ (g), 0°C, 10 min; vi) PPh₃, CCl₄, NEt₃, benzene, dichloromethane, 40°C, 5 - 22 h.

Thermal Analysis

We examined the thermal properties of the organophosphazenes **OP1-OP3** and **CP1-CP3** by thermal gravimetric analysis (TGA) and differential scanning calorimetry (DSC) in a nitrogen atmosphere at a scanning rate of 10 K min⁻¹.

For the application in small molecule OLEDs the materials have to be processible by thermal evaporation. Therefore, the molecular weight of the compounds should not be too high to exclude decomposition during evaporation. As the cyclic phosphazene core bears six substituents it is particularly important to choose confined aromatic units as substituents. In this study we concentrate on phenyl substituents at the inorganic phosphazene core. All results of the thermal characterization are listed in Table 1.

The phenoxy substituted cyclic phosphazene **OP1-OP3** are thermally stable up to at least 260°C. However, the high rotational freedom given by the oxygen-linkage leads to very low glass transition temperature of -12°C and 1°C for compounds **OP1** and **OP2**. Thus, films of **OP1** and **OP2** crystallize readily. In the case of **OP3**, the bifunctional substituents introduce more structural rigidity leading to a much higher melting temperature of 251°C. Yet, the material does not sublime without decomposition.

We prepared a second series of cyclic phosphazenes with the substituents being attached via direct phosphorus-carbon bonds (**CP1-CP3**). All materials show high thermal stability up to at least 280°C in the TGA measurements and much higher melting temperatures than their phenoxy substituted analogues. **CP1** melts at 235°C and crystallizes at 191°C upon cooling. The observed low supercooling of only 44°C demonstrates the high tendency of **CP1** to crystallize. **CP2** reveals a melting peak at 214°C and crystallizes upon cooling at 138°C. Compared to **CP1** the crystallization tendency could be slightly decreased by introducing additional methyl groups as evident from the higher supercooling of 76°C. **CP3** melts at a temperature of 281°C and crystallizes at 221°C upon cooling. Contrary to the twelve methyl groups in **CP2**, the six methoxy groups in **CP3** cause only a slight hindrance of crystallization compared to hexaphenylcyclotriphosphazene **CP1** which is indicated by a supercooling of only 54°C. In a second DSC experiment the isotropic melts of the samples were quenched with liquid nitrogen before measuring the glass transition temperatures (T_g s). The pretreated samples of **CP2** and **CP3** revealed T_g s of 68°C and 73°C, respectively. Although **CP1-CP3** show crystalline behavior in the DSC measurements amorphous films can be prepared from solution and evaporation which are morphologically stable over several months at room temperature. To summarize, due to the low glass transition temperatures of **OP1** and **OP2** no morphological stable films can be prepared. In contrast, **OP3** reveals higher

transition temperatures, however, **OP3** cannot be sublimed without decomposition. Because of their detrimental thermal properties the phenoxy substituted cyclic phosphazenes **OP1-OP3** were not further considered in this study.

Table 1. Thermal properties of **OP1-3** and **CP1-3**.

	$T_m/^\circ\text{C}$	$T_{cr}/^\circ\text{C}$	$T_g/^\circ\text{C}$	$T_{ID}^a/^\circ\text{C}$
OP1	116	38 ^b	-12	260
OP2	107	--	1	314
OP3	251	173	--	271
CP1	235	191	--	285
CP2	214	137	68 ^c	280
CP3	281	221	73 ^c	337

T_m : melting temperature, T_{cr} : crystallization temperature, T_g : glass transition temperature and T_{ID} : initial decomposition temperature.

^a T_{ID} is the temperature at which an initial loss of mass was observed in a thermogravimetric experiment with a heating rate of 10 K min⁻¹ under nitrogen.

^b Observed only during the heating scan.

^c Observed only during heating scan after quenching from melt.

Optical Analysis

For the optical characterization we measured the UV/Vis and photoluminescence spectra of **CP1-CP3** in thin films and in cyclohexane solutions (see Figure 3). All materials have an absorption edge in the UV-region between 277 nm and 295 nm. While the absorption of **CP1** and **CP2** are very similar, the absorption of **CP3** is of a different shape and at slightly higher wavelengths. We assign this to the electron donating effect of the methoxy substituents at the *para*-positions of the phenyl rings. At room temperature we did not detect any photoluminescence neither in solution nor in film samples. From the wavelength of the absorption edge the optical band gap $\Delta E(S_0-S_1)$ can be calculated. All cyclic phosphazenes reveal very large band gaps in the range of 4.2 eV to 4.5 eV. Since the exchange energy of many small molecules is typically in the range of 0.7 eV to 1 eV³³ a large triplet energy is expected for **CP1-CP3**. As estimate for the exchange energy the energy difference ΔE_{ST} between the singlet and triplet emission transitions is taken.³⁴

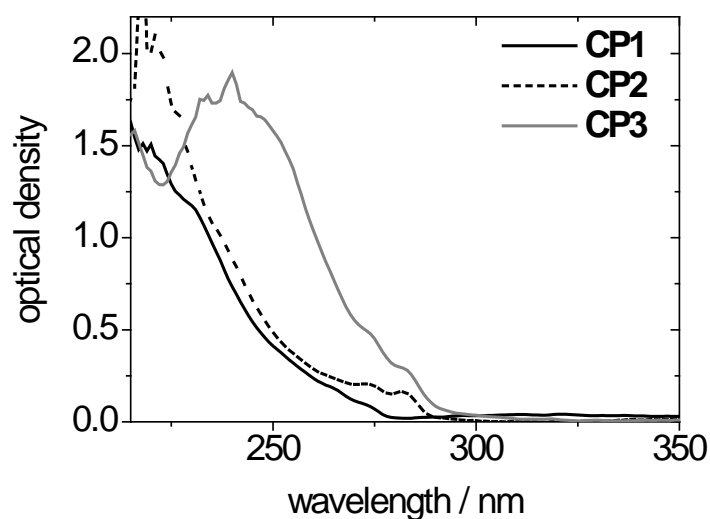


Figure 3. Absorption spectra of thin films of **CP1-CP3**.

Table 2. Optical properties of the materials **CP1-CP3**.

	λ_{EA}^a /nm	λ_{EA}^b /nm	$\Delta E(S_0-S_1)^c$ /eV	λ_{77K}^d /nm	$\Delta E(T_1-S_0)$ /eV
CP1	278	277	4.5	363	3.41
CP2	288	288	4.3	382	3.24
CP3	294	295	4.2	382	3.24

^a Absorption edge measured in 10^{-5} M cyclohexane solution at room temperature.

^b Absorption edge measured on neat films at room temperature.

^c The optical band gap was estimated from the onset of the UV/Vis absorption of neat films.

^d Wavelength of the highest energy shoulder in the phosphorescence spectra of 100 % films at 5 K.

At low temperatures (5 K) we were able to detect phosphorescence. The phosphorescence spectra are shown in Figure 4. The emission maxima are centered at around 395 nm for **CP1** and 410 nm for **CP2** and **CP3**. The highest energy peak is visible as a small shoulder at 363 nm for **CP1** and 382 nm for **CP2** and **CP3** corresponding to very high triplet energies of 3.41 eV and 3.24 eV, respectively. All results from the photo physical investigations are summarized in Table 2.

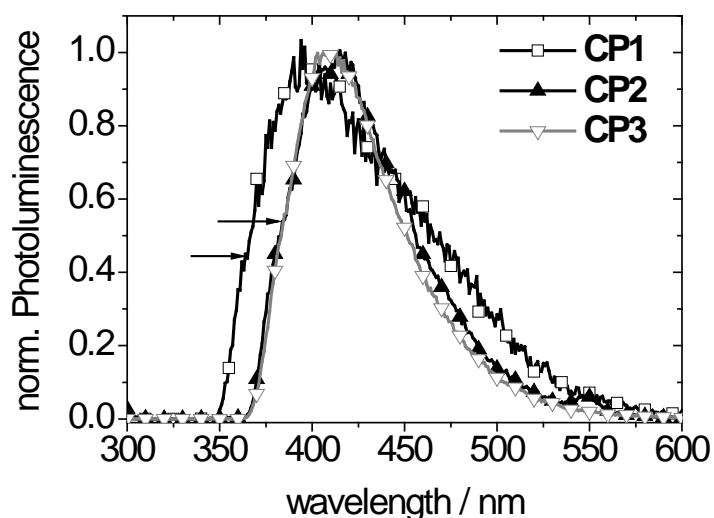


Figure 4. Phosphorescence spectra of **CP1- CP3** measured on neat films at 5 K; the arrows indicate the shoulder in the emission spectra taken for the determination of the triplet energy of the compounds.

Considering the spatial molecular structure of **CP1** helps to explain the experimental findings. As evident from the geometry optimized molecular structure shown in Figure 5 the pendant phenyl rings are aligned above and below the central plane formed by the P_3N_3 -ring. The calculated dihedral angles between the outer phenyl rings and the central ring plane are 48° to 56° . The calculated dihedral angles and bond lengths are consistent with experimental crystallographic data of **CP1**.³⁵ As no conjugation over the central ring takes place all phenyl rings are electronically isolated from each other. Thus, in the experiments the absorption and emission properties of isolated substituted phenyl rings are observed with nearly no influence of the P_3N_3 -core.

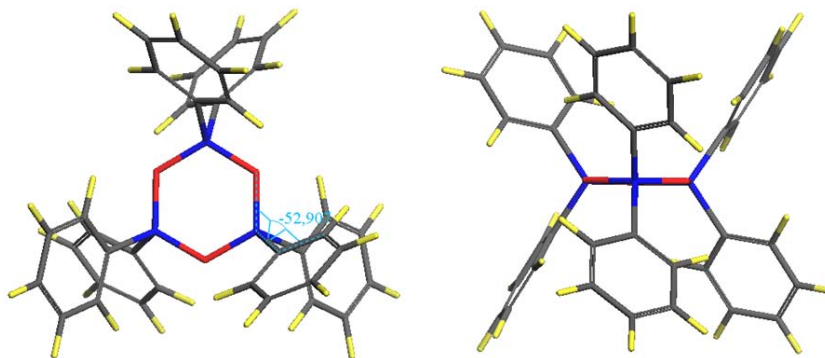


Figure 5. Geometry optimized molecular structure of **CP1**.

Experimental and calculated energy levels

The energy levels were determined by measuring ultra-violet photoelectron spectroscopy (UPS). Very low HOMO levels of 6.51 eV for **CP1** and 6.56 eV for **CP2** were measured. By adding the optical band gap to the HOMO values the LUMO values of 2.01 eV for **CP1** and 2.23 eV for **CP2** can be derived.

Table 3. Energy values and triplet energies of **CP1-CP3**.

	calculated		experimental	
	HOMO ^a /eV	LUMO ^a /eV	HOMO ^b /eV	LUMO ^c /eV
CP1	6.47	1.53	6.51	2.01
CP2	5.98	1.35	6.56	2.23
CP3	5.71	1.14	--	--

^a Calculated energy values.

^b Experimentally determined value from UPS measurements.

^c Estimated by adding the optical band gap to the experimental HOMO level.

Single carrier devices

In order to get a more comprehensive understanding about the charge carrier transport properties of the novel class of host materials we prepared single carrier devices. Because of its high morphological stability we chose **CP2** for the single carrier device tests. Here, the material in varying thicknesses is sandwiched between two chemically doped hole or electron transport layers with high mobilities for holes or electrons. The IV-characteristics and the device setup are shown in Figure 6.

CP2 is a good hole conductor and a current density of 1 mA cm⁻² is achieved at 1.6 V for holes. For electrons the current density of 1 mA cm⁻² is achieved at an even lower voltage of 1 V. The JV-characteristics show that **CP2** has balanced transport properties for both types of charge carriers.

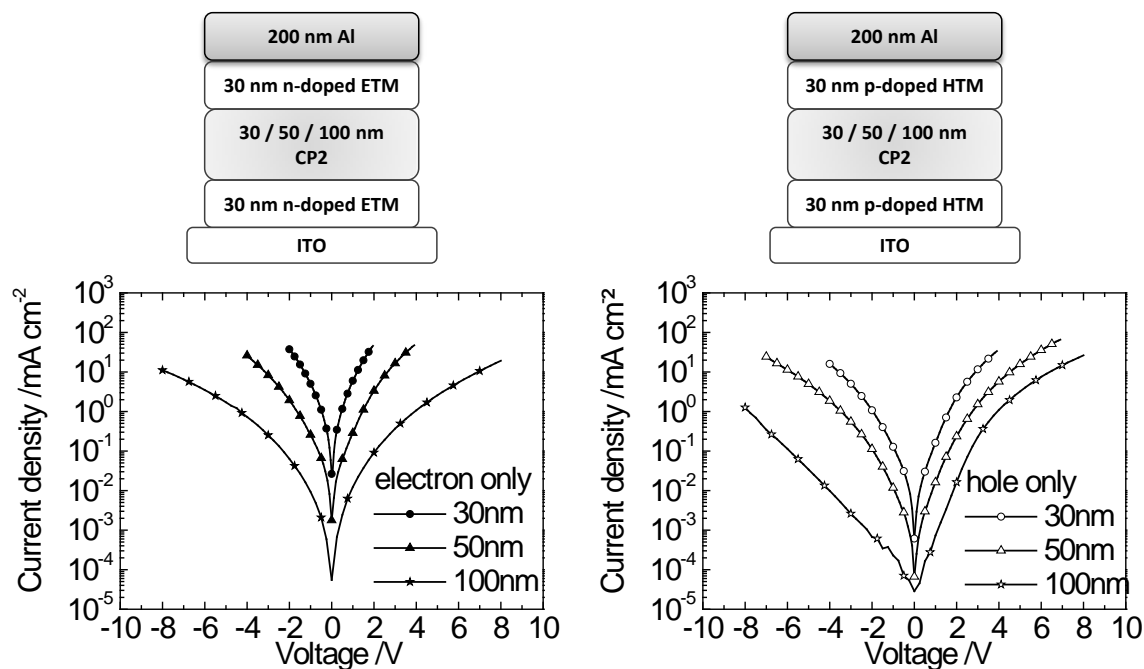


Figure 6. JV-characteristics of CP2 in e-only device (left) and h-only device (right).

Phosphorescent Organic Light-Emitting Diodes

We employed CP2 in an OLED device as host material for the saturated blue emitter Ir(dbfmfi). The device structure is shown in Figure 7. On top of the indium-tin-oxide (ITO) anode 120 nm of α -NPD p-doped with 10 wt-% molybdenum(VI) oxide were deposited as hole-injection and hole-transporting layer. The additional 10 nm thick hole transporting layer of DPBIC³⁶ prevents quenching of triplet excitons at the doped NPD-layer. On top a double emission layer of 10 nm of DPBIC doped with 8 % Ir(dbfmfi) and 40 nm of CP2 doped with 8 % Ir(dbfmfi) was deposited. The electron transport within the emission layer takes place over the host CP2. The thin emitter doped DPBIC interlayer allows residual electrons to recombine and emit efficiently on the emitter. 10 nm of the hole and exciton blocking material 2,8-bis(triphenylsilyl)-dibenzofuran (DBFSi)³⁷ and 40 nm of the electron-transporting material 1,3,5-tris(2-*N*-phenylbenzimidazolyl)-benzene (TPBi) were deposited. As cathode LiF (0.5 nm)/ Al (100 nm) was used.

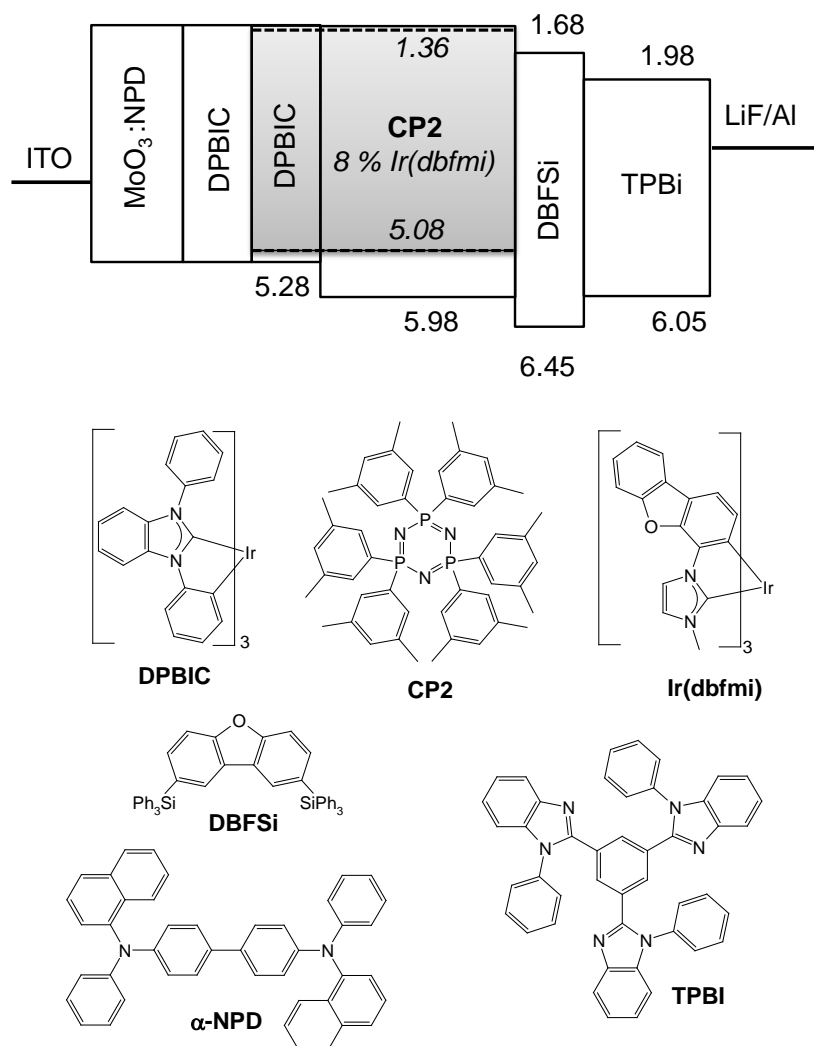


Figure 7. Energy level diagram of the device with **CP2** as host for Ir(dbfmi) and the molecular structures of all materials. Ionization potentials and electron affinity levels of the materials are indicated. The dotted lines represent the levels of the emitter Ir(dbfmi). All HOMO and LUMO levels were taken from density functional theory (DFT) calculations.

Figure 8 (top) shows the current density-voltage-luminance characteristics of the device. The peak power efficiency of 7.6 lm W^{-1} is achieved at 5.5 V. A peak luminance of 5000 cd/m^2 was reached at 13.5 V. At 100 cd m^{-2} and 1000 cd m^{-2} the power efficiencies are 4.9 lm W^{-1} and 2.3 lm W^{-1} , respectively. To the best of our knowledge, this work represents the first report about cyclic phosphazene compounds as host materials for an emitter with saturated blue phosphorescence which can be processed by thermal evaporation.

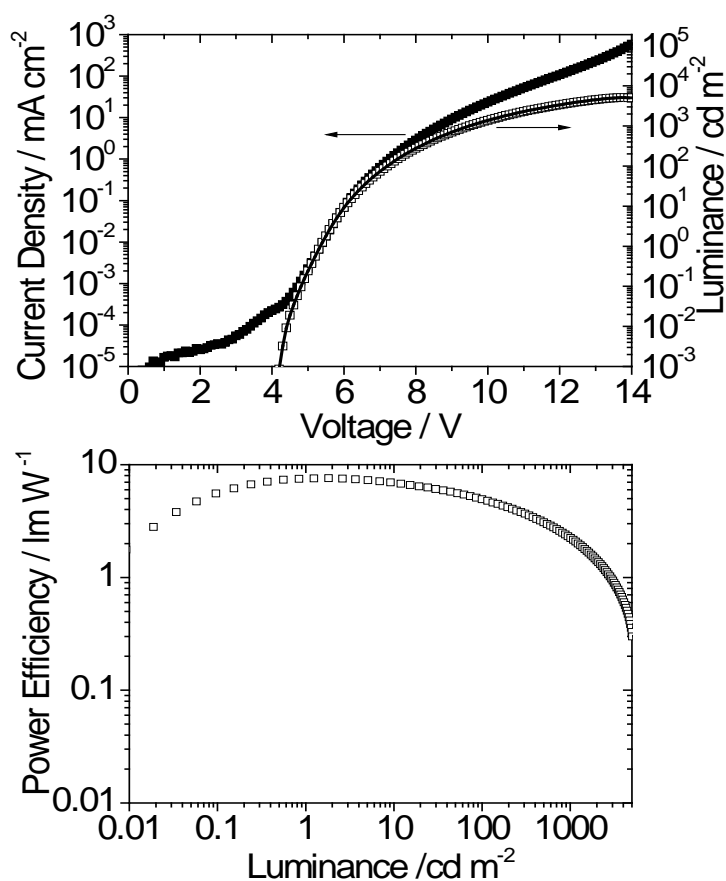


Figure 8. Top: Current density-voltage characteristics (open squares) and luminance-voltage plot (filled squares). **Bottom:** Power efficiency-luminance plot.

Conclusion

We have described a novel series of host materials based on cyclic phosphazenes. Substituted phenyl rings were attached to the central phosphazene core either via phosphorus-oxygen bonds (**OP1-OP3**) or via phosphorus-carbon bonds (**CP1-CP3**). The phenoxy substituted phosphazenes **OP1-OP3** revealed high crystallization tendency and poor thermal stability. In contrast, the phenyl substituted phosphazenes **CP1-CP3** form morphologically stable films. Due to the non-conjugated linkage via the central phosphazene rings **CP1-CP3** exhibit very high triplet energies of more than 3 eV. Thus, energy transfer to even deep blue emitters is possible. The phenyl substituted phosphazenes reveal balanced transport characteristic for both holes and electrons. In an OLED device **CP2** was successfully tested as host material for the emitter Ir(dbfmi) with saturated blue emission.

Acknowledgements

We thank Dr. Evelyn Fuchs, Dr. Hans-Hermann Johannes, Dr. Nicolle Langer, Dr. Oliver Molt and Dr. Ingo Münster for stimulating discussions. Financial support from the BMBF projects OPAL 2008 (FKZ 13N 8992) and TOPAS 2012 (FKZ 13N 10447) is gratefully acknowledged. P.S. thanks the Universität Bayern e.V. for a grant.

References

- ¹ Tang, C. W.; van Slyke, S. A.; *Appl. Phys. Lett.* **1987**, 51, 913.
- ² Yersin, H. (Ed.); *Highly Efficient OLED's with Phosphorescent Materials*; Wiley-VCH:Weinheim, Germany, **2008**.
- ³ Reinecke, S.; Lindner, F.; Schwartz, G.; Seidler, N.; Walzer, K.; Lüssem, B.; Leo, K.; *Nature*, **2009**, 459, 234-238.
- ⁴ Baldo, M. A.; O'Brien, D. F.; You, Y.; Shoustikov, A.; Silbey, S.; Thompson, M. E.; Forrest, S. R.; *Nature* **1998**, 395, 151-154.
- ⁵ Adachi, C.; Baldo, M. A.; Thompson, M. E.; Forrest, S. R.; *J. Appl. Phys.* **2001**, 90, 5048-5051.
- ⁶ Tsai, M.-H.; Lin, H.-W.; Su, H.-C.; Ke, T.-H.; Wu, C.-C.; Fang, F.-C.; Liao, Y.-L.; Wong, K.-T.; Wu, C.-I.; *Adv. Mater.* **2006**, 18, 1216-1220.
- ⁷ He, J.; Liu, H.; Dai, Y.; Ou, X.; Wang, J.; Tao, S.; Zhang, X.; Wang, P.; Ma, D.; *J. Phys. Chem. C* **2009**, 113, 6761-6767.
- ⁸ Adams, J. E.; Mantulin, W. W.; Huber, J. R.; *J. Am. Chem. Soc.* **1973**, 95, 5477.
- ⁹ Ren, X.; Li, J.; Holmes, R. J.; Djurovich, P. I.; Forrest, S. R.; Thompson, M. E. *Chem. Mater.* **2004**, 16, 4743.
- ¹⁰ Holmes, R. J.; D'Andrade, B. W.; Forrest, S. R.; Ren, X.; Li, J.; Thompson, M. E. *Appl. Phys. Lett.* **2003**, 83, 3818.
- ¹¹ Li, J.; Djurovich, P. I.; Alleyne, B. D.; Tsyba, I.; Ho, N. N.; Bau, R.; Thompson, M. E. *Polyhedron* **2004**, 23, 419-428.
- ¹² Eom, S.-H., Zheng, Y.; Chopra, N.; Lee, J.; So, F.; Xue, J.; *Appl. Phys. Lett.*, **2008**, 93, 133309.

- 13 Burrows, P. E.; Padmaperuma, A. B.; Sapochak, L. S.; Djurovich, P.; Thompson, M. E. *Appl. Phys. Lett.* **2006**, *88*, 183503.
- 14 Padmaperuma, A. B.; Sapochak, L. S.; Burrows, P. E.; *Chem. Mater.* **2006**, *18*, 2389-2396.
- 15 Mamada, M.; Ergun, S.; Pérez-Bolívar, C.; Anzenbacher, P. Jr.; *Appl. Phys. Lett.* **2011**, *98*, 073305.
- 16 Sudhakar, S.; Sellinger, A.; *Macromol. Rapid. Comm.* **2006**, *27*, 247-254.
- 17 Bolink, H. J.; Barea, E.; Costa, R. D.; Coronado, E.; Sudhakar, S.; Zhen, C.; Sellinger, A.; *Org. Electr.* **2008**, *9*, 155-163.
- 18 Bolink, H. J.; Santamaria, S. G.; Sudhakar, S.; Zhen, C.; Sellinger, A.; *Chem. Commun.* **2008**, 618-620.
- 19 Soh, M. S.; Santamaria, S. A. G.; Williams, E. L.; Perez-Morales, M.; Bolink, H. J.; Sellinger, A.; *J. Polym. Sci. B: Polym. Phys.* **2011**, *49*, 531-539.
- 20 Perdew, J. P.; Yue, W.; *Phys. Rev. B: Condens. Matter Mater. Phys.* **1986**, *33*, 8800-8802.
- 21 Becke, A. D.; *Phys. Rev. A: At., Mol., Opt. Phys.* **1988**, *36*, 3098-3100.
- 22 Schäfer, A.; Horn, H.; Ahlrichs, R.; *J. Chem. Phys.* **1992**, *97*, 2571-2577.
- 23 Andrae, D.; Häußermann, U.; Dolg, M.; Stoll, H.; Preuss, H.; *Theor. Chim. Acta* **1990**, *77*, 123-141.
- 24 Schäfer, A.; Huber, C.; Ahlrichs, R.; *J. Chem. Phys.* **1994**, *100*, 5829-5835.
- 25 Klamt, A.; *J. Phys. Chem.*, 1995, **99**, 2224-2235.
- 26 Ahlrichs, R.; Bär, M.; Häser, M.; Horn, H.; Kölmel, C.; *Chem. Phys. Lett.* **1989**, *162*, 165-169.
- 27 Sasabe, H.; Takamatsu, J.; Motoyama, T.; Watanabe, S.; Wagenblast, G.; Langer, N.; Molt, O.; Fuchs, E.; Lennartz, C.; Kido, J.; *Adv. Mater.* **2010**, *22*, 5003-5007.
- 28 Allcock, H. R.; Sunderland, N. J.; Primrose, A. P.; Rheingold, A. L.; Guzei, I. A.; Parvez, M.; *Chem. Mater.* 1999, *11*, 2478-2485.
- 29 Bode, H.; Bach, H.; *Ber. Dt. Chem. Ges.* **1942**, *75*, 215-226.
- 30 Acock, K. G.; Shaw, R. A.; Wells, F. B. G.; *J. Chem. Soc.* **1964**, 121-130.

- ³¹ Mashima, K.; Kusano, K.; Sato, N.; Matsumura, Y.; Nozaki, K.; Kumobayashi, H.; Sayo, N.; Hori, Y.; Ishizaki, T.; Akutagawa, S.; Takaya, H.; *J. Org. Chem.* **1994**, *59*, 3064-39076.
- ³² Appel, R.; Einig, H.; *Chem. Ber.* **1975**, *108*, 914-918.
- ³³ H. Bässler, V. I. Arkhipov, E. V. Emelianova, A. Gerhard, A. Hayer, C. Im, J. Rissler, J.; *Synth. Metals* **2003**, *135-136*, 377.
- ³⁴ Brunner, K.; van Dijken, A.; Börner, H.; Bastiaansen, J. J. A. M.; Kiggen, N. M. M.; Langeveld, B. M. W.; *J. Am. Chem. Soc.* **2004**, *126*, 6035.
- ³⁵ Dietrich, A.; Neumüller, B.; Dehnicke, K.; *Z. Anorg. Allg. Chem.* **2000**, *626*, 2035.
- ³⁶ Bold, M.; Lennartz, C.; Prinz, M.; Schmidt, H.-W.; Thelakkat, M.; Bäte, M.; Neuber, C.; Kowalsky, W.; Schildknecht, C.; Johannes, H.-H.; WO Patent 2005, 019373.
- ³⁷ Langer, N.; Kahle, K.; Lennartz, C.; Molt, O.; Fuchs, E.; Rudolph, J.; Schildknecht, C.; Watanabe, S.; Wagenblast, G.; WO Patent 2009, 003898.

9 Appendix: Triplet Excimer Emission in a Series of 4,4'-Bis(*N*-carbazolyl)-2,2'-biphenyl Derivatives

S. T. Hoffmann,[†] P. Schrögel,[‡] M. Rothmann,[‡] R. Albuquerque,[†]

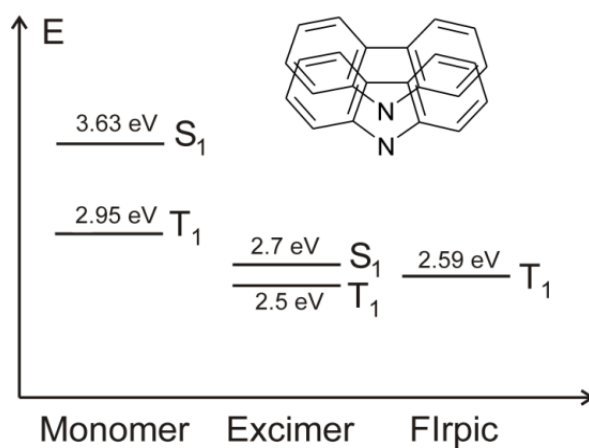
P. Strohriegl,[‡] and A. Köhler^{†}*

[†]Lehrstuhl Experimentalphysik II, Universität Bayreuth, 95440 Bayreuth, Germany,

[‡]Lehrstuhl Makromolekulare Chemie I, Universität Bayreuth, 95440 Bayreuth,

Germany

*Corresponding author: anna.koehler@uni-bayreuth.de



Reprinted with permission from

Journal of Physical Chemistry B, **2011**, 115, 414-421.

Copyright 2011, American Chemical Society

doi.org/10.1021/jp107408e

Abstract

Carbazole-based materials such as 4,4'-bis(N-carbazolyl)-2,2'-biphenyl (CBP) and its derivatives are frequently used as matrix materials for phosphorescent emitters in organic light emitting diodes (OLED)s. An essential requirement for such matrix materials is a high energy of their first triplet excited state. Here we present a detailed spectroscopic investigation supported by density functional theory calculations on two series of CBP derivatives, where CH₃ and CF₃ substituents on the 2 - and 2' - position of the biphenyl introduce strong torsion into the molecular structure. We find that the resulting poor coupling between the two halves of the molecules leads to an electronic structure similar to that of *N*-phenyl-3,6-dimethyl-carbazole, with a high triplet state energy of 2.95 eV. However, we also observe a triplet excimer emission centered at about 2.5-2.6 eV in all compounds. We associate this triplet excimer with a sandwich geometry of neighboring carbazole moieties. For compounds with the more polar CF₃ substituents, the lifetime of the intermolecular triplet excited state extends into the millisecond range for neat films at room temperature. We attribute this to an increased charge-transfer character of the intermolecular excited state for the more polar substituents.

Keywords

carbazole, triplet excimer, DFT calculation, OLEDs

Introduction

While organic semiconductor materials are of current interest for a range of applications such as solar cells, displays, sensing or radio-frequency identification tags (RFIDs),¹ they offer particularly promising opportunities for solid state lighting since they allow for the engineering of efficient white organic light emitting devices (WOLEDs).^{2,3} One approach to WOLEDs consists in the use of red, green and blue emissive dopants that are incorporated into carefully designed multilayer structures or suitably attached as side groups to a polymer backbone.^{2,3,4} As an alternative method, the incorporation of a single emitter with efficient broad excimer emission has been demonstrated successfully.⁵ In either case, the emitters used in WOLEDs require host materials that need to fulfill several constraints. To allow for efficient charge injection from both electrodes, the energy separating the highest occupied molecular orbital (HOMO) and the lowest unoccupied molecular orbital (LUMO) should be not too high. At the same time, the energy of the first triplet excited state needs to be high enough so that phosphorescence from blue or green emitters is not quenched by energy transfer to the host.

Host materials that are considered suitable and that are therefore used frequently for WOLED applications are often based on carbazole structures,⁵⁻⁹ such as CBP (CBP=4,4'-bis(9-carbazolyl)-biphenyl) or polyvinyl carbazole like polymers.¹⁰⁻¹⁵ Approaches to obtain high triplet energies include reducing the size of the conjugated system, e.g., by replacing the biphenyl bridging between the two carbazoles with a single phenyl as in mCP (mCP = 3,5-bis(9-carbazolyl)-benzene),¹⁶ or by introducing torsion between the two biphenyls as in 4,4'-bis(9-carbazolyl)-2,2'-dimethyl-biphenyl (CDBP).⁷ This substitution leads to good results with respect to emission and efficiency. We have recently reported the synthesis of a set of CBP derivatives with triplet excited state energies of about 2.95 eV.¹⁷ As for CDPB, the high triplet energy is obtained by introducing torsion between the biphenyls through substitution with a CH₃ group or a CF₃ group. Further substitution with CH₃-groups on the carbazole moiety was employed to fine-tune HOMO and LUMO levels for optimized charge injection.

We present here a detailed spectroscopic and quantum mechanical study on the electronic structure of these compounds, focusing on the influence of the electron-rich CH_3 group compared to the electron-withdrawing CF_3 group on the nature of the optical transitions. In addition to fluorescence and phosphorescence from the monomer, we observe phosphorescence that can be attributed to a sandwich excimer of adjacent carbazole moieties. While this intermolecular triplet state emission is present for both types of compounds, the radiative excimer emission rate is higher for the CH_3 -substituted compounds than for the compounds with the more polar CF_3 group, where the intermolecular excited state seems to acquire a stronger charge-transfer component. With a view to the ubiquitous use of CBP derivatives as hosts for WOLED applications we note that the well-known propensity of this general class of materials to form excimer states (and the polarity dependence of triplet excimer formation) deserves more attention.^{11,18-28} The presence of poorly emissive triplet excimers by the host can easily go unnoticed, in particular when combined with efficient phosphorescent emitters that cover a broad spectral range as is the case in WOLEDs. Nevertheless, long-lived triplet excimers may present non-radiative decay channels, and they can reduce device efficiency and device lifetime if not suitably managed. On the other hand, when the radiative decay rate of the host triplet excimer is high enough, they could be contemplated as emitter materials for WOLEDs by themselves. In the context of the study presented here, we focus on understanding the electronic structure of the CBP derivatives by spectroscopic studies in combination with quantum chemical calculations.

Experimental Section

The series of CBP derivatives were synthesized as described by Schrögel and co-workers.¹⁷ For optical measurements, 10^{-5} M cyclohexane solutions of the materials as well as thin films on quartz substrates were prepared. Both, neat films and films with 10 wt-% of compound in poly(methylmethacrylate) were prepared by spin coating. The ultraviolet-visible (UV/Vis) absorption spectra were measured in solution and on neat films with a Hitachi U-3000 spectrometer. Room temperature steady state emission spectra from solution and from thin films were obtained from a Shimadzu spectrofluorophotometer RF-5301PC using excitation at 300 nm.

The phosphorescence spectra were taken with the thin film samples mounted in a continuous flow helium cryostat. The temperature was controlled with an Oxford Intelligent temperature controller-4 (ITC-502). Excitation was provided by a pulsed, frequency-tripled Nd-YAG laser at 355 nm (3.49 eV) (Spectron SL401). This wavelength corresponds to the red tail of the first absorption band in our compounds. The duration of the laser pulses was 6 ns and the laser was operated at a repetition rate of 10 Hz by a self made electronic delay generator. The light emitted by the sample was dispersed and subsequently detected by a time gated intensified CCD camera (Andor iStar DH734-18F-9AM). The measurements were taken with a delay time of 500 ns and a gate width of 60 ns. The measurements were carried out at an excitation density of about $250 \mu\text{Jcm}^{-2}\text{pulse}^{-1}$ on films of about 150 nm thickness as determined by a Dektak profilometer. To increase the signal-to-noise-ratio, all spectra were obtained by averaging over 2000 laser shots.

Density Functional Theory (DFT) calculations were carried out for the compounds **3** and **6** using the B3LYP hybrid functional together with the basis set 6-31G*.^{29,30} The excited states were calculated by using Time-Dependent-DFT with the optimized ground-state geometries. All DFT calculations were carried out with the Gaussian 03 program.

Results and Discussion

(i) Absorption and Fluorescence

We use the widely employed CBP as our reference compound. Figure 1 shows the general structure of the compounds along with a table that details the substitution pattern. In order to obtain torsion, the 2- and 2'-positions of the biphenyl unit were substituted with electron withdrawing CF_3 groups or with electron-rich CH_3 moieties. In order to assess the degree of electronic decoupling obtained by torsion, we compare our materials to *N*-phenyl-3,6-dimethyl-carbazole. The structure for *N*-phenyl-3,6-dimethyl-carbazole is also displayed in Figure 1. In order to block the reactive 3 and 6 positions of the carbazole unit methyl groups have been introduced. In addition, this leads to a further fine-tuning of the electronic structure. Thus, compounds **1-6** form two sets of materials, with the group formed by **1** (CDBP), **2** and **3** based on the methyl-substituted

biphenyl centre and the compounds **4-6** based on the trifluoromethyl substituted core. Within each set, the amount of CH₃-substitution on the carbazole unit rises.

	CBP	1 (CDBP)	2	3	4	5	6
R ₁	H	H	CH ₃	CH ₃	H	CH ₃	CH ₃
R ₂	H	H	H	CH ₃	H	H	CH ₃
R ₃	H	CH ₃	CH ₃	CH ₃	CF ₃	CF ₃	CF ₃

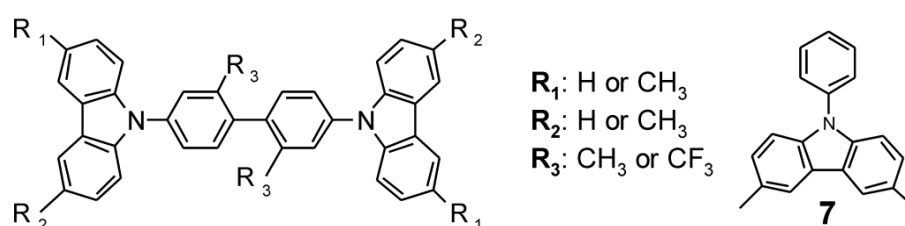


Figure 1. Chemical structures of 4,4'-bis(9-carbazolyl)-biphenyl (CBP), the substituted derivatives **1-6** and of N-phenyl-3,6-dimethyl-carbazole (compound **7**).

To understand how the substitutions affect the excited states of these compounds, we first consider the effect of torsion by comparing the compounds CBP and CDBP. CDBP differs from CBP only by the presence of the methyl group at the 2,2'-positions of the central biphenyl unit. According to DFT calculations, the methyl group increases the ground state torsion angle between the two central phenyl rings from about 33° to 81°.¹⁷ Parts a and b of Figure 2 display the room temperature absorption and fluorescence spectra taken from 10⁻⁵ M cyclohexane solutions of both compounds. Despite the different ground state geometry, both CBP and CDBP display a first absorption band at the same energy, that is with a S₁←S₀ 0-0 peak at 3.70 eV and the 0-1 vibrational replica at 3.88 eV, yet for the more planar CBP the molar extinction of this first band is more than twice that found for CDBP. In contrast to CDBP, there is also some intensity at 3.95 eV in CBP. The next absorption band with a 0-0 peak at 4.30 eV and a 0-1 vibrational sideband at 4.45 eV is at the same energy and at very similar intensity for both compounds.

When considering the absorption spectrum of CDBP, we note a striking similarity to the absorption of N-phenyl-3,6-dimethyl-carbazole that is also displayed in Figure 2 for ease of comparison. In the same way, the fluorescence spectra of N-phenyl-3,6-dimethyl-

carbazole and CDBP coincide. In contrast to the absorption, the emission of CBP is red shifted compared to CDBP. We attribute this to the planarization of CBP after the transition to the excited state, while such a geometric relaxation is not possible for CDBP due to the bulkier side groups. From this comparison of the three compounds it is evident that the torsion induced by the methyl unit at the central biphenyl reduces conjugation between the two parts of the molecule such that the optical transitions in CDBP are dominated by just the separate *N*-phenyl-carbazole moieties.

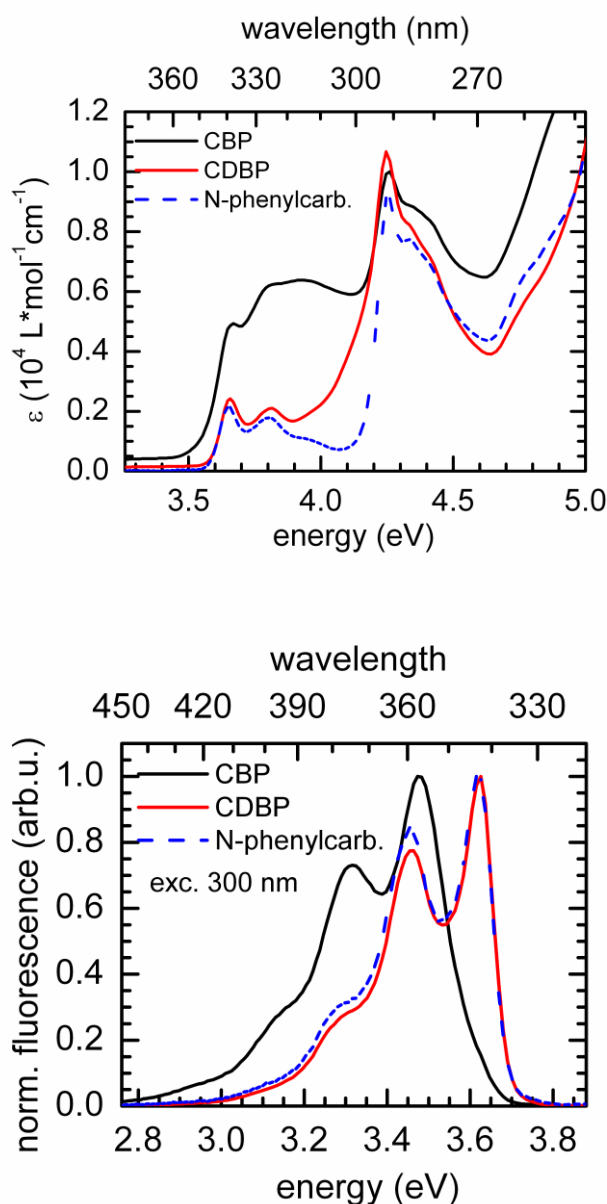


Figure 2. (a) Absorption spectra and (b) fluorescence spectra, both taken at room temperature for CBP, CDBP and the *N*-phenyl-3,6-dimethyl-carbazole **7** in 10^{-5} M cyclohexane solution.

If the biphenyl is substituted with the electron-withdrawing trifluoromethyl group instead of the electron-rich methyl unit, we observe only minor changes in the absorption, yet an entirely different spectrum in emission. For example, the only differences in the absorption of compounds **3** and **6** (Figure 3a) are a slightly higher extinction at about 3.85 eV and a significantly reduced extinction in the band around 4 eV for the CF₃ substituted compound while the energetic positions and spectral shapes of the absorption features remain essentially unaltered. In contrast, in the fluorescence spectra the emission energy and vibrational structure differ strongly. The emission of compound **3** closely resembles that of the parent molecule CBP in both energy and structure, while the luminescence of **6** consists of a broad unstructured peak centered at about 3.25 eV with a small shoulder at 3.55 eV.

Before considering the difference between the CF₃ and the CH₃ substituted compounds in more detail, we briefly comment on the minor modifications to the excited state energies obtained by introducing additional methyl substituents at the pendant carbazole moieties. We consider compounds **1** (CDBP), **2** and **3** (Figure 3b). For all compounds, we observe a small bathochromic shift with increasing amount of methyl substituents. Otherwise the spectra retain the features of the carbazole-emission. We attribute this to a slight upshift of the HOMO due to the electron donating character of the methyl group, as confirmed by quantum chemical calculations. The same effect occurs in the trifluoromethyl series **4**, **5** and **6** upon CH₃ substitution on the carbazole moiety.

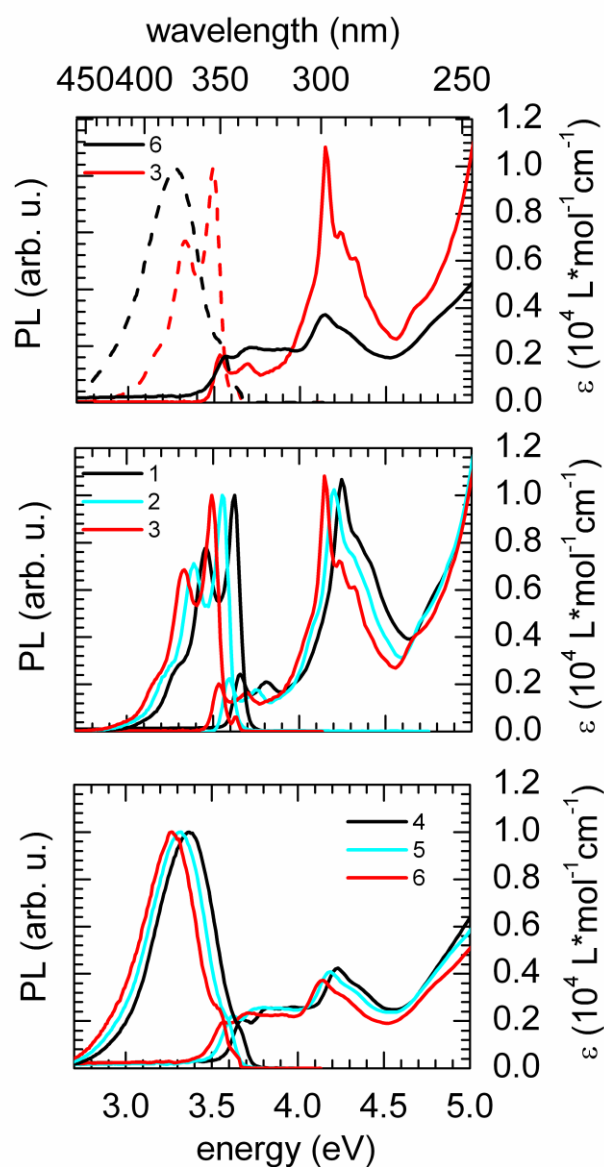


Figure 3. Room temperature absorption and fluorescence spectra in 10^{-5} M cyclohexane solution (a) for compounds **6** and **3**, (b) for the CH_3 -substituted compounds **1** - **3** and (c) for the CF_3 -substituted compounds **4** - **6**.

To understand what causes the striking difference in the emission spectra of the CF_3 -substituted series compared to the CH_3 -substituted one, we compare solution spectra with spectra taken on thin films. The fluorescence spectra taken from the liquid solution (10^{-5} M of host compound in cyclohexane) are, apart from a very minor bathochromic shift of 50 meV, identical to those taken from thin films of solid state solution (10 wt% of host compound in poly(methylmethacrylate)). For the neat films, however, we observe

an additional broad emission feature in the CH₃-substituted compound **3** centered at about 2.6 eV. (Figure 4) Such a broad red emission that only occurs in the neat film yet not in solutions is typical for an intermolecular excited state. If we correct for the slight energy shift between the solid solution spectrum and the neat spectrum and then form the difference spectrum between the two, we find that the broad emission centered at 2.6 eV contributes about 40 % to the overall neat film emission in **3**. In contrast for **6**, the same red emission only becomes evident after forming the difference spectrum as it amounts to merely 7 % of the integrated neat film emission.

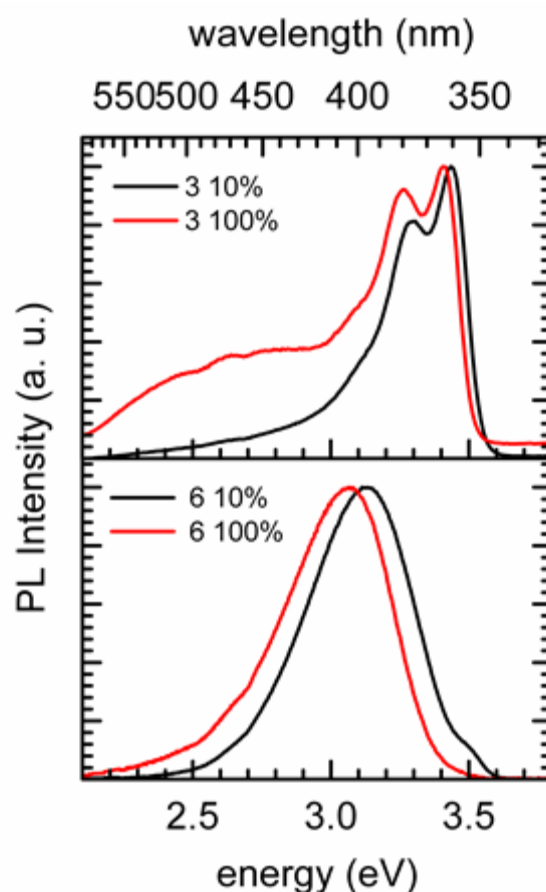


Figure 4. Room temperature steady state emission spectra of neat films (labelled 100%) and solid state solution in PMMA (labelled 10 %) normalized to unity (a) for the CH₃-substituted compound **3** (b) and for the CF₃-substituted compound **6**.

We carried out DFT calculations of the molecular orbitals and excited state energies for the compounds **3** and **6** in order to understand the influence of CF₃ substitution on the

central biphenyl compared to the CH₃ substitution. The HOMO and LUMO electron densities are displayed in Figure 5 and the resulting term scheme is shown in Figure 6. For compound **3**, the torsion between the central biphenyl ring due to the CH₃ groups leads to a localization of the electron wave function on each of the carbazole units. As a result, HOMO and HOMO-1, as well as LUMO and LUMO+1 are nearly degenerate, separated by only 1-2 meV. The lowest excited singlet state, S₁, involves mainly transitions from HOMO→LUMO+1 and HOMO-1→LUMO. Only the former of the two is illustrated in Figure 6. In the HOMO, the lone pair on the nitrogen mixes with the π-conjugated system of the rings. The transitions contributing to S₁ have predominantly a π→π* character and the vertical transition energy is calculated to be at 3.97 eV. At slightly higher energy, that is at 4.10 eV, we find the second excited singlet state which involves transitions from orbitals localized on the carbazole unit to an orbital localized on the central biphenyl section of the molecule, such as the HOMO→LUMO+2 transition illustrated in Figure 5. S₂ has thus a strong charge transfer character.

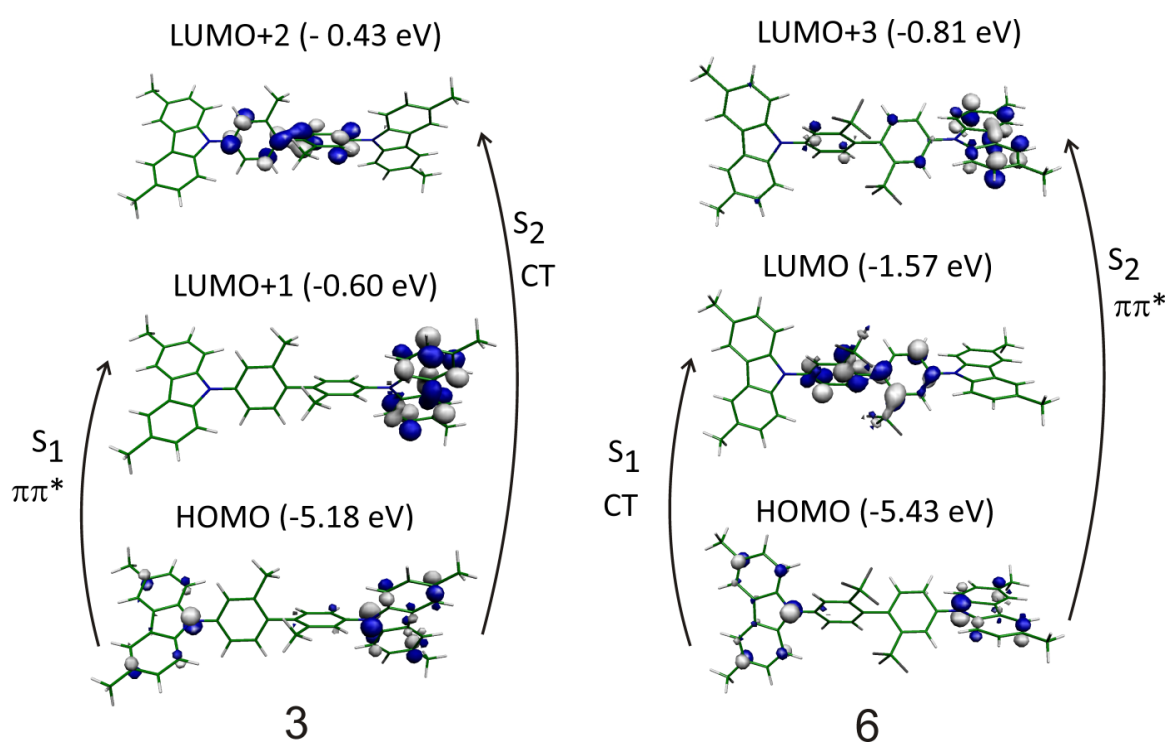


Figure 5. The DFT optimized chemical structures and relevant orbitals for compounds **3** (left side) and **6** (right side). The energies of the orbitals with respect to the vacuum level are also indicated. The arrows indicate the transitions into S₁ and S₂ along with their dominant character.

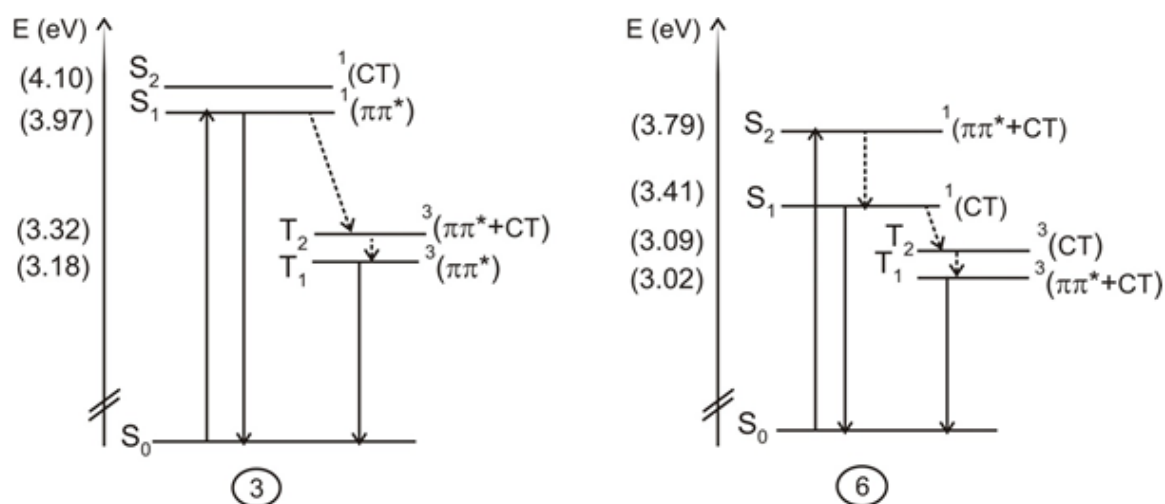


Figure 6. Scheme of the singlet and triplet energy levels based on the DFT calculations for compound **3** and **6**. The predominant nature of the transitions involved, i.e. charge transfer (CT) or $\pi\pi^*$, is indicated next to the energy levels.

In contrast to **3**, compound **6** is substituted with electron withdrawing CF_3 groups on the biphenyl. As a result, the orbital localized on the central biphenyl is stabilized and becomes the LUMO. LUMO+1 and LUMO+2 are also centered on the biphenyl. Only orbitals from LUMO+3 onwards contain some non-negligible electron density on the carbazole units. Transitions from a HOMO localized on the carbazole to the LUMO on the biphenyl group lead to a singlet excited state with a strong intramolecular charge transfer character (and concomitantly a very small oscillator strength) at a vertical transition energy of 3.41 eV. The second excited singlet state S_2 comprises both carbazole-carbazole centered $\pi \rightarrow \pi^*$ transitions such as $\text{HOMO} \rightarrow \text{LUMO}+3$ and carbazole-biphenyl charge-transfer type transitions. With 3.79 eV, it is at energy similar than the $\pi \rightarrow \pi^*$ based S_1 state in **3**.

With these calculations, we can now interpret the absorption and fluorescence spectra. Absorption requires reasonable oscillator strength. Consequently, the absorption observed experimentally at 3.54 eV takes place into the S_1 state of **3** and into the S_2 state of **6**. The S_1 state of **6** cannot be seen in the absorption spectrum due to the low oscillator strength associated with this intramolecular charge-transfer-type transition. After absorption, fluorescence in **3** occurs from the same S_1 state that has been excited, resulting in a small Stokes' shift and clear vibrational structure that mirrors the

absorption band (see Figure 3a). In contrast for **6**, fast internal conversion to the lower energy S_1 takes place, in agreement with Kasha's rule.³¹ The intramolecular charge-transfer character of the $S_1 \rightarrow S_0$ transition precludes a vibrational structure and causes the broad emission.

(ii) Phosphorescence

To experimentally observe the triplet state emission, we measured the 10 K luminescence from thin films at a delay time of 500 ns after an excitation pulse and using a detector with a large gate width of 60 ms. Figure 7 shows the spectra obtained for **1** (CDBP), **2** and **3**, normalized to unity at about 2.95 eV. The corresponding spectra for **4**, **5** and **6** are displayed in Figure 8.

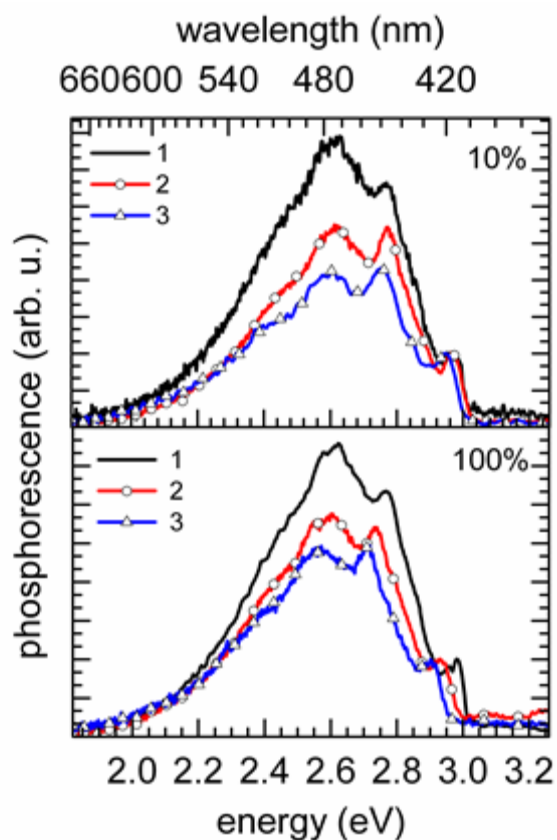


Figure 7. Emission spectra taken at 10 K with a delay time of 500 ns and a gate width of 60 ms for the CH_3 -substituted compounds **1-3** (a) in a 10 wt% solid state solution of PMMA and (b) in pure film. The spectra are normalized to unity at the first emission peak.

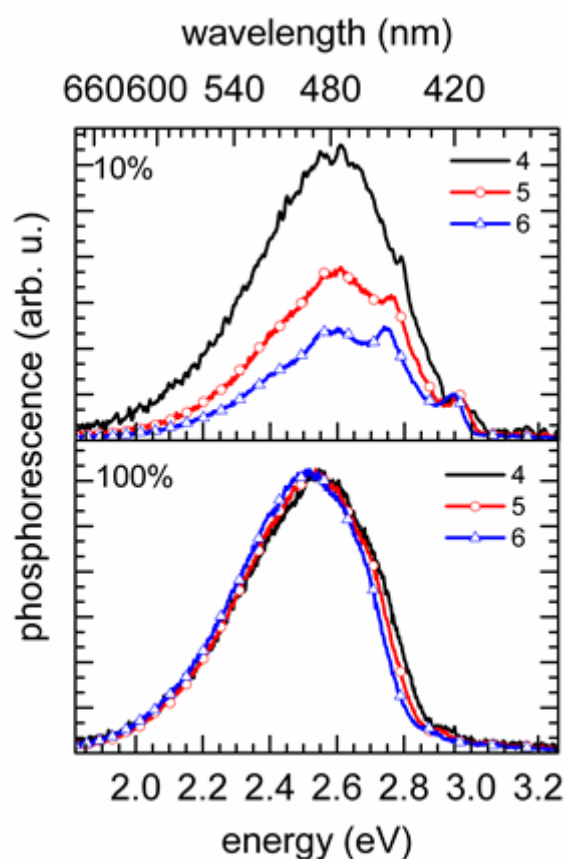


Figure 8. Emission spectra taken at 10 K with a delay time of 500 ns and a gate width of 60 ms for the CF_3 -substituted compounds **4-6** (a) in a 10 wt% solid state solution of PMMA and (b) in pure film. The spectra are normalized to unity at the first emission peak.

For all spectra taken in a solid state solution (Figures 7a and 8a), we observe two sharp peaks at 2.95 eV and at 2.76 eV as well as a broad peak centered at 2.6 eV. The intensity of this broad peak reduces when the number of methyl substituents on the pendant carbazoles is increased along the series **1** (CDBP), **2** and **3**, and along the series **4**, **5** and **6**.

Increasing the concentration by using a pure film of compounds (figures 7b and 8b) does not change the spectral shape any further for the series with the methyl substituents on the biphenyl, except for a small bathochromic shift with increasing CH_3 -content. In contrast, for the compounds with CF_3 at the central biphenyl, the sharp features are lost and the emission is entirely dominated by the broad peak now centered at 2.5 eV. Furthermore, the spectra do not change with increasing amount of CH_3 -content, except again for a small bathochromic shift.

We consider that the broad peak may be associated with intermolecular interactions since it reduces in relative intensity when the molecule is in a solid solution (compare Figure 8b and 8a), and when the number of bulky CH₃ groups on the molecule increases. For compound **6**, some vibrational structure is clearly visible in the emission from solid solution, while the luminescence from the neat film contains only the broad feature. We therefore use these two spectra to separate the contributions. Figure 9a shows the emission from the solid state solution for compound **6**. Also shown is the emission obtained from the neat film, scaled to the red tail of the solid state solution spectrum. Subtracting the scaled neat film spectrum from the solid state solution spectrum results in a well-structured difference spectrum, with a 0-0 peak at 2.95 eV and clear vibrational replica at 2.75, 2.60, and 2.44 eV. In Figure 9b, we compare the so obtained difference spectrum to the phosphorescence spectrum we found for *N*-phenyl-3,6-dimethylcarbazole **7** in a neat film. The spectra are very similar. From this analysis it is evident that the emission from compounds **4**, **5** and **6** is due to a superposition of the well-structured carbazole phosphorescence with the 0-0 peak at 2.95 eV and a broad unstructured emission centered around 2.5-2.6 eV that we attribute to intermolecular interactions as detailed further below. The same applies analogously to **1** (CDBP), **2** and **3**, albeit with a lower contribution by the intermolecular peak in the neat film.

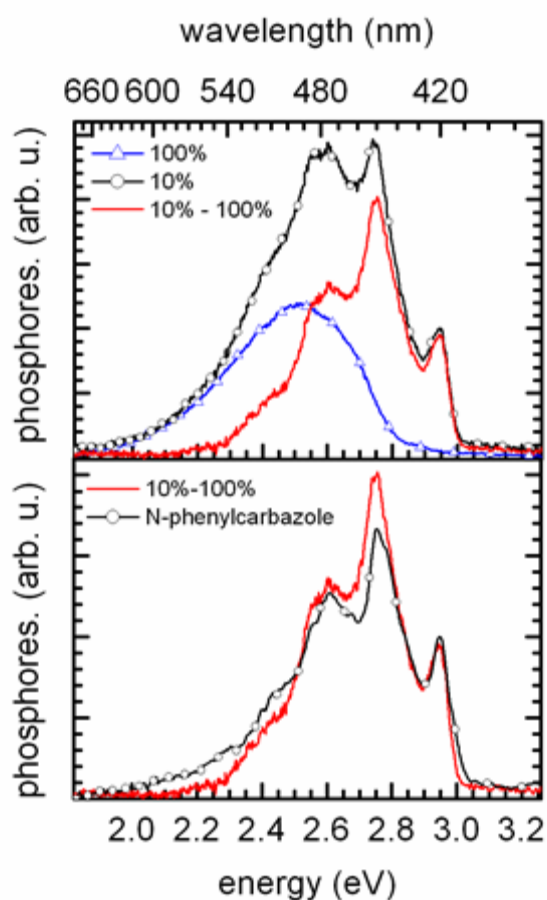


Figure 9. (a) 10 K phosphorescence spectra of compound **6** in a pure film (blue line with triangles) and in a 10 wt % solid state solution in PMMA (black line with circles), normalized to unity at the first peak of emission, along with the difference spectrum between the pure film spectrum and the solid state solution spectrum (red line). (b) Comparison of the difference spectrum (red line) with the 10 K phosphorescence spectrum from **7** in a pure film (black line with circles).

The well-resolved vibrational structure of the phosphorescence in contrast to the broad fluorescence for the CF_3 -substituted compounds implies that the state giving rise to phosphorescence is of a different nature to the state causing the fluorescence. This is confirmed by the quantum chemical calculations. The nature of the optical transitions directly affects the position of the associated triplet excited states. The exchange energy, and thus the energy gap between a singlet and the associated triplet state, is well-known to scale with the overlap of the orbitals involved.³² In consequence, $\pi \rightarrow \pi^*$ transitions result in a larger exchange energy than the charge-transfer type transitions. For compound **6** this implies that the $\pi \rightarrow \pi^*$ transitions that contribute to S_2 lead to a large calculated singlet-triplet splitting of 0.77 eV, while the charge-transfer type

transitions involved in S_1 give rise to a calculated singlet-triplet splitting of only 0.32 eV (see Figure 6). In consequence, charge-transfer type transitions cause the second lowest triplet excited state, T_2 , while the lowest energy triplet excited state, T_1 , has some $\pi - \pi^*$ character that leads to vibrational structure, as in compound **3**.

To summarize the results obtained so far, we find that the CH_3 substituted molecules have a first excited singlet state with 0-0 $S_1 \rightarrow S_0$ transition energies are in the range from 3.5 eV to 3.7 eV, depending on the substituents on the carbazole moiety. Phosphorescence takes place with the 0-0 $T_1 \rightarrow S_0$ transition in the range of 2.9-3.0 eV, and it is superimposed by a broad additional emission band. The strong torsion within the biphenyl unit implies that the $\pi \rightarrow \pi^*$ transition causing the S_1 and T_1 state is localized on the carbazole moieties. As a result, absorption, fluorescence and phosphorescence are essentially identical to the spectra reported for *N*-arylcarbazoles in the pioneering works by Klöpffer¹³ and Johnson.^{12,18} We have shown this by direct comparison of **1** (CDBP), **2** and **3** to *N*-phenyl-3,6-dimethyl-carbazole **7**, and by DFT calculations. Our calculations only consider the vertical $S_1 \leftarrow S_0$ and $T_1 \leftarrow S_0$ transitions. In the excited state, there is likely to be some degree of planarization, yet the similarity between the emission spectra of compounds **1-3** and **7** confirms the essentially localized character of the excited states.

When using CF_3 instead of CH_3 for the biphenyl substitution, the absorption and phosphorescence spectra remain very similar, yet the fluorescence shifts to the red and loses all structure. This is because absorption and phosphorescence still involve the $\pi - \pi^*$ transition localized on the carbazole, while fluorescence takes place from an intramolecular charge-transfer (CT) state. Essentially, the result of the CF_3 substitution is to stabilize an unoccupied orbital centered on the biphenyl, so that an intramolecular CT transition from the carbazole to the biphenyl moiety requires less energy than the carbazole-based $\pi \rightarrow \pi^*$ transition. Without the CF_3 substitution, this order is reversed.

(iii) Excimer emission

We now consider the broad emission found around 2.5-2.6 eV (Figures 4, 7 and 8) in more detail. First we note that for the spectra taken under steady state conditions at room temperature (Figure 4), the broad emission is particularly prominent for the CH₃-substituted compound **3**, while it contributes only little to the spectrum of the CF₃-substituted compound **6**. However, when the emission is recorded at 10K with a delay time of 500 ns after the excitation pulse and with a long detector gate width of 60ms (Figures 7 and 8), the broad emission features more strongly in the spectra of the CF₃-substituted materials. This difference in intensity is easily resolved when considering the detection modes used in more detail. With use of steady state detection all the photons emitted from an excited state are integrated, and so excitations that decay with a high radiative decay rate show up more strongly. Naturally, these excitations have already decayed when waiting for a delay of 500 ns after excitation, and the collected signal intensity is mostly due to excitations with a lower radiative decay rate. Comparison of Figures 4, 7 and 8 suggests therefore that the broad emission centered at around 2.5-2.6 eV is present in both classes of materials, yet with a faster decay rate for the CH₃-substituted compounds compared to the CF₃-substituted counterparts. To confirm this hypothesis we measured the decay time at 2.4 eV in a neat film at room temperature (Figure 10). The emission decays in a non-monomolecular fashion to about 1/e of its initial value in 240 μ s for **3**, yet in 1.2 ms for **6**.

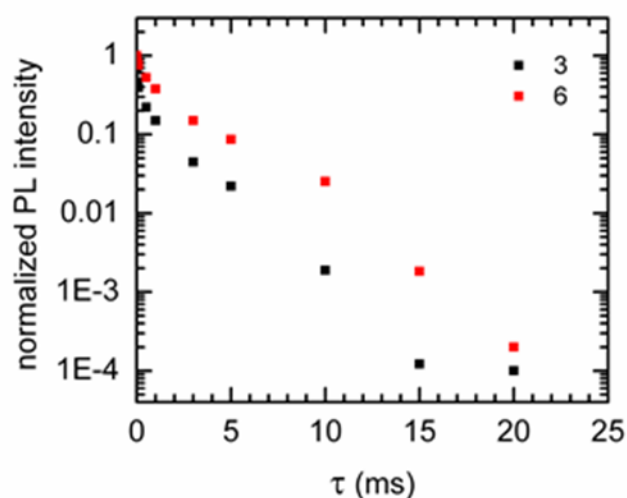


Figure 10. Normalized decay curves of the photoluminescence intensity for compounds **3** and **6** in neat film (where, for example, 1E-3 represents 1×10^{-3}).

Next we draw attention to the fact that the relative contribution of the broad emission decreases when the molecule has more bulky substituents on the carbazole or when the molecule is diluted into a solid state solution, suggesting that the broad emission is associated with intermolecular interactions. Furthermore, there is no corresponding absorption feature. We therefore attribute the broad emission to an excimer. We use the term excimer to refer to an intermolecular state that is only stable in the excited state and that has both, covalent and ionic contributions to the overall excited state wave function, Ψ . This can be expressed as

$$\Psi = c_1\Psi(A^*B) + c_2\Psi(AB^*) + c_3\Psi(A^-B^+) + c_4\Psi(A^+B^-) \quad (1)$$

where A and B refer to different molecules, the symbols $*$, $^+$ and $^-$ indicate the excited or charged state, and c denotes a constant.³² Usually it is understood that the covalent contribution, given by the first two terms in equation (1), dominate the character of the excited state.

We now consider the subtle differences between the excimer in the CH_3 -substituted compounds such as **3** and in the CF_3 -substituted ones such as **6**. The energy and shape of the emission are identical, yet for **6** compared to **3**, the lifetime of the excimer emission is about five times longer and the intensity under steady state detection is lower. As already mentioned above, this implies a lower radiative decay rate in **6** than in **3**. We interpret this as an indication that the more polar character of a neat film of **6** increases the ionic contribution to the overall excimer wave function expressed in (1). A stronger charge-transfer character of the intermolecular state reduces the wave function overlap that is needed according to Fermi's golden rule to give a high radiative decay rate. The fact that the substitution with the CF_3 group increases the charge-transfer character of the intermolecular excitation is a remarkable detail. The relative amount of the covalent to the ionic contribution in an intermolecular excitation such as an excimer or, in the case of a heterojunction, such as an exciplex is one of the factors that control the efficiency of charge separation at the intermolecular interface.^{33,34} It is therefore desirable to be able to fine-tune this property by a simple mechanism such as substitution. From the present data we are not able to differentiate whether the longer

lifetime of the excimer is caused by the increased polarity of the two molecules constituting the excimer, or whether it can be attributed to the enhanced polarity of the excimer's environment, or both.³⁵

We have already shown that the strong torsion in the biphenyl unit in compounds **1-6** electronically decouples the two halves of the molecule to some degree, resulting in absorption and phosphorescence spectra that are identical to those of *N*-phenyl-carbazole. *N*-arylcarbazoles and *N*-alkylcarbazoles have been studied extensively in the past by Klöpffer, Johnson and many others^{11,18-28}, and it is well known that they are prone to form excimers. Given the similar electronic structure, it is instructive to compare the excimer emission we find for compounds **1-6** with the existing literature on excimers in *N*-arylcarbazoles and *N*-alkylcarbazoles. These materials can form two different kinds of excimers, depending on their geometric arrangement.

If the carbazoles overlap by only one phenyl ring, a partial overlap excimer is formed. This excimer fluoresces in broad unstructured fashion at about 3.1 eV (400nm)^{19,26}. For carbazolophanes that are used as model compounds for the partial overlap excimer, Tani and coworkers²⁶ also report phosphorescence, though we note that this phosphorescence has vibrational structure with a 0-0 peak about 2.91 eV (425 nm), like the corresponding *N*-ethylcarbazole monomer. Since the triplet is strongly localized, it is conceivable that the resonance interaction is not sufficient to form a stable triplet excimer. A different conformation is that of a sandwich excimer where the two carbazole-derivatives involved overlap fully.^{19,26,36} Broad and unstructured fluorescence and phosphorescence are reported centered at about 2.7 eV (460 nm) and at about 2.5 eV (500 nm), respectively, for the sandwich excimer.^{19,26,36}

Triplet excimers are not reported often since the singlet-triplet splitting in excimers is small. As a result, triplet excimers are often energetically above the triplet state in the monomer and they become quenched by it.³² Triplet excimers can be observed if the stabilization energy of the excimer formation is large compared to the S_1 - T_1 energy splitting of the monomer, so that the energy level of the excimer triplet is lower than the monomer triplet (Figure 11). For carbazole sandwich excimers, this is the case.^{24,26,37}

The monomer S_1 - T_1 energy splitting is about 0.7 eV (see Figures 2 and 9 for *N*-phenyl-carbazole, or Figure 3 in reference²⁶ for *N*-ethyl-carbazole). In contrast the energetic

stabilization associated with the excimer formation is 0.9 eV, as is evident from the change in S_1 energy from 3.6 eV to 2.7 eV. We consider that this large stabilization energy is associated with a significant wave function overlap of the π -system in the carbazole sandwich excimer.

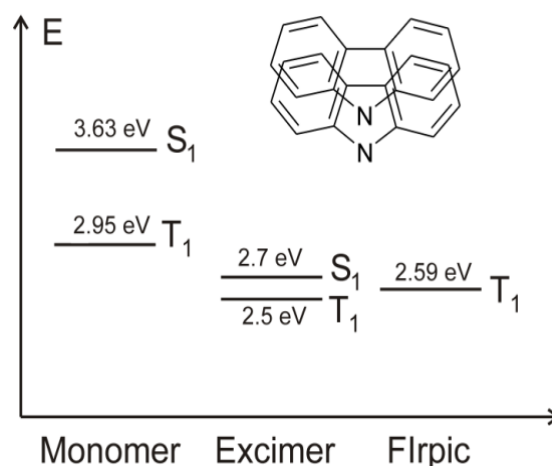


Figure 11. Energy diagram illustrating the singlet and triplet energy levels for the carbazole monomer, for the carbazole excimer and of the emitter Flrpc.

If we compare the excimer emission observed in compounds **1-6** to the excimer emission reported for *N*-arylcarbazoles and *N*-alkylcarbazoles, we find that our excimer emission centered at around 2.5 - 2.6 eV is energetically identical to the triplet of the carbazole sandwich excimer. Furthermore, the lifetime of the excimer in our compounds is on the order of a few hundred microseconds to milliseconds (Figure 10). This is too long for a singlet excimer, which is typically in the range of tens of nanoseconds,^{33,34,38,39} yet it is consistent with a typical phosphorescence lifetime at room temperature for organic solids.⁴⁰ On this basis we conclude that the excimer emission observed in compounds **1-6** can be assigned to a triplet excimer that is localized on two carbazole moieties in a sandwich configuration. On passing we remind the reader that we attributed the longer lifetime found for the CF_3 -substituted **6** to a stronger charge-transfer character of the intermolecular state. This is consistent with reports by Haggquist and coworkers who considered how the balance between geminate pair recombination, triplet excimer formation and triplet-triplet annihilation in the sandwich excimer of *N*-ethyl-carbazole depends on the dielectric constant of the solvent.³⁶ It also

confirms earlier work by Tani et al. on sandwich-type carbazole-derivatives^{24,26,37} and by Lim et al. on triplet excimers in naphthalene-derivatives that arrange in a skewed or L-shaped geometry.^{28,41} Both groups pointed out that triplet excimers are stabilized if charge resonance adds to the usual electronic resonance associated with excimers, i.e. if the third and fourth terms in equation (1) also contribute substantially. This is in contrast to singlet excimers, where electronic resonance alone, i.e. the first two terms in equation (1), is often sufficient.

Having established that there is a non-negligible amount of triplet excimers present in neat films of compounds **1-6**, we may now question whether these materials are suitable as hosts for blue triplet emitters. There are a number of reports where compound **1**, that is CDBP, was used as a host for the Iridium complex Flrpic. The OLED performance was found to be very good and certainly superior to that with CBP as host material.^{7,42} The reason for the good performance of **1** (CDBP) may be that Flrpic has a 0-0 triplet energy of 2.64 eV and the triplet excimer in CDBP is centered at around 2.6 eV, i.e. nearly isoenergetic as indicated in Figure 11. The energy transfer rates for forward transfer and back transfer therefore have to be very similar. Since the lifetime of Flrpic is only in the range of microseconds whereas the triplet excimer lives for several hundreds of microseconds this implies that almost all of the excited triplet states still decay from the Flrpic site. To which degree this balance shifts when the energy of the triplet in the phosphorescent emitter is higher than that in the excimer still needs to be investigated in a quantitative fashion.

Summary and conclusion

We have shown that the substitution on the central biphenyl unit successfully raises the triplet T_1 energy from 2.58 eV in the more planar CBP to 2.95 eV in the twisted compounds **1-6**. The monomeric phosphorescence is superimposed by triplet emission centered at 2.6 eV from a sandwich type excimer localized on the carbazole moiety. This triplet excimer emission can be reduced by increasing the number of bulky substituents on the carbazole. When using CF_3 instead of CH_3 as substituents on the central biphenyl, the fluorescence acquires a charge-transfer character, and the radiative recombination of the triplet excimer reduces. This is attributed to a larger ionic character of the

intermolecular triplet excited state for the more polar compounds. It implies that depending on the local molecular polarization, the intermolecular excited state may vary between having a dominant resonance character (more excimer-like) or a stronger coulomb contribution (more charge-transfer like). A partially similar dependence of the nature of the intermolecular excited state on the local molecular environment has also been observed for molecular heterojunctions, where this effect is known to contribute decisively to the recombination or dissociation rate of excited states.³⁵ Given the structural similarity of compounds **1-6** to the widely used host materials CBP or mCP and the relevant role of long-lived excimer states to device efficiency and lifetime, the possible existence of only weakly emissive triplet excimers from the host materials needs to be taken into account and requires consideration when evaluating the performance of device structures such as WOLEDs.

Acknowledgements

We thank Christian Lennartz for fruitful discussions relating to the DFT calculations. The German-Israeli Foundation is acknowledged for financial support. Support from the Graduiertenkolleg 1640 is gratefully acknowledged.

References

- ¹ Hadziioannou, G.; Malliaras, G. *Semiconducting Polymers*; Wiley-VCH: Weinheim, Germany, 2007.
- ² Sun, Y. R.; Giebink, N. C.; Kanno, H.; Ma, B. W.; Thompson, M. E.; Forrest, S. R. *Nature* **2006**, *440*, 908.
- ³ Kamtekar, K. T.; Monkman, A. P.; Bryce, M. R. *Adv. Mater.* **2010**, *22*, 572.
- ⁴ Schütz, C.; Hofer, B.; Jaiser, F.; Krueger, H.; Thesen, M.; Janietz, S.; Kohler, A. *Phys. Status Solidi B* **2008**, *245*, 810.
- ⁵ D'Andrade, B. W.; Brooks, J.; Adamovich, V.; Thompson, M. E.; Forrest, S. R. *Adv. Mater.* **2002**, *14*, 1032.
- ⁶ Su, S. J.; Sasabe, H.; Takeda, T.; Kido, J. *Chem. Mater.* **2008**, *20*, 1691.

- 7 Tanaka, I.; Tabata, Y.; Tokito, S. *Chem. Phys. Lett.* **2004**, *400*, 86.
- 8 van Dijken, A.; Bastiaansen, J. J. A. M.; Kigger, N. M. M.; Langeveld, B. M. W.;
Rothe, C.; Monkman, A.; Bach, I.; Stossel, P.; Brunner, K. *J. Am. Chem. Soc.* **2004**,
126, 7718.
- 9 Brunner, K.; van Dijken, A.; Borner, H.; Bastiaansen, J. J. A. M.; Kigger, N. M. M.;
Langeveld, B. M. W. *J. Am. Chem. Soc.* **2004**, *126*, 6035.
- 10 Klöpffer, W. *Ber. Bunsen-Ges.* **1969**, *73*, 864.
- 11 Klöpffer, W.; Fischer, D. *J. Polym. Sci., Polym. Symp.* **1973**, *40*, 43.
- 12 Klöpffer, W. *ACS Symp. Ser.* **1987**, *358*, 264.
- 13 Rippen, G.; Kaufmann, G.; Klöpffer, W. *Chem. Phys.* **1980**, *52*, 165.
- 14 Itaya, A.; Okamoto, K. I.; Kusabayashi, S. *Bull. Chem. Soc. Jpn.* **1976**, *49*, 2037.
- 15 Vala, M. T.; Haebig, J.; Rice, S. A. *J. Chem. Phys.* **1965**, *43*, 886.
- 16 Adachi, C.; Forrest, S. R.; Thompson, M. E. *New J. Chem.* **2002**, *26*, 1171.
- 17 Schrögel, P.; Rothmann, M.; Strohrriegl, P.; Hoffmann, S. T.; Köhler, A.; Lennartz,
C. J. Mater. Chem. **2011**, *21*, 2266.
- 18 Johnson, P. C.; Offen, H. W. *J. Chem. Phys.* **1971**, *55*, 2945.
- 19 Qian, L.; Bera, D.; Holloway, P. H. *J. Chem. Phys.* **2007**, *127*, 244707.
- 20 Williams, E. L.; Haavisto, K.; Li, J.; Jabbour, G. E. *Adv. Mater.* **2007**, *19*, 197.
- 21 Burkhart, R. D.; Jhon, N. I.; Boileau, S. *Macromolecules* **1991**, *24*, 6310.
- 22 Abia, A. A.; Burkhart, R. D. *Macromolecules* **1984**, *17*, 2739.
- 23 Katayama, H.; Hisada, K.; Yanagida, M.; Ohmori, S.; Ito, S.; Yamamoto, M. *Thin
Solid Films* **1993**, *224*, 253.
- 24 Benten, H.; Guo, J.; Ohkita, H.; Ito, S.; Yamamoto, M.; Sakumoto, N.; Hori, K.;
Tohda, Y.; Tani, K. *J. Phys. Chem. B* **2007**, *111*, 10905.
- 25 Shimizu, H.; Kakinoya, Y.; Takehira, K.; Yoshihara, T.; Tobita, S.; Nakamura, Y.;
Nishimura, J. *Bull. Chem. Soc. Jpn.* **2009**, *82*, 860.
- 26 Tani, K.; Tohda, Y.; Takemura, H.; Ohkita, H.; Ito, S.; Yamamoto, M. *Chem.
Commun. (Cambridge, U.K.)* **2001**, *19*, 1914.
- 27 Cai, J. J.; Lim, E. C. *J. Chem. Phys.* **1992**, *97*, 3892.
- 28 Cai, J. J.; Lim, E. C. *J. Phys. Chem.* **1994**, *98*, 2515.
- 29 Becke, A. D. *J. Chem. Phys.* **1993**, *98*, 5648.

- 30 Lee, C. T.; Yang, W. T.; Parr, R. G. *Phys. Rev. B* **1988**, *37*, 785.
- 31 Kasha, M. *Discuss. Faraday Soc.* **1950**, *9*, 14.
- 32 Köhler, A.; Bässler, H. *Mater. Sci. Eng. R* **2009**, *66*, 71.
- 33 Morteani, A. C.; Sreearunothai, P.; Herz, L. M.; Friend, R. H.; Silva, C. *Phys. Rev. Lett.* **2004**, *92*, 247402.
- 34 Veldman, D.; Ipek, O.; Meskers, S. C. J.; Sweelssen, J.; Koetse, M. M.; Veenstra, S. C.; Kroon, J. M.; van Bavel, S. S.; Loos, J.; Janssen, R. A. J. *J. Am. Chem. Soc.* **2008**, *130*, 7721.
- 35 Huang, Y. S.; Westenhoff, S.; Avilov, I.; Sreearunothai, P.; Hodgkiss, J. M.; Deleener, C.; Friend, R. H.; Beljonne, D. *Nat. Mater.* **2008**, *7*, 483.
- 36 Haggquist, G. W.; Burkhart, R. D. *J. Phys. Chem.* **1993**, *97*, 2576.
- 37 Tani, K.; Yamamoto, S.; Kubono, K.; Hori, K.; Tohda, Y.; Takemura, H.; Nakamura, Y.; Nishimura, J.; Benten, H.; Ohkita, H.; Ito, S.; Yamamoto, M. *Chem. Lett.* **2007**, *36*, 460.
- 38 Winnik, F. M. *Chem. Rev.* **1993**, *93*, 587.
- 39 Yin, C.; Schubert, M.; Bange, S.; Stiller, B.; Castellani, M.; Neher, D.; Kumke, M.; Hörhold, H. H. *J. Phys. Chem. C* **2008**, *112*, 14607.
- 40 Turro, N. J. *Modern Molecular Photochemistry*: University Science Books: Sausalito, CA, 1991.
- 41 Lim, E. C. *Acc. Chem. Res.* **1987**, *20*, 8.
- 42 Tokito, S.; Iijima, T.; Tsuzuki, T.; Sato, F. *Appl. Phys. Lett.* **2003**, *83*, 2459.

10 List of Publications

P. Schrögel, A. Tomkevičienė, P. Strohrig, S. T. Hoffmann, A. Köhler, C. Lennartz

“A Series of CBP-Derivatives as Host Materials for Blue Phosphorescent Organic Light-Emitting Diodes”

Journal of Materials Chemistry **2011**, *21*, 2266-2273.

S. T. Hoffmann, **P. Schrögel**, M. Rothmann, R. Albuquerque, P. Strohrig, A. Köhler

“Triplet Excimer Emission in a Series of 4,4'-bis(*N*-carbazolyl)-2,2'-biphenyl Derivatives”

Journal of Physical Chemistry B **2011**, *115*, 414-421.

P. Schrögel, N. Langer, C. Schildknecht, G. Wagenblast, C. Lennartz, P. Strohrig

“Meta-linked CBP-derivatives As Host Materials For A Blue Iridium Carbene Complex”

accepted by *Organic Electronics*, **2011**.

P. Schrögel, M. Hopping, W. Kowalsky, A. Hunze, H. Börner, G. Wagenblast, C. Lennartz, P. Strohrig

“Phosphazene-based Host Materials for the Use in Blue Phosphorescent OLEDs”

submitted to *Chemistry of Materials*, 2011

Patent application

E. Fuchs, O. Molt, N. Langer, C. Lennartz, P. Strohrig, **P. Schrögel**

“Cyclic phosphazene compounds and the use thereof in organic light-emitting diodes”

WO 2009153276 A1, BASF SE, Germany

Danksagung

An dieser Stelle möchte ich mich bei allen bedanken, die mich während meiner Doktorarbeit auf vielfältige Art und Weise unterstützt haben.

Allen voran danke ich herzlich meinem Doktorvater Prof. Dr. Peter Strohmriegl für die interessante und anwendungsbezogene Themenstellung, seine stete Diskussionsbereitschaft und die umfassende Unterstützung während meines Auslandsaufenthaltes.

Dem Lehrstuhlinhaber, Prof. Dr. Hans-Werner Schmidt, möchte ich für die Bereitstellung eines sehr gut ausgestatteten Laborplatzes danken.

Für die finanzielle Unterstützung im Rahmen der Projekte „OPAL 2008“ und „TOPAS 2012“ sei dem Bundesministerium für Bildung und Forschung (BMBF) und der BASF SE gedankt. Darüber hinaus danke ich der Universität Bayreuth e.V. für ein Graduiertenstipendium.

Sebastian Hoffmann und Prof. Dr. Anna Köhler vom Lehrstuhl Experimentalphysik II danke ich für die nette Zusammenarbeit.

Bei allen Kooperationspartnern außerhalb der Universität Bayreuth, insbesondere bei Dr. Nicolle Langer, Dr. Evelyn Fuchs, Dr. Ingo Münster, Dr. Christian Lennartz, Dr. Christian Schildknecht, Dr. Gerhard Wagenblast, Dr. Soichi Watanabe, Dr. Thomas Geßner, Dr. Thomas Schäfer (BASF), Dr. Herbert Börner (Philips), Dr. Günter Schmid, Dr. Arvid Hunze (Siemens), Dr. Matthias Hoping (TU Braunschweig), Dr. Stephan Haneder, Raffael Tautz und Dr. Enrico Da Como (LMU München) möchte ich mich für ihre Hilfe bei fachlichen Fragen, für verschiedene Messungen und die gute Zusammenarbeit bedanken.

Allen Mitarbeitern des Lehrstuhls MCI danke ich für die angenehme und unterhaltsame Arbeitsatmosphäre. Großer Dank gilt Dr. Christian Neuber und Dr. Klaus Kreger für ihren reichen Erfahrungs- und Wissensschatz, den sie stets gerne und geduldig teilen. Dr. Klaus Kreger und Christina Löffler sei darüber hinaus für die zahlreichen GPC-Messungen, Doris Hanft und Florian Wieberger für HPLC-Messungen, Dr. Esther Scheler und Ruth Lohwasser für MALDI-TOF-Messungen und Dr. Michael Rothmann, Robin Pettau und Andreas Küst für ihre Hilfe bei Computerfragen gedankt.

Bei Irene Bauer möchte ich mich ganz herzlich für ihre tatkräftige Unterstützung bei der Synthese bedanken! Katlen Frenzel, Nadine Popp, Daniel Wagner und Moritz Tebbe bin ich sehr dankbar für ihre Hilfe im Labor während verschiedener Forschungspraktika.

Dr. Michael Rothmann, Dr. Esther Scheler, Andrea Jahreis und Andreas Ringk danke ich herzlich für ihr großes Interesse, für die vielen hilfreichen Diskussionen und Anregungen und für ihre freundschaftliche Unterstützung im Labor- und Büroalltag.

Der größte Dank gilt meinen Eltern für ihre uneingeschränkte Unterstützung in allen Lebenslagen und den persönlichen Rückhalt während meiner gesamten Ausbildung. Auch bei meiner Schwester Kathrin, meinem Schwager Oliver und meiner wertvollen Freundin Martina Eiser möchte ich mich ganz herzlich dafür bedanken, dass sie mir stets mit Rat und Tat zur Seite stehen.

Danke!

Erklärung

Hiermit erkläre ich, dass ich die Arbeit selbstständig verfasst und keine anderen als die angegebenen Hilfsmittel verwendet habe.

Ferner erkläre ich, dass ich nicht versucht habe, anderweitig mit oder ohne Erfolg, eine Dissertation einzureichen oder mich der Doktorprüfung zu unterziehen.

Bayreuth, Mai 2011

Pamela Schrögel

